Centro de Investigación Científica de Yucatán, A.C.

Posgrado en Ciencias Biológicas

FLUJOS DE METANO Y DIÓXIDO DE CARBONO EN ÁRBOLES DE MANGLE EN YUCATÁN

Tesis que presenta

Julio Alberto Salas Rabaza

En opción al título de

DOCTOR EN CIENCIAS
(Ciencias Biológicas: Recursos Naturales)

Mérida, Yucatán, México

2024

CENTRO DE INVESTIGACIÓN CIENTÍFICA DE YUCATÁN, A. C.
POSGRADO EN CIENCIAS BIOLÓGICAS

CICY

RECONOCIMIENTO

Por medio de la presente, hago constar que el trabajo de tesis de **Julio Alberto Salas Rabaza** titulado **Flujos de metano y dióxido de carbono en árboles de mangle en Yucatán,** fue realizado en la Unidad de Recursos Naturales, en la línea de investigación Servicios Ambientales de la Biodiversidad, en el Laboratorio de Fisiología Ambiental de Plantas del Centro de Investigación Científica de Yucatán, A.C. bajo la dirección del Dr. José Luis Andrade Torres, dentro de la opción de Recursos Naturales, perteneciente al Programa de Posgrado en Ciencias Biológicas de este Centro.

Atentamente

Dr. José Luis Hernández Stefanoni
Director de Docencia

Mérida, Yucatán, México, a 16 de octubre de 2024

DECLARACIÓN DE PROPIEDAD

Declaro que la información contenida en la sección de Materiales y Métodos, los Resultados y Discusión de este documento proviene de las actividades de investigación realizadas durante el período que se me asignó para desarrollar mi trabajo de tesis, en las Unidades y Laboratorios del Centro de Investigación Científica de Yucatán, A.C., y que a razón de lo anterior y en contraprestación de los servicios educativos o de apoyo que me fueron brindados, dicha información, en términos de la Ley Federal del Derecho de Autor y la Ley de la Propiedad Industrial, le pertenece patrimonialmente a dicho Centro de Investigación. Por otra parte, en virtud de lo ya manifestado, reconozco que de igual manera los productos intelectuales o desarrollos tecnológicos que deriven o pudieran derivar de lo correspondiente a dicha información, le pertenecen patrimonialmente al Centro de Investigación Científica de Yucatán, A.C., y en el mismo tenor, reconozco que si derivaran de este trabajo productos intelectuales o desarrollos tecnológicos, en lo especial, estos se regirán en todo caso por lo dispuesto por la Ley Federal del Derecho de Autor y la Ley de la Propiedad Industrial, en el tenor de lo expuesto en la presente Declaración.

Firma: 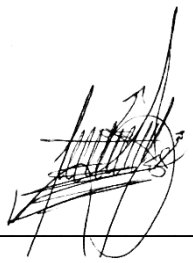

Julio Alberto Salas Rabaza

Este trabajo se llevó a cabo en la Unidad de Recursos Naturales del Centro de Investigación Científica de Yucatán, A.C., y no formó parte de ningún proyecto específico financiado. Sin embargo, para la realización del trabajo de campo en Yucatán se contó con la beca de la International Tropical Timber Organization (ITTO; Yokohama, Japón) con número de referencia 050/20A. Adicionalmente, se contó con el apoyo del Cape Horn International Center (CHIC; Puerto Williams, Chile) con número de referencia ANID-CHIC-FB210018, para la realización de la estancia y trabajo de campo en Isla Navarino.

AGRADECIMIENTOS

Al Consejo Nacional de Humanidades Ciencias y Tecnologías (CONAHCYT) por la beca número 760092, la cual me permitió realizar mis estudios de posgrado. Al Centro de Investigación Científica de Yucatán A.C. (CICY; Mérida, México) por abrirme las puertas y darme la oportunidad de realizar mis estudios en sus instalaciones. Asimismo, a la International Tropical Timber Organization (ITTO; Yokohama, Japón) por la beca otorgada para la realización del trabajo de campo (número de referencia 050/20A) y al Cape Horn International Center for global changes studies and biocultural conservation (CHIC; Puerto Williams, Chile) por el apoyo para la realización de la estancia de investigación en Isla Navarino (número de referencia ANID-CHIC-FB210018).

Al Centro de Investigación y de Estudios Avanzados del Instituto Politécnico Nacional (CINVESTAV; Zacatenco, México) y a la Universidad Autónoma de San Luis Potosí (UASLP; San Luis Potosí, México), por todas las facilidades brindadas directa e indirectamente a mi persona para el uso del equipo de medición de gases de efecto invernadero, así como el equipo de microtecnia; tanto en campo como en laboratorio. Asimismo, a la ONG Idea Wild (Colorado, Estados Unidos) por la subvención otorgada para la adquisición de equipo especializado para la toma de muestras de madera en árboles.

Agradezco nuevamente a la ITTO (número de referencia 091/23A), así como a la International Union of Forest Research Organizations (IUFRO; Viena, Austria), a través del Programa Especial para el Desarrollo de Capacidades (SPDC), por la beca y el apoyo otorgados para la asistencia al 26th IUFRO World Congress 2024 en Estocolmo, Suecia. Igualmente, extiendo mis agradecimientos a la Society of Wetland Scientists (SWS, Virginia, Estados Unidos) por el International Travel Award otorgado para la asistencia a la Reunión Anual 2025 a realizarse en Rhode Island, EEUU del 15-18 de julio de 2025. Todos ellos permitiéndome compartir los resultados de la presente tesis y extender las redes de colaboración para el futuro.

A mi asesor de tesis Dr. José Luis Andrade, quien ha sido un claro y buen ejemplo de lo que es ser un excelente gurú académico y de vida. Siempre estaré agradecido JLA, por tu aprecio, tu conocimiento, tus seminarios memorables, tu pasión por que la ciencia sea para todas y todos, tus consejos y tu amistad. Espero compartir tus enseñanzas y generosidades con futuros estudiantes. Gracias, por tanto.

A todos los integrantes de mi comité tutorial, les agradezco por sus enseñanzas académicas, así como por sus preguntas, comentarios y sugerencias en cada examen tutorial, sin los cuales esta tesis no hubiese sido concebida. Sepan que se les aprecia enormemente. Muchas gracias desde mi duramen sí vivo.

Au Dr. Frédéric Thalasso. *Mon ami, mon maître*, merci beaucoup d'avoir partagé ta science et ta façon de voir la vie avec moi. Je te remercie pour toutes les expériences incroyables que tu m'as permis de vivre au bout du monde, ainsi que de me laisser rencontrer ta belle famille. Tu es une des personnes les plus gentilles (et souriantes haha) que je connaisse. Sois assuré que je chercherai à créer des opportunités pour que d'autres étudiants soient aussi passionnés par la science sans frontières.

A la Dra. Laura Yáñez Espinosa. Le agradezco mucho por sus enseñanzas en anatomía, por recibirme en su laboratorio en la UASLP, así como por sus largas pláticas mientras me encontraba en el microtomo. Aprecio mucho su apoyo, sin el cual no hubiera sido posible expandir mi visión sobre cómo lo "pequeño" puede impactar al mundo.

Al Dr. Eduardo Cejudo Espinosa. Muchas gracias por sus siempre acertados comentarios a mi documento de tesis, los cuales han sido invaluables. Agradezco su entusiasmo para con mi tema, así como su perseverancia en involucrarme en los temas biogeoquímicos.

A los integrantes de mis comités de revisión predoctoral y de tesis de doctorado: Dra. Casandra Reyes García, Dra. María Azucena Canto Aguilar, Dr. Javier Orlando Mijangos Cortés y Dr. Rodrigo Méndez Alonzo, a quienes agradezco mucho por su valioso tiempo y disposición en la lectura de la presente tesis (en sus diferentes etapas), así como por sus acertados comentarios para su mejora. Asimismo, a la Dra. Azucena por el préstamo del microscopio óptico y la cámara para la toma de fotografías de las muestras anatómicas.

Agradezco a las autoridades de la CONANP, quienes han permitido que este trabajo fuera realizado con respeto en cada uno de los sitios de muestreo.

Al técnico del CICY, el Ing. Roberth Us Santamaría por su invaluable colaboración durante el doctorado, así como por su apoyo logístico y de campo requerido para la realización de la presente tesis. Los tiempos en el laboratorio y en el manglar han sido marcados por su presencia. Asimismo, agradezco mucho a la técnica Lic. María Rosalina Rodríguez Román por su apoyo en el uso del microscopio. Agradezco igualmente al Ing. Samuel Flores Mena

e Ing. Leonardo Gus Peltinovich del Depto. de Instrumentación, quienes siempre han tenido las puertas abiertas de sus talleres, así como una creatividad innata para apoyarme con mis locas ideas.

A la Dra. Francisca Massardo y al Dr. Ricardo Rozzi. Gracias por sus gestiones antes, durante y posterior a mi estancia en su bello país Chile. Junto con Fred, me permitieron conocer lo impresionante del Sur (o Norte) del mundo. Gracias por confiar en mí.

A la Lic. Eugenia M. Gade Palma, al Dr. Francisco Javier Aguirre y al Biól. Vicente Fecci Machuca por su apoyo y excelente compañía durante los trabajos de campo en Isla Navarino. Personas tan diversas de quienes aprendí muchas lecciones. Particularmente Eugenia, por su cualidad para escuchar y empatizar, muito obrigado.

A la C. Dra. Gabriela Cerón, Ing. Karina González, Dra. Gisela Mayora, C. Dr. Pablo Morales, C. Jesús Garrido, M.C. Juan Andrés y M.C. Aarón Casanova, quienes viajaron desde lejos (o cerca) para unirse al equipo de medición en campo en Yucatán. Las risas y el trabajo nunca faltaron con ustedes. Muchas gracias por su amistad y por el apoyo más allá de lo académico, se les quiere bonito.

A la Dra. Brenda Riquelme, Geof. Matías Troncoso, Geól. Camilo Quidel, Biól. Mar. Gabriel Múñoz y Bió. Amb. Katherine Chávez, los sap* más bacanes de Chile. Gracias por su apoyo dentro y fuera del bosque. Por su amistad y por todo lo que compartimos en Isla Navarino (y más allá). Lo atesoro enormemente. Nos vemos pronto.

Al M.C. David Balderas, Dra. Patricia González, M.C. Mauricio Collí y Biól. Eduardo Martínez, por su apoyo, amistad y compañía en el Laboratorio de Anatomía y en casa en SLP. Gracias por soportarme unos meses, en los cuales me hicieron sentir bien adoptado con todo y mamá.

A la Dra. Sunitha Pangala y al Dr. Rodrigo González Valencia, quienes fueron precursores de mi interés en el estudio del metano en ecosistemas tropicales y con quienes tuve la oportunidad de realizar mis primeras mediciones en manglares. Asimismo, a la Dra. Pangala, quién a través del proyecto EAA7572 de la Universidad Lancaster ha apoyado nuestros estudios preliminares sobre las emisiones de metano a nivel de hoja en manglares chaparros.

Agradezco igualmente a los integrantes (de ayer y hoy) de los laboratorios de Fisiología del CICY, de Gases de Efecto Invernadero en el CINVESTAV-Zacatenco y de Anatomía Funcional de la UASLP. Igualmente, al equipo que labora en la Dirección de Docencia del CICY y del Centro Subantártico Cabo de Hornos que siempre fueron amables y brindaron el apoyo requerido para hacer de mis estancias y trámites algo más fácil.

A mi madre y mi padre, quienes a través del ejemplo me llevaron por el camino del amor, el esfuerzo y el agradecimiento. No terminaré de gratificar ni en este ciclo del carbono ni en el siguiente. A mis hermanos, Ricardo y Rolando por brindar un hombro invisible en todo momento. Todos ellos, junto con mis sobrinos, hacen que el camino a casa siempre valga la pena… los amo enormemente.

A mon homme d'amour, Gilles, qui a maintenu son soutien même quand je m'éloignais. De qui j'ai appris que la vie ne peut pas être seulement le travail, et que tout travail vaut la peine si la vie est partagée. Tout comme le repos n'est pas un luxe. Merci beaucoup aussi de m'avoir prêté ta langue pour que je puisse continuer à raconter des histoires, et d'avoir fait grandir ma famille.

A mis amigos y familiares de todas las vidas que he vivido en este mundo, en Chiapas, en Guatemala, en Chapingo, en Coyoacán, en Mérida, en Québec y en Chile. Todos ellos han sido pilares que me han sostenido en los días más nublados, pero también en los más cálidos. Gracias por su amistad, los quiero un cocao.

DEDICATORIA

A la memoria de aquellos seres queridos que se han adelantado en el ciclo del carbono. En júbilo de los nuevos integrantes de la familia que hoy respiran y expiran CO_2. En ventura de aquellos que seguimos por la vida que evoluciona y florece, en presencia y en ausencia de oxígeno.

PRODUCTOS GENERADOS

ARTÍCULOS CIENTÍFICOS DEL DOCTORADO

- **Salas-Rabaza, J.A.**, Andrade, J.L., Us-Santamaría, R., Morales-Rico, P., Mayora, G., Aguirre, F.J., Fecci-Machuca, V., Gade-Palma, E.M., Thalasso, F., 2023. Impacts of leaks and gas accumulation on closed chamber methods for measuring methane and carbon dioxide fluxes from tree stems. Science of The Total Environment 904 (166358). https://doi.org/10.1016/j.scitotenv.2023.166358
- **Salas-Rabaza JA**, Yáñez-Espinosa L, Cejudo E, Cerón-Aguilera SG, Us-Santamaría R and Andrade JL. 2024. Pneumatophore CO_2 effluxes decrease with increased salinity in mangrove forests of Yucatan, Mexico. Scientific Reports 14 (18449). https://doi.org/10.1038/s41598-024-68822-9

OTROS ARTÍCULOS CIENTÍFICOS DEL PERÍODO

- **Salas-Rabaza JA**, Reyes-García C, Méndez-Alonzo R, Us-Santamaría R, Flores-Mena S and Andrade JL. 2023. Hydroperiod modulates early growth and biomass partitioning in *Rhizophora mangle* L. Aquatic Botany. https://doi.org/10.1016/j.aquabot.2023.103747
- Riquelme-del Río B, Sepulveda-Jauregui A, **Salas-Rabaza JA**, Mackenzie R and Thalasso F. 2024. Fine-scale spatial variability of greenhouse gas emissions from a subantarctic peatland bog. Environmental Science & Technology. https://doi.org/10.1021/acs.est.3c10746

ESTANCIAS

- *Balance de gases de efecto invernadero en ecosistemas subantárticos.* Realizado en el Centro Internacional Cabo de Hornos (CHIC, Puerto Williams) de la Universidad de Magallanes, Chile. Investigador receptor: Dr. Frédéric Thalasso. Período: 6 febrero – 13 de marzo (2022); 16 de julio – 9 de agosto (2022) y 24 de enero – 24 de julio (2023).
- *Atributos anatómicos de la madera y corteza en especies de manglar.* Realizada en el Instituto de Investigación en Zonas Desérticas de la Universidad Autónoma de San Luis Potosí (UASLP). Investigadora receptora: Dra. Laura Yáñez Espinosa. Período: 17 agosto – 20 diciembre (2022) y 26 de julio – 7 de septiembre (2023).

PARTICIPACIONES EN CONGRESOS

- *The bark side of mangrove methane emissions.* En la SWS 2025 Annual Meeting. Julio, 2025. Rhode Island, EEUU (a venir).
- *Do tree-mediated greenhouse gas emissions offset blue carbon in mangroves?* En el 26th IUFRO World Congress. Junio, 2024. Estocolmo, Suecia. Obteniendo el premio a mejor póster.
- *Más allá de la hoja: intercambio de gases en otros tejidos vegetales*. En el 5° Congreso Mexicano de Fisiología Vegetal. Octubre, 2023. Yucatán, México.
- *Implicaciones fisio-anatómicas en las emisiones de CH_4 y CO_2 en manglares.* En el III Simposio Latinoamericano de Ecofisiología Vegetal. Diciembre, 2022. En línea.

- *Implicaciones fisio-anatómicas en los flujos de gases de efecto invernadero en el mangle rojo.* En el 4° Congreso Mexicano de Fisiología Vegetal. Noviembre, 2022. Quintana Roo, México.
- *Emisiones de CH_4 y CO_2 en árboles de manglar, ¿el eslabón perdido de carbono?* En el XIII Simposio Internacional del Carbono en México. Octubre, 2022. Veracruz, México (En línea).
- *Flujos de CH_4 y CO_2 en árboles de manglar.* En el 2do Congreso de Manglares de América. Octubre, 2022. Yucatán, México.
- *Contribución de los neumatóforos de Avicennia germinans (L.) L. al flujo de CO_2 en manglares.* En el VIII Congreso Mexicano de Ecología. Mayo, 2022. Oaxaca, México. Obteniendo el segundo lugar como mejor presentación oral.

ACTIVIDADES DE DIVULGACIÓN

- **Salas-Rabaza, JA**. 2024. Understanding mangroves to better combat climate change. ITTO Tropical Forest Update 33 (2). ttps://www.itto.int/tfu/2024/08/28/lighting_the_path_to_sustainable_development/
- Exposición en formato Pecha Kucha con el tema: *Árboles de mil patas*. En el Foro de Árboles ciudadanos organizado por el Ayuntamiento de Mérida. Febrero, 2024.
- Participación en la Obra musical *"Árboles ciudadanos"* durante los eventos del Eclipse anular en el Parque Metropolitano Yumtsil (Octubre, 2023), CICY Casa Abierta (Noviembre, 2023) y Foro de árboles de las ciudades (Febrero, 2024).
- Exposición en formato Pecha Kucha con el tema*: Cazafantasmas de las plantas*. En la Telesecundaria Leandro Valle en San Pedro Chimay, Yuc.; la Preparatoria Estatal No. 13 Plantel Azteca, en Mérida, Yuc.; y el Telebachillerato Comunitario de Bolón, en Bolón, Yuc. Octubre, 2023.
- Entrevista para una nota periodística de la Agencia EFE de noticias sobre el impacto del castor norteamericano en las emisiones de metano en Tierra del Fuego. Mayo, 2023. https://n9.cl/castores_en_chile
- Participación como ponente en los seminarios de estudiantes de la Unidad de Recursos Naturales del CICY en los semestres 2021-I, 2021-II y 2023-I.
- **Salas-Rabaza, JA**. 2022. Tomemos un respiro para entender los bosques. Entrada en el Blog del XV World Forestry Congress Korea. https://worldforestvoices.wordpress.com/2022/03/22/tomemos-un-respiro-para-entender-a-los-bosques/
- Cerón-Aguilera, G., Alvarado-Barrientos, S., **Salas-Rabaza, JA**. 2022. Manglares: dioses del agua. En: Crónica y Portal Comunicación Veracruzana, INECOL. https://www.cronica.com.mx/academia/manglares-dioses-agua.html
- Participación en el Podcast Dondequiera con Ciencia con el tema: *La otra cara de la moneda de Carbono en manglares*. Marzo de 2022.
- Participación en Radio – Amor de 4 huellas con el tema: *"Los manglares, su importancia y los servicios que brindan*". Mérida, Yuc. Enero, 2022.
- Presentación "*Si el manglar tuviera Instagram"* a alumnos de la Preparatoria República de México. Mérida, Yuc. Octubre, 2020.
- Presentación *"Servicios ambientales de la biodiversidad*" a cargo de la Fundación R. de la Gala A.C. Facebook Live. Julio, 2020.

ÍNDICE

LISTA DE FIGURAS

LISTA DE CUADROS

En el principio todo eran gases …

RESUMEN

Los humedales tropicales son la mayor fuente natural de gases de efecto invernadero (GEI), pero también tienen un gran potencial como sumidero de carbono. Los ecosistemas de manglar son uno de los principales reservorios de este carbono. Sin embargo, parte del carbono es emitido como metano (CH_4) y dióxido de carbono (CO_2). Adicionalmente, los árboles pueden mediar el transporte de los GEI producidos en los suelos. Por lo tanto, es importante realizar mediciones precisas para mejorar los inventarios de CH_4 y CO_2. No obstante, la contribución atribuida a los árboles en la producción, el transporte y la emisión de CH_4 y CO_2 sigue siendo poco conocida. Además, las magnitudes y los moduladores de estas emisiones no están claros. Asimismo, no hay un consenso sobre las técnicas de medición de GEI en árboles, lo que dificulta las comparaciones entre especies y ecosistemas, representando otra fuente de error en las estimaciones de GEI. En este contexto, se buscó conocer los posibles sesgos en las estimaciones de GEI en manglares por *i*) el efecto de las fugas y la acumulación de gas en los métodos de medición en tallos, *ii*) la inclusión de estructuras biogénicas como los neumatóforos de *Avicennia germinans*, y *iii*) la emisión de GEI a través de los tejidos interconectados en los zancos y tallos de *Rhizophora mangle*. Así, se estimó la variación de CH_4 y CO_2 de tallos y raíces aéreas de tres especies de mangle (*R. mangle*, *A. germinans*, y *Laguncularia racemosa*) en diferentes tipos ecológicos de manglar (chaparro, cuenca, petén y franja) en Yucatán durante la estación lluviosa y la de sequía. Por un lado, las fugas son una fuente importante de error, mientras que la acumulación de gas en las cámaras de medición puede reducir el gradiente de presión parcial del gas, que disminuye su capacidad de intercambio. Ambos efectos condujeron a una subestimación del 40 ± 20 % de las emisiones de CH_4 y del 22 ± 22% de las emisiones de CO_2, dependiendo de la rugosidad de la corteza. En general, los zancos de *R. mangle* chaparro tuvieron las mayores tasas de emisión de CH_4. El manglar de cuenca contribuyó al aumento de los flujos de CO_2 a través de los tallos y neumatóforos de *A. germinans* y *L. racemosa*. La época de lluvias y la interfaz agua-aire limitaron los flujos de CO_2 pero promovieron las emisiones de CH_4. Los zancos de *R. mangle* cercanos al suelo – con mayor aerénquima – presentaron los mayores flujos de GEI. Además, las mayores emisiones de CO_2 provinieron de los neumatóforos del manglar de franja. Nuestros resultados, sugieren que las estimaciones actuales de los flujos de GEI en árboles están siendo subestimadas. Por lo tanto, no sólo deben incluirse en los balances y modelos de carbono, sino también deben entenderse desde la fisiología y anatomía de plantas.

ABSTRACT

Tropical wetlands are the most important source of natural greenhouse gas (GHG) emissions, mainly from soils. But they also have a great potential as a carbon sink. Mangrove ecosystems are one of the major blue carbon reservoirs. Conversely, some of the stored carbon is emitted, mainly as CH_4 and CO_2. Additionally, trees can mediate the transport of GHG produced in soils to the atmosphere, suggesting that our current CH_4 and CO_2 budgets are being underestimated. Accurate measurements of GHG emissions from trees is therefore important, to improve our current estimates and to provide better GHG inventories. However, the contribution of trees to production, transport, and emission of CH_4 and CO_2 remains poorly understood. Moreover, magnitudes, patterns, and drivers of these emissions are still unclear. Yet, there is no consensus on the techniques to measure GHG from trees, which make comparisons between species and ecosystems a big challenge, representing another source of GHG underestimation. In this context, we aimed to quantify the potential underestimations of GHG in mangroves due to *i*) the effect of leaks and gas accumulation on measuring methods, *ii*) lack of representation of biogenic structures such as pneumatophores, and *iii*) the soil-produced gas diffusion through the interconnected tissues in stilt roots and stems. Thus, we estimated the variation of CH_4 and CO_2 from tree stems and aerial roots of three mangrove species (*Rhizophora mangle*, *Avicennia germinans*, and *Laguncularia racemosa*) along different mangrove ecological types (scrub, basin, hammock and fringe) in Yucatan during both rainy and dry season. We found that the combined effects of leaks and concentration buildup can lead to an underestimation of CH_4 emissions by an average of 40 ± 20 % and CO_2 emissions by 22 ± 22 %, depending on the bark roughness. Overall, scrub *R. mangle* had the highest CH_4 emission rates from stilt roots. Basin mangrove forest contributed to increased CO_2 fluxes through the stems and pneumatophores of *A. germinans* and *L. racemosa*. Both the rainy season and the water-air interface limited CO_2 fluxes but enhanced CH_4 emissions. CH_4 and CO_2 were higher in near-ground tissues such as third-order stilt roots in *R. mangle* – which had a higher aerenchymatous tissue – both in scrub and hammock mangrove forests. Also, the greater CO_2 emissions came from pneumatophores in fringe mangrove. All our results, combined with a literature review, suggest that our current estimates of GHG fluxes from trees are being underestimated. Therefore, these fluxes must not only be included into our current carbon budgets and models, but also must be understood from a physiological and anatomical perspective.

RÉSUMÉ

Les zones humides tropicales sont une source majeure d'émissions de gaz à effet de serre (GES), tout en ayant un grand potentiel comme puits de carbone. Les écosystèmes de mangroves sont parmi les principaux réservoirs de carbone bleu. Cependant, une partie de ce carbone stocké est émise sous les formes de CH_4 et de CO_2. De plus, les arbres peuvent transporter les GES produits dans les sols vers l'atmosphère, suggérant que nos budgets actuels de CH_4 et de CO_2 sont sous-estimés. Il est donc essentiel de mesurer avec précision les émissions de GES des arbres afin d'améliorer nos estimations et d'obtenir de meilleurs inventaires. Néanmoins, la contribution des arbres à la production, au transport et aux émissions de CH_4 et de CO_2 reste peu comprise. En outre, les magnitudes, tendances et facteurs de ces émissions ne sont pas encore établis. L'absence de consensus sur les techniques de mesure des GES des arbres complique la comparaison entre espèces et écosystèmes, ce qui constitue aussi une source de sous-estimation. Dans ce contexte, nous avons cherché à quantifier les sous-estimations potentielles de GES dans les mangroves, dues à i) l'effet des fuites et de l'accumulation de gaz, ii) l'absence de prise en compte des structures biogènes telles que les pneumatophores, et iii) la diffusion des gaz depuis le sol à travers les tissus interconnectés des tiges et racines aériennes. Nous avons estimé les variations de CH_4 et de CO_2 à partir des tiges et racines aériennes de trois espèces de mangroves (*Rhizophora mangle*, *Avicennia germinans* et *Laguncularia racemosa*) le long de différents types écologiques (côtière, bassin, arbustive, petén) au Yucatán, pendant les saisons des pluies et de la sécheresse. Les effets combinés des fuites et de l'accumulation peuvent entraîner une sous-estimation moyenne des émissions de CH_4 de 40 ± 20 % et de celles de CO_2 de 22 ± 22 % selon la rugosité de l'écorce. Les taux d'émission de CH_4 étaient les plus élevés chez *R. mangle* dans les racine-échasses. Les forêts de mangrove du bassin ont montré une augmentation des flux de CO_2 par les tiges et pneumatophores *d'A. germinans* et de *L. racemosa*. La saison des pluies et l'interface eau-air ont réduit les flux de CO_2 mais augmenté les émissions de CH_4. Ces gaz étaient plus élevés dans les tissus proches du sol, notamment les racine-échasses de *R. mangle*, qui possèdent davantage d'aérenchyme dans les forêts arbustives et de petén. Par ailleurs, les émissions de CO_2 les plus élevées provenaient des pneumatophores dans les mangroves côtières. Nos résultats, soutenus par une revue de la littérature, suggèrent que les flux actuels de GES issus des arbres sont sous-estimés. Ces flux doivent donc être inclus dans les modèles actuels de carbone et être mieux compris d'un point de vue physiologique et anatomique.

INTRODUCCIÓN

El dióxido de carbono (CO_2) y el metano (CH_4) son los dos gases de efecto invernadero (GEI) que contribuyen al 80% del calentamiento global del planeta (Jackson *et al.,* 2024; Saunois *et al.,* 2024; Myhre *et al.,* 2013; Dalal y Allen, 2008). Según científicos del Panel Intergubernamental sobre Cambio Climático, la concentración de CO_2 podría duplicarse pronto, tal como es el caso del CH_4 (IPCC, 2021). Por tanto, hay un gran interés en la disminución de las concentraciones de estos GEI en la atmósfera. En este sentido, los bosques tienen una gran influencia sobre la dinámica del CO_2 y el CH_4 (Anderson *et al.,* 2010), ya que son sistemas naturales que extraen y retienen moléculas de carbono de la atmósfera, es decir, actúan como sumideros de carbono.

Los manglares fueron reconocidos como un gran sumidero de carbono debido a su alta productividad y potencial de secuestro de carbono, principalmente en el suelo (Bouillon *et al.,* 2008; Alongi, 2012). En este sentido, ha surgido un interés por entender los procesos que rigen la dinámica de carbono en los ecosistemas de manglar. Debido a sus características intrínsecas, estos ecosistemas se consideran una de las opciones para mitigar el cambio climático (Siikamäki *et al.,* 2012) mediante la compensación de los efectos de los GEI a través de la restauración efectiva (Pendleton *et al.,* 2012), o a través de la conservación de áreas naturales para evitar la emisión de GEI por degradación (Alongi y Mukhopadhyay, 2015).

Estos enfoques de mitigación y adaptación al cambio climático requieren de un conocimiento no sólo de las entradas de CO_2 y CH_4 al ecosistema, sino también de las emisiones de GEI del ecosistema hacia la atmósfera. Dichas emisiones provienen de diferentes interfaces, pero los suelos han recibido particular atención debido a que son las fuentes principales. Asimismo, ha sido reconocido que los árboles son capaces de movilizar gases que son producidos en el suelo. Esta facilitación ocurre a nivel de raíces y tallos, tanto en especies de humedales arbóreos como en bosques no inundables. En el caso de los humedales, como los manglares, el metano es el GEI mayormente estudiado; ya que tiene un potencial de calentamiento de 25-32 veces más que el CO_2, en una escala de 100 años. Empero, el estudio del CO_2 continúa siendo importante de contrastar, debido a que éste está involucrado en procesos fisiológicos de las plantas. Estudiando y cuantificando la dinámica de emisión y facilitación de estos dos gases, nos permite conocer la importancia

de los árboles en la regulación de los flujos de gases, a la vez que es posible entender el funcionamiento del ecosistema.

Los flujos de carbono, en su conjunto, son de especial importancia en la península de Yucatán debido a que esta región alberga el 60.12% de la superficie de manglares de México (Velázquez-Salazar *et al.,* 2021). Además, esta región cuenta con cuatro tipos ecológicos de manglar (Zaldívar-Jiménez *et al.,* 2010): manglar de franja, de cuenca, de petén y chaparro. Estos ecotipos de manglar difieren en su dominancia y composición de especies, el hidroperíodo y la salinidad, principalmente. Por tanto, a continuación, se detalla un enfoque anatómico y fisiológico sobre el entendimiento de la variación espaciotemporal de los flujos de moléculas de carbono, CO_2 y CH_4, en el continuo suelo-planta-atmósfera en los diferentes tipos ecológicos de manglar en la península de Yucatán. Esto con el fin de resaltar su importancia en el balance global de C (y particularmente del CO_2 y el CH_4); y, por consiguiente, el papel de estos ecosistemas en la mitigación y adaptación del cambio climático.

Particularmente, en la presente tesis se hace énfasis en las posibles subestimaciones potenciales de nuestra línea base de emisiones, debido a 1) los métodos de medición de GEI en tejidos vegetales no convencionales (*i.e.,* tallo y raíces); y 2) la exclusión de tejidos, como las raíces aéreas, en los inventarios y reportes de emisiones de GEI.

CAPÍTULO I.

1.1. ANTECEDENTES

1.1.1. GASES DE EFECTO INVERNADERO Y CAMBIO CLIMÁTICO

Los principales gases de efecto invernadero (GEI) son el dióxido de carbono (CO_2) y el metano (CH_4), los cuales contribuyen con el 60% y 20% del calentamiento global, respectivamente (Jackson *et al.,* 2024; Saunois *et al.,* 2024; Myhre *et al.,* 2013; Dalal y Allen, 2008). Aunque el CO_2 es el principal gas de efecto invernadero, el CH_4 tiene un potencial de calentamiento de 25 a 32 veces mayor que el CO_2 (Neubauer y Megonigal, 2015; Stocker *et al.,* 2013). El potencial de calentamiento se debe a la capacidad de estos gases para absorber y reemitir la radiación infrarroja emitidas por la superficie terrestre, contribuyendo al incremento de la temperatura media global. De esta forma estos GEI tienen un impacto directo sobre la variabilidad climática del planeta, contribuyendo a la formación de eventos hidrometeorológicos extremos que ponen en riesgo a millones de personas y contribuyen a la amenaza de extinción de especies y biomas en todo el mundo.

Según la última actualización (mayo de 2024) de la Estación Mauna Loa, Hawái, de la Administración Nacional Oceánica y Atmosférica (NOAA) de los Estados Unidos y del Instituto Scripps de Oceanografía (Universidad de California en San Diego), la concentración atmosférica de dióxido de carbono y metano es de 427 ppm CO_2 y 1929 ppb CH_4, lo cual representa un incremento respectivo del 51.70% y del 142.20% en la concentración de estos gases desde la era preindustrial. Debido, justamente, al potencial de calentamiento y a la concentración de estos gases en la atmósfera, se han registrado anomalías en la temperatura media global de hasta 1.1°C en el período comprendido desde 1880 hasta 2023 y de hasta 1.5°C entre 2023-2024 (Cattiaux *et al.,* 2024; NOAA, 2024). Este aumento en la temperatura media global influencia los regímenes de temperatura y precipitación a diversas escalas; haciendo que el clima cambie (Trumbore, 2000). Por lo que las acciones de mitigación y adaptación al cambio climático se hacen imperativas, dentro de las cuales se encuentra el desentrañar los procesos de intercambio de GEI entre la atmósfera y los ecosistemas, y viceversa.

1.1.2. EL PAPEL DE LOS BOSQUES DE MANGLAR EN LA DINÁMICA DE LOS GEI

Los bosques constantemente intercambian especies químicas basadas en el carbono con la atmósfera. La principal molécula de intercambio es el dióxido de carbono (CO_2), la cual entra a la biósfera a través de la fotosíntesis y es emitida de vuelta por medio de la respiración (Chapin III *et al.,* 2009; Smith y Smith, 2007); dejando en este trayecto otras formas de carbono, como constituyentes de la biomasa y en formas no estructurales en las plantas. Sin embargo, en bosques de humedales, otras moléculas, como el metano (CH_4), también son emitidas. En este caso, el flujo neto de CH_4 depende de la producción (metanogénesis) y la oxidación (metanotrofía; Barba *et al.,* 2019a). Tanto los procesos fisiológicos de las plantas en los que está involucrado el CO_2 (*i e.,* fotosíntesis y respiración) así como los procesos que involucran al CH_4, ocurren simultáneamente con procesos de intercambio de moléculas de carbono entre el suelo y la atmósfera; e incluso entre los suelos y las plantas. Se estima que cada año, alrededor del 10% del CO_2 atmosférico entra y sale por los suelos del mundo (Stockman *et al.,* 2013). El suelo gana C principalmente de la vegetación; y éste es liberado como CO_2 y CH_4 por medio de procesos aeróbios como la respiración de raíces y microorganismos, así como por procesos anaeróbios (metanogénesis) y abióticos (Luo y Zhou, 2006).

El balance entre los procesos de intercambio de estos GEI en el continuo suelo-planta-atmósfera, determina si el ecosistema actúa como un emisor neto o como un sumidero neto de carbono. En este sentido, los bosques tienen una gran influencia sobre la dinámica de los GEI en la atmósfera (Anderson *et al.,* 2010), ya que capturan y almacenan moléculas de carbono, actuando como sumideros bajo condiciones naturales. No obstante, los humedales también contribuyen en las emisiones de GEI, siendo la fuente natural más grande de CH_4 atmosférico (Saunois *et al.,* 2024). Aproximadamente, el 60% del área global total de estos humedales son bosques inundables (Prigent *et al.,* 2007). Esto sugiere que, aunque los manglares son sumideros netos de carbono (la captura excede a la emisión), también pueden aportar metano a la atmósfera.

Se estima que entre el 49-98% del carbono almacenado en los manglares se encuentra en el suelo debido a su alta productividad y potencial de secuestro (Alongi, 2014; Donato *et al.,* 2011; Bouillon *et al.,* 2008). Sin embargo, el equilibrio entre la captura y la emisión bruta que determina este carbono almacenado puede llegar a ser alterado por actividades antropogénicas y naturales. El sistema de raíces, las altas tasas de sedimentación y las

condiciones anóxicas del suelo en manglares, resulta en una tasa neta de almacenamiento de carbono (burial) substancialmente alta comparado con cualquier otro bosque terrestre (Alongi, 2012; McLeod *et al.,* 2011). La captura y el secuestro de carbono son dos servicios ecosistémicos muy importantes del manglar; siendo este bosque junto con los pastos marinos y las marismas saladas los principales contribuyentes al almacén de carbono azul (Herrera-Silveira *et al.,* 2020; Lovelock y Duarte, 2019; Sanders *et al.,* 2016). Por tanto, los manglares juegan un papel muy importante en el ciclo del carbono, en la regulación de los GEI en la atmósfera y, por ende, contribuyen a la mitigación del cambio climático.

1.1.3. LOS MANGLARES DE LA PENÍNSULA DE YUCATÁN

Los manglares son comunidades de árboles, arbustos o helechos que se distribuyen en las zonas costeras de los trópicos y subtrópicos. Estas comunidades poseen adaptaciones que les permiten tolerar un rango amplio de salinidad e inundación como son sus raíces aéreas (*e.g.,* neumatóforos y zancos), glándulas excretoras de sales, entre otras (Tomlinson, 2016; Rodríguez-Zúñiga *et al.,* 2013; Lugo y Snedaker, 1974).

México cuenta con una amplia extensión de manglares, la cual lo posiciona como el cuarto país con mayor superficie de manglar en el mundo, el sexto en diversidad de especies (Rodríguez-Zúñiga *et al.,* 2013; Giri *et al.,* 2011; Spaldin *et al.,* 2010) y a su vez en el sexto lugar en capacidad de almacenamiento de carbono (Herrera-Silveira *et al.,* 2020). De la extensión total en México, el 60.12% de manglares se encuentra en la península de Yucatán (Velázquez-Salazar *et al.,* 2021). En esta región, podemos encontrar las tres principales especies de mangles “verdaderos” (según la definición de Tomlinson, 2016) del país, las cuales son: el mangle rojo, *Rhizophora mangle* L.; el mangle negro, *Avicennia germinans* (L.) y el mangle blanco, *Laguncularia racemosa* (L.) C. F Gaertn (Figura 1.1.A). Estas especies difieren principalmente en su tolerancia a la salinidad y la inundación, por lo que es común que éstas se distribuyan siguiendo una zonación microtopográfica (Spaldin *et al.,* 2010; McKee, 1995). Estos factores microtopográficos, así como los hidrológicos y de nutrimentos dan como resultado diferentes tipos ecológicos (o ecotipos) de manglar (Feller y Sitnik, 1996), que presentan diferencias en su estructura (Figura 1.1.B) y composición de especies. Es así como, de acuerdo con Lugo y Snedaker (1974), se distinguen seis principales tipos fisionómicos de manglar (tipos ecológicos o ecotipos), de los cuales cuatro se presentan en la península de Yucatán (Figura 1.1.C; Zaldívar-Jiménez *et al.,* 2010). A saber, son: el manglar de franja, de cuenca, de petén y el manglar chaparro.

- *Manglar de franja.* Se encuentra sobre la línea de costa, en islas o al borde de lagunas; por tanto, están expuestos a los regímenes hidrológicos de estos cuerpos de agua adyacentes y los niveles de inundación suelen ser altos, con una salinidad variable. En estos bosques podemos encontrar las tres especies de manglar, pero la que domina suele ser *R. mangle*.

- *Manglar de cuenca.* Se localiza detrás del manglar de franja hacia tierra dentro y suelen formarse en depresiones topográficas. Se inunda sólo durante mareas altas y se drena pronto, por tanto, puede presentar altas salinidades. La dominancia de una especie depende de la salinidad, siendo *A. germinans* la dominante a salinidades mayores a 40 ppm y *L. racemosa* a salinidades menores a 35 ppm (Zaldívar-Jiménez et al., 2010). Sin embargo, tierra adentro, es posible también encontrar este tipo de manglar a salinidades bajas.

- *Manglar de petén.* Son una variante del manglar de cuenca, pero se encuentran sobre una mayor elevación del sustrato. Están asociados a descargas de agua dulce subterránea (localmente llamados “ojos de agua”). Por tanto, la salinidad es muy baja y el aporte de nutrientes es alta; lo que permite que los árboles alcancen mayores alturas. Las especies dominantes son *R. mangle* y *L. racemosa*.

- *Manglar chaparro*. Es un tipo de manglar muy particular, formado por árboles de baja altura que crecen en suelos con limitaciones de nutrientes y con salinidades elevadas, así como en sitios expuestos a altos niveles de radiación solar. El aporte de agua depende mucho de la época de lluvias, pero pueden estar asociados a dinámicas de mareas. Son bosques monoespecíficos, principalmente de *R. mangle* o *A. germinans*.

Por tanto, para entender la variabilidad espacial y temporal de los flujos de moléculas de C (CO_2 y CH_4) en bosques de manglar, es sumamente importante considerar: 1) la tolerancia y adaptación de las diferentes especies a la inundación y la salinidad; 2) la diferenciación estructural intra- e inter-específica en los diversos tipos fisionómicos de árboles de mangle; y, 3) las características hidrológicas, el microambiente y la biogeoquímica de los diferentes ecotipos de manglar.

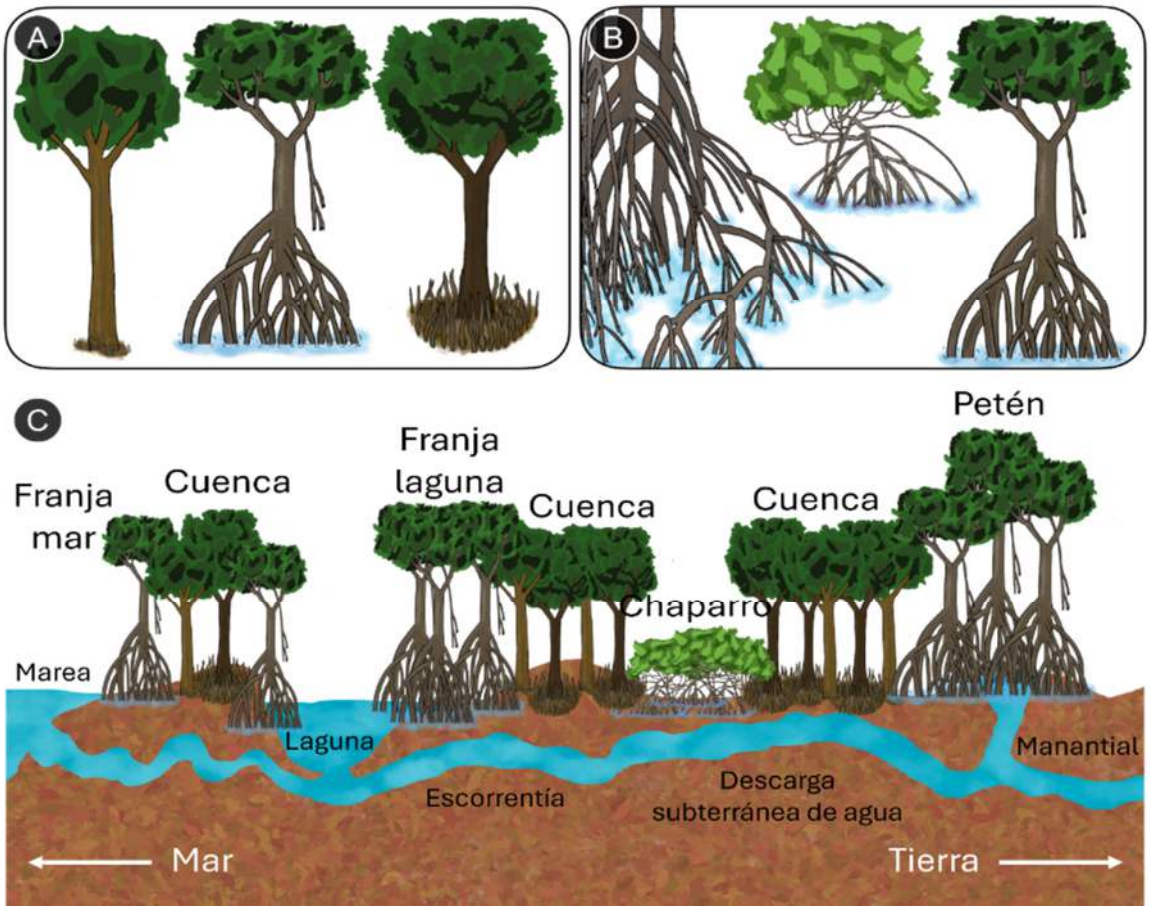

Figura 1.1. A. Diferenciación estructural interespecífica entre las especies de manglar. De izquierda a derecha tenemos *L. racemosa*, *R. mangle* y *A. germinans*. B. Diferencias estructurales intraespecíficas de *R. mangle* según el tipo ecológico en el que crece. C. Gradiente de zonación de los tipos ecológicos de manglar en Celestún, Yucatán. Modificado de Zaldívar-Jiménez *et al.,* 2010.

1.1.4. FLUJOS DE CH_4 Y CO_2 EN ECOSISTEMAS DE MANGLAR

La investigación en bosques en el contexto del ciclo del carbono se ha enfocado principalmente en la dinámica del dióxido de carbono (Schlesinger y Andrews, 2000; Smith et al., 2018). Sin embargo, recientemente, se ha demostrado que las emisiones de metano en suelos de manglares pueden compensar parcialmente hasta el 20% del carbono azul almacenado en el suelo (Rosentreter *et al.,* 2018). Por ello, la investigación de los flujos de gases de efecto invernadero en los bosques se ha centrado en las emisiones provenientes de suelos. No obstante, los árboles también actúan como fuentes o sumideros de CO_2 y CH_4 a través de sus tallos y raíces (Covey y Megonigal, 2019; Maier *et al.,* 2018; Pangala

et al., 2017). Lo cual juega un papel muy importante en el balance de C del ecosistema. Por lo tanto, cuantificar los presupuestos de C es un desafío porque los bosques constituyen un complejo sistema de procesos, ambientes y superficies que producen, "consumen", transportan y emiten GEI (Covey y Megonigal, 2019; Teskey et al., 2017).

Al hablar de los flujos de CH_4 y CO_2 en el manglar, hay que distinguir que éstas se mueven en el continuo suelo-planta-atmósfera, en el cual existe un intercambio constante de moléculas a tres principales niveles (Figura 1.2): 1) entre el suelo y la atmósfera; 2) entre el suelo y las plantas, que envuelve a los procesos fisiológicos naturales que transportan gases; y 3) entre las plantas y la atmósfera, que incluye procesos que toman lugar en el interior de las plantas; pero adicionalmente, también existe un intercambio de gases entre los cuerpos de agua y la atmósfera. Sin embargo, el origen, las magnitudes de los flujos, así como la variación espacial y temporal en tallos y raíces de manglares permanece casi desconocido (Barba *et al.,* 2019a; Akhand *et al.,* 2019; Teskey *et al.,* 2008). Aún más, poco se sabe sobre los procesos biofísicos, fisiológicos y anatómicos implicados en esos flujos.

1.1.4.1. Flujos de gases entre el suelo y la atmósfera

Los flujos de CO_2 del suelo, se deben principalmente a la producción de CO_2 por medio de la actividad microbiana durante la mineralización de la materia orgánica y la respiración aeróbica de raíces (Chen *et al.,* 2012; Lovelock *et al.,* 2011; Lovelock, 2008; Luo y Zhou, 2006). Sin embargo, en bosques continuamente inundados como los manglares, el oxígeno se agota rápidamente, el potencial de óxido reducción (Eh) disminuye y otras moléculas son usadas como aceptores de electrones (Nóbrega *et al.,* 2016; Alongi *et al.,* 2001). Estas condiciones anóxicas favorecen otros procesos como la respiración anaeróbica y la metanogénesis (Inglet *et al.,* 2013; Luo y Zhou, 2006). Asimismo, la oxidación del CH_4 ocurre en la superficie del suelo sobre la columna de agua, y alrededor de las raíces; donde el oxígeno transportado por las plantas se difunde hacia los suelos anaeróbicos (Covey y Megonigal, 2019). Estos procesos de producción y consumo de CO_2 y CH_4 ocurren simultáneamente y están influenciados por las características fisicoquímicas del suelo como la salinidad, el potencial de óxido reducción, la temperatura, la humedad del suelo, la inundación (Chen *et al.,* 2016; Troxler *et al.,* 2015; Kirui *et al.,* 2009), así como por la composición de especies, el contenido de agua y de materia orgánica (Lin *et al.,* 2020; Chen *et al.,* 2012; Chen *et al.,* 2010) y la presencia de neumatóforos (Troxler *et al.,* 2015; Pangala *et al.,* 2013; Kristensen *et al.,* 2008).

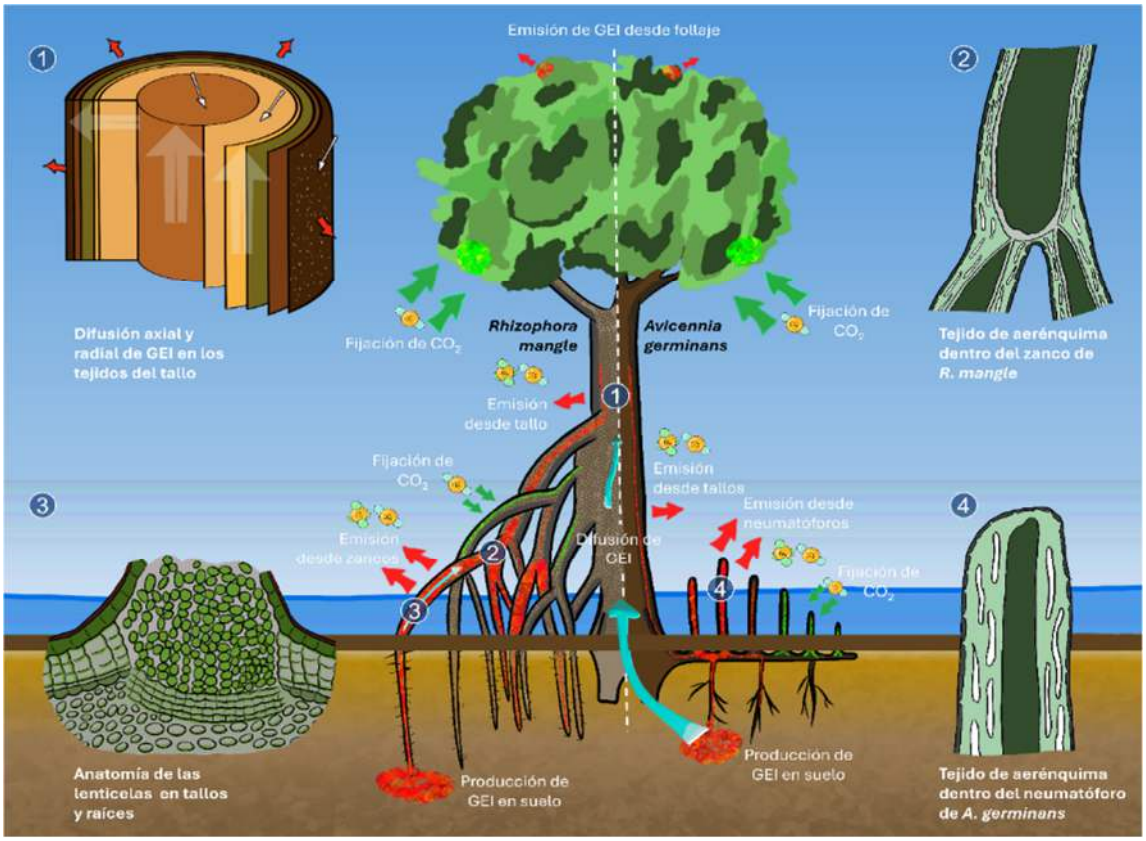

Figura 1.2. Sitios de producción, consumo, movimiento y emisión de GEI en el continuo suelo-planta-atmósfera en especies con estructura tipo *R. mangle* (izq.) y *A. germinans* (der.) en el ecosistema de manglar. Morfología y anatomía de tallos (1), zancos (2), lenticela (3) y neumatóforos (4). Puntos rojos denotan producción y movimiento, mientras puntos verdes denotan consumo, fijación u oxidación de GHG. Flechas señalan las emisiones de gases hacia la atmósfera (rojas); captura (verdes); y transporte (azul) de moléculas. Modificado de Barba *et al.,* 2019a.

Las principales características que han sido responsables de las variaciones estacionales de los flujos de CO_2 en suelos de manglar son la temperatura y la humedad del suelo. La mayoría de los estudios han encontrado una relación positiva entre los flujos de CO_2 y la temperatura del suelo (Poungparn *et al.,* 2009; Lovelock, 2008), pero también otros estudios no han encontrado dicha relación (Kirui *et al.,* 2009). Esta relación es atribuida a las altas temperaturas que favorecen la actividad microbiana en el suelo y por tanto conduce a mayores flujos de CO_2, mientras que la humedad del suelo ha tenido una correlación negativa con los flujos (Akhand *et al.,* 2019). Asimismo, las emisiones de CH_4 en manglares son afectadas por la temperatura y la humedad del suelo, aportando a la variabilidad estacional de los flujos. Por ejemplo, se ha reportado que las estaciones con mayor flujo de CH_4 son las temporadas calientes y menor en las temporadas más frías (Nóbrega *et al.,*

2016; Chen *et al.,* 2016; Purjava y Ramesh, 2001), lo cual apoya el hecho del papel que juega la temperatura en la regulación de los flujos de moléculas con carbono.

Igualmente, los suelos ricos en carbono orgánico y con mayor presencia de nutrientes como N, P y Fe favorecen mayores flujos de CO_2 (Chen *et al.,* 2012; 2010); pero no en todos los casos (Chen *et al.,* 2014). Además, el estancamiento del agua y la mayor cantidad de materia orgánica también inducen una mayor producción de CH_4 (Lin *et al.,* 2020; Allen *et al.,* 2007). Sin embargo, estos parámetros del suelo pueden influenciar las emisiones de CH_4 dependiendo de las especies dominantes en el manglar (Lin *et al.,* 2020). Esto resalta que la composición o la estructura de las raíces también afectan las emisiones de gases provenientes del suelo, pues, se ha observado que los suelos con neumatóforos tienen flujos de CO_2 y CH_4 más altos que en suelos sin ellos (Lin *et al.,* 2021, Lin *et al.,* 2020; Troxler *et al.,* 2015; Pangala *et al.,* 2013; Kristensen *et al.,* 2008). Por tanto, la medición de los flujos de estos gases en suelos sin neumatóforos podría subestimar la respiración y la metanogénesis global del suelo en gran medida.

Los flujos de CO_2 del suelo también han sido correlacionados positivamente con la productividad primaria (medida como tasa de caída de hojarasca), y el índice de área foliar (Lovelock*,* 2008); que son factores de la vegetación que contribuyen al aporte de materia orgánica en los suelos. También hay muchos estudios que demuestran que altas salinidades inhiben la actividad metanogénica de las bacterias (Rosentreter *et al.,* 2018; Chen *et al.,* 2016; Chauhan *et al.,* 2015), mientras que el potencial de óxido-reducción ha tenido un efecto inverso (Lin *et al.,* 2020; Rosentreter *et al.,* 2018). Esto se debe principalmente a que el sulfato puede ser adquirido del agua de mar, y, por tanto, la reacción de reducción de sulfatos en suelos ocurre antes que la metanogénesis en sitios con altas salinidades (Nóbrega *et al.,* 2016). Sin embargo, otros factores como el hidroperíodo, que influencia la salinidad, la temperatura y la humedad del suelo en manglares, así como la disponibilidad de nutrientes y características fisicoquímicas han recibido menos atención (Leopold *et al.,* 2013); aunque se ha encontrado que, durante los momentos de inundación del suelo, éstos presentan menor flujo de CO_2 (Troxler *et al.,* 2015).

Por tanto, las mediciones de los flujos de CO_2 y CH_4 del suelo deben hacerse simultáneamente con la cuantificación de las emisiones del tallo y las raíces, para comparar los procesos que tienen lugar en el suelo y en las plantas (Pitz *et al.,* 2018; Pangala *et al.,*

2017; 2013), y para mejorar los enfoques de escalamiento a nivel de ecosistema y a escala regional (Pangala *et al.,* 2017).

1.1.4.2. Flujos de gases entre los árboles y la atmósfera

Los flujos de carbono han sido mejor caracterizados en suelos, aun cuando los árboles también pueden emitir CO_2 y CH_4 a través de sus tallos, raíces y follaje (Tenhovirta *et al.,* 2024; Saunois *et al.,* 2024; Covey y Megonigal, 2019; Barba *et al.,* 2019a; Teskey *et al.,* 2017). Sin embargo, las magnitudes de estas emisiones en el contexto del balance global de carbono aún son inciertas y permanecen bajo debate. Respecto a los manglares, se conoce muy poco sobre los flujos de CO_2 (Vinh *et al.,* 2019), y CH_4 en tallos (Liao *et al.,* 2024; Zhang *et al.,* 2022; Dušek *et al.,* 2021; Gao *et al.,* 2021; He *et al,* 2019; Jeffrey *et al.,* 2019; Zhang *et al.,* 2019). Por tanto, esta sección está basada, en su gran mayoría, en lo que se conoce de los flujos de CO_2 y CH_4 provenientes de tallos de especies arbóreas diferentes al manglar.

Procesos que liberan o consumen CO_2 y CH_4 en tallos

La mayoría de CO_2 dentro de los tallos es originado por la respiración de células vivas en tallos y raíces. En el tallo, estas células se encuentran en la corteza interna, en el cambium vascular y en las células rayo de la albura (Teskey *et al.,* 2008). La tasa de respiración celular difiere sustancialmente con la profundidad radial en el tallo. Por ejemplo, se ha reportado que el flujo de CO_2 de tejidos de la corteza interna son mayores que en la albura (Teskey y McGuire, 2007; Pruyn *et al.,* 2003), lo cual ha sido relacionado con la disponibilidad de carbohidratos o la concentración de nitrógeno (Pruyn *et al.,* 2005). Sin embargo, a pesar de que se ha asumido que el CO_2 derivado de la respiración es liberado hacia la atmósfera, se ha demostrado que grandes cantidades de ese CO_2 se mantiene dentro de los árboles (Teskey y McGuire, 2007) y que incluso una porción es disuelta en la savia y transportada fuera de los sitios de origen (Figura 1.3.A; Teskey *et al.* 2008; Teskey y McGuire, 2005).

Los procesos que regulan la dinámica de gases en tallos de árboles están poco entendidos, pero revisiones hechas por Teskey *et al.,* (2017; 2008) sobre el CO_2, sugieren que existe una traslocación de CO_2 disuelto por la corriente de transpiración y también un consumo de CO_2 por fotosíntesis cortical. En el caso del metano, la metanogénesis y la metanotrofía también están presentes en los tallos de los árboles y dependen de características

anaeróbicas dentro de los tejidos (Covey y Megonigal, 2019); pero también son dependientes de la comunidad microbiana asociada a ellos, que son capaces de consumir hasta un tercio del CH_4 durante su transporte axial en el tallo (Jeffrey *et al.,* 2021a, 2021b).

El comportamiento de los flujos de metano varía por tipo de tejido y posición en el árbol. Las emisiones tienden a decrecer conforme aumenta la altura en el tronco, hacia las ramas y hojas (Covey y Megonigal, 2019; Pangala *et al.,* 2017); un comportamiento que podría ser causado por diversos factores como el volumen del tejido, tipo de tejido (duramen o albura) o distancia desde la fuente de emisión (Covey y Megonigal, 2019; Wang *et al.,* 2016). Algunos estudios realizados en humedales sugieren que árboles de diámetros pequeños emiten mayor CH_4 que árboles maduros de diámetros mayores (Pangala *et al.,* 2017, 2015). Los árboles muertos también pueden difundir y emitir metano producido en suelos (Jeffrey *et al.,* 2019); además, la materia muerta emite metano producido en el interior del tallo por microorganismos, o por procesos fotoquímicos abióticos (Covey y Megonigal, 2019).

Para que la fotosíntesis cortical o de la madera se produzca se requiere de tejidos que contengan cloroplastos, además de que haya un suficiente aporte de CO_2 y que la luz penetre al interior del tallo. Algunos tejidos que contienen cloroplastos pueden encontrarse en diferentes partes del tallo, incluyendo sitios adyacentes al cambium, dentro del floema en la corteza interna, en los rayos del xilema e incluso en la médula (Pfanz *et al.,* 2002; Pfanz y Aschan, 2001). En comparación con la fotosíntesis en hojas, la fotosíntesis cortical y de la madera tiene dos ventajas principales: 1) hay menor pérdida de agua, debido a que no hay estomas involucrados en el proceso; y 2) la fotorrespiración es baja o no detectable, debido a las altas concentraciones de CO_2 en los tejidos de la madera (Teskey *et al.,* 2017; Teskey *et al.,* 2008; Cernusak y Marshall, 2000). En especies de humedales, como los manglares, la fotosíntesis cortical puede jugar un papel muy importante para el mantenimiento de oxígeno en tallos o raíces aéreas para evitar la anoxia (Yabuki, 2004; Pfanz *et al.,* 2002; Pfanz y Aschan, 2001; Aiga *et al.,* 1995), y por tanto también podrían inhibir la producción de metano y dióxido de carbono.

Barreras y conductos de gases dentro de árboles

Los flujos de moléculas de CO_2 y CH_4 al interior de los tallos y raíces, así como de éstos hacia la atmósfera, no sólo dependen de las tasas de producción (respiración y metanogénesis) o consumo (fotosíntesis cortical y metanotrofía). Es también dependiente

del tipo y composición de los tejidos internos, que funcionan como barreras biofísicas; así como de las estructuras y tejidos que sirven como canales de transporte; y por tanto también depende de las sustancias que actúan como transportadores de las moléculas de C a lo largo de esos canales (Figura 1.3). Por tanto, las interacciones que existan entre estas barreras, conductos y transportadores, determinarán el flujo neto de CO_2 y CH_4 hacia la atmósfera.

1. Respiración (crecimiento)
2. Mantenimiento de la respiración
3. Transpiración
4. Transporte por floema
5. Disolución, en función de temperatura y pH.
6. Intercambio de gases
7-8. Fijación de CO_2 por fotosíntesis (PEP-C o Rubisco) en xilema

DsV. Difusión vertical (axial)
DsD. Difusión en duramen
DsA. Difusión en albura
DsC. Difusión en corteza

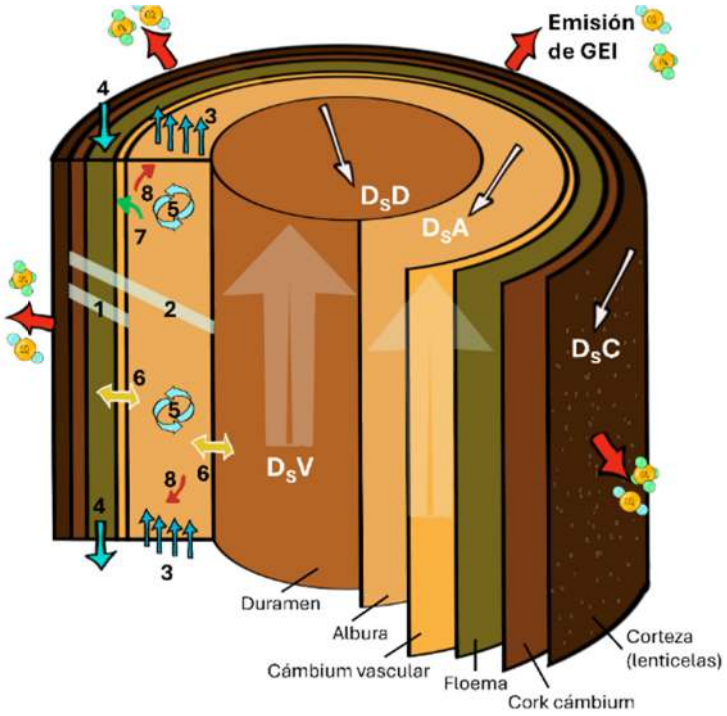

Figura 1.3. Segmento del tallo que muestra los sitios de producción, consumo y transporte de gases; y tejidos que pueden cumplir la función de barrera, conducto o transportador (Modificado de Trumbore *et al.,* 2013 y Barba *et al.,* 2019a).

Altas concentraciones de CH_4 dentro de los tallos de árboles demuestran que hay barreras para el trasporte y la difusión de gases relacionados con la anatomía de la madera y la corteza (Covey y Megonigal, 2019). Estos tejidos protegen al árbol contra la pérdida de agua, la entrada de insectos y patógenos; pero también limitan el intercambio de gases con la atmósfera (Teskey *et al.,* 2008; Teskey y McGuire, 2007). Estas resistencias dependen principalmente de la cantidad de ligninas, suberinas, lípidos, ceras y del grosor de la corteza (Lendzian, 2006) y por tanto difiere sustancialmente entre especies y la edad del tejido (Teskey *et al.,* 2008).

Las emisiones de CH_4 en tallos de especies de humedales han sido relacionadas positivamente con la concentración de CH_4 en el agua capilar (Terazawa *et al.,* 2015; Pangala *et al.,* 2015, 2014) y negativamente con la densidad de la madera (Pangala *et al.,* 2013). Asimismo, las emisiones disminuyen rápidamente con la altura del tallo por encima del nivel de inundación (Pangala *et al.,* 2017).

En especies de manglar, que crecen en ambientes inundados, una adaptación importante en la corteza es la presencia de lenticelas, que son tejidos especializados que facilitan el intercambio de gases con la atmósfera. Por ejemplo, se ha encontrado que la densidad de lenticelas y la concentración de CH_4 en el agua capilar explican el 84% de la variación en las emisiones de metano de tallos en *Alnus glutinosa* (Pangala *et al.,* 2014). Otra adaptación importante para las especies de manglar es la formación de aerénquima (Armstrong y Armstrong, 2005; Colmer, 2003), el cual es un tejido especializado que se caracteriza por ampliar los espacios de aire en raíces y tallos (Figura 1.3.A-B), permitiendo soportar condiciones anóxicas del suelo (Evans, 2004; Colmer, 2003; Drew *et al.,* 2000). Por tanto, el aerénquima es un tejido que facilita el flujo de gases al interior de los árboles, y permiten el movimiento axial del CO_2 y CH_4.

La transpiración también puede favorecer el flujo de gases entre el suelo o las raíces y la atmósfera. Esto ha sido demostrado en diferentes especies donde el CH_4 disuelto en el suelo es transportado hacia la atmósfera a través de plántulas de especies arbóreas en humedales (Rice *et al.,* 2010; Garnet *et al.,* 2005). También se han encontrado relaciones negativas entre los flujos de savia (velocidad y densidad del flujo) y la transpiración con los flujos de CO_2 (Bowman *et al.,* 2005; Gansert y Burgdorf, 2005). La cantidad total de CO_2 disuelto en savia es dependiente de la temperatura, el pH y el CO_2 en fase gaseosa que está en contacto con la savia (Teskey et al., 2008; Teskey y McGuire, 2007).

En el caso de las raíces, su contribución a los flujos de moléculas de C emitidos en tallos es poco conocida, especialmente en raíces de especies adaptadas a la inundación (como los manglares), donde las características anatómicas y morfológicas crean barreras para la pérdida radial de oxígeno hacia el suelo (Armstrong y Armstrong, 2005; Colmer, 2003). Además, en estas especies se forma una capa de suberina en la exodermis de las raíces que reduce el flujo de oxígeno (De Simone *et al.,* 2003), pero puede también tener la misma función para los flujos de CO_2 y CH_4. Estas mismas características tienen un impacto sobre el paso, a través de los árboles, de gases de C desde el suelo hacia la atmósfera.

1.1.4.3. Flujos de gases entre el suelo y las plantas

En humedales, los tallos de árboles pueden ser una ruta de escape de gases producidos en micrositios en el suelo o bajo tierra (Covey y Megonigal, 2019; Pangala *et al.,* 2017). Debido a que los árboles son capaces de transportar y emitir metano producido en el suelo, ya sea por difusión o por transporte en el xilema (Bloemen *et al.,* 2014), este transporte de gases desde el suelo hacia la atmósfera – a través de los árboles – es gobernado por la ley de Fick, es decir, el flujo de gases es proporcional al gradiente de concentración. No obstante, también depende de la distancia desde la fuente hacia la atmósfera, y la resistencia al flujo a través del tallo (Covey y Megonigal, 2019). Sin embargo, los árboles no sólo funcionan como transportadores de gases desde el suelo, sino también juegan un papel como reguladores de esos flujos a través de las interacciones planta-suelo-microbioma.

Los árboles controlan las tasas de producción, oxidación y exportación de gases producidos en el suelo, actuando como donadores y aceptores de electrones para la respiración microbiana (Covey y Megonigal, 2019; Megonigal *et al.,* 2004) e inhibiendo las emisiones de CH_4 debido a la generación de óxidos de Fe (III), que compiten como aceptores de electrones, limitando así la metanogénesis (Covey y Megonigal, 2019). Por tanto, un gran desafío para explicar la variación espacial y temporal en los flujos de CO_2 y CH_4 en tallos y raíces aéreas es discernir entre las moléculas de C que fueron producidas en el suelo de aquellas producidas al interior de los árboles.

1.1.5. CUANTIFICACIÓN DE FLUJOS DE GEI

La exclusión de tejidos como los tallos y raíces aéreas para la cuantificación de GEI, puede conducir a subestimaciones en los reportes de emisiones de estos gases, sobre todo en un enfoque *bottom-up* o de escalamiento de abajo hacia arriba. Es decir, cuando se realizan mediciones en estructuras e interfaces bajo el dosel y se extrapolan a escalas espaciales más grandes como el ecosistema. Su contraparte, las aproximaciones *top-down* o de arriba hacia abajo, nos permiten capturar con mayor detalle la variación temporal a nivel de ecosistema, ya que las mediciones se realizan sobre el dosel del bosque. Para ello, las estimaciones se realizan mediante técnicas y métodos tales como las torres de flujo de covarianza de torbellinos (eddy covariance) o de sensores remotos (*e.g.,* Lidar o radar). Ambas aproximaciones son importantes, pero las estimaciones bajo el dosel nos ayudan a

entender mejor la dinámica de CO_2 y CH_4 de forma más precisa por componente y no sólo como ecosistema. Por tal motivo, se deben de considerar todas las posibles fuentes de GEI.

Por sí mismo, los métodos de medición de gases son muy variados, pero se basan todos en encapsular un espacio de la fuente de GEI, en áreas y volúmenes determinados, para registrar la acumulación de gases a través del tiempo. Con esta información es posible calcular una tasa de emisión/absorción o flujo (*i.e.,* flux) que corresponde en términos "generales" a la pendiente que se forma entre la concentración cuantificada a lo largo del tiempo. Para ello, se recurre al uso de cámaras (*"chambers*; Fig. 1.4) que nos permiten justamente cubrir un espacio de interés, de nueva cuenta, en un área y volumen definidos. Sin embargo, a pesar de que existen diferentes modelos de cámaras caseras y comerciales, aún no existe un consenso en las metodologías; y, por tanto, el uso de una cámara u otra depende de factores propios del estudio, así como de la accesibilidad a los sitios de medición, el presupuesto o la disponibilidad de equipo de laboratorio (para muestras *ex situ*), así como de la intensidad del muestreo y la precisión en la medición de los gases. No obstante, en la cuantificación de gases de efecto invernadero, existe cierta preferencia en la utilización de cada tipo de cámaras, según el gas en cuestión o la interfaz de medición (*i.e.,* suelo, planta, agua).

1.1.5.1. Medición en suelos y neumatóforos

El método de cámara cerrada estática (*non-flow-through-non-steady state chamber*), con mediciones discretas, es el método más ampliamente usado para la medición de flujos de gases de efecto invernadero – especialmente el metano – entre el suelo y la atmósfera en manglares (Akhand *et al.,* 2019; Chauhan *et al.,* 2008). El principio básico de esta técnica es cubrir un área conocida del suelo con la cámara cerrada, permitiendo el intercambio de gases entre el suelo debajo de la cámara y la cabeza de la cámara (Pihlatie *et al.,* 2013; Inglett *et al.,* 2013; Yu *et al.,* 2013). Estas cámaras cuentan con una válvula que permite la extracción muestras de gases. La concentración del gas dentro de la cámara aumenta con el tiempo, por lo que deben tomare múltiples muestras para ser cuantificadas *ex situ* con un cromatógrafo de gases u otro analizador (Luo y Zhou, 2006) y ser transformadas a una tasa de flujo. El método más común para calcular los flujos de CH_4 es la regresión lineal, aunque pueden provocar subestimaciones en la cuantificación de los flujos (Pihlatie *et al.,* 2013; Pedersen *et al.,* 2010). Debido a su versatilidad para la medición *ex situ*, este método permite cuantificar diferentes gases de efecto invernadero. Sin embargo, para las

mediciones *in situ*, las cámaras cerradas dinámicas (*non-steady-state trough-flow chamber*), con mediciones continuas, son ampliamente utilizadas. Estas cámaras cuentan con mecanismos para mezclar el aire al interior de la cámara y son conectadas a analizadores de gases (Figura 1.4.F– I; Heinemeyer y McNamara, 2011; Luo y Zhou, 2006), que permiten la cuantificación de la concentración de gases al interior de la cámara.

Un problema muy importante en las cámaras estáticas para las tomas discretas de gases son los largos períodos de muestreo manual, que pueden subestimar los flujos debido a un aumento asintótico en las concentraciones de gases dentro de la cámara que modifica la dinámica de intercambio de gases; no obstante, Heinemeyer y McNamara (2011), demostraron que las mediciones con cámaras estáticas pueden proporcionar valores de flujos de gases comparables con las cámaras dinámicas en mediciones continuas; siempre y cuando se tomen muestras iniciales más frecuentes durante períodos de tiempo más cortos; evitando así, la subestimación del flujo debido a la acumulación gases dentro de la cámara. Este error en la subestimación también puede disminuirse al aumentar la altura de la cámara, el área y el volumen (Pihlatie *et al.,* 2013).

1.1.5.2. Medición en tallos y zancos

Mucha de la metodología para la cuantificación de GEI en suelos ha sido trasladada a interfaces más complicadas como son los tallos o los zancos. Para la medición de gases emitidos por tallos o raíces aéreas, también se puede contar con cámaras estáticas y dinámicas. Sin embargo, en este caso particular, no existen cámaras comerciales para tallos, debido a la alta heterogeneidad de las superficies de medición que varían con la edad y la especie. Por tanto, las cámaras “caseras” (Figura 1.4) han sido las más ampliamente utilizadas para la medición de CO_2 y CH_4 (He *et al.,* 2019; Vinh et al., 2019 Jeffrey *et al.,* 2019; Pangala *et al.,* 2015); pero también se ha recurrido a la modificación de la superficie de los tallos para la colocación de cámaras dinámicas de suelos (Li-COR 8100-104, Lincoln, Nebraska) de forma vertical, permitiendo su automatización (Barba *et al.,* 2019b; Vargas y Barba, 2019). No obstante, se ha propuesto un diseño de cámaras rígidas y semirrígidas manuales para tallos (Figura 1.4. A-E; Siegenthaler *et al.,* 2016); las cuales reducen la permeabilidad de los gases, se adaptan a diferentes superficies, permiten un mejor mezclado al interior, son fáciles de construir, transportar e implementar en campo. Lo cual favorece una alta replicación y puede mejorar los modelos de flujos de gases en tallos con enfoques a diferentes escalas (Covey y Megonigal, 2019). Estas cámaras semirrígidas

pueden funcionar como cámaras dinámicas, y, por tanto, permiten su adaptación con analizadores de gases.

No obstante, un reto en la medición de flujos de GEI en tallos es asegurar un sellado hermético de la cámara con el tejido, para evitar fugas (*i.e.,* el intercambio de gases entre la atmósfera y el volumen interno de la cámara). Sin embargo, aun si la cámara está perfectamente sellada, pueden aparecer fugas en el circuito neumático o dentro del detector (Wilkinson *et al.,* 2018). Además de las fugas, otro efecto potencial, es debido a un aumento en la concentración de los gases dentro de la cámara. Esta acumulación reduce el gradiente de presión parcial de los gases entre el tallo y la atmósfera, disminuyendo así su intercambio. A su vez, este fenómeno puede dar lugar a errores en las estimaciones, como se sugiere en ecosistemas acuáticos (Xiao *et al.,* 2016), suelos (Welles et al., 2001; Kutzbach *et al.,* 2007; Juszczak, 2013) y observado en árboles (Jeffrey *et al.,* 2020; Bréchet *et al.,* 2021; Kohl *et al.,* 2021; van Haren *et al.,* 2021).

Por lo cual, es importante contrastar el impacto que esos efectos, solos y combinados, puede tener sobre la cuantificación de GEI de tallos. Adicionalmente, existen otro tipo de cámaras abiertas, las cuales permiten el intercambio continuo de gases entre la cámara y la atmósfera, que lo acerca más a la realidad (Fig. 1.4H). Pero, requiriendo un mayor entendimiento del balance de masas del sistema y la toma correcta de las variables (Thalasso *et al.,* 2023). Sea cual sea el tipo de cámara, éstas son conectadas a diferentes analizadores de gases, por ejemplo: microelectrodos o sensores de infrarrojo no dispersivo (NDIR), sensores en el infrarrojo (IRGA) o espectróscopia láser, entre otros.

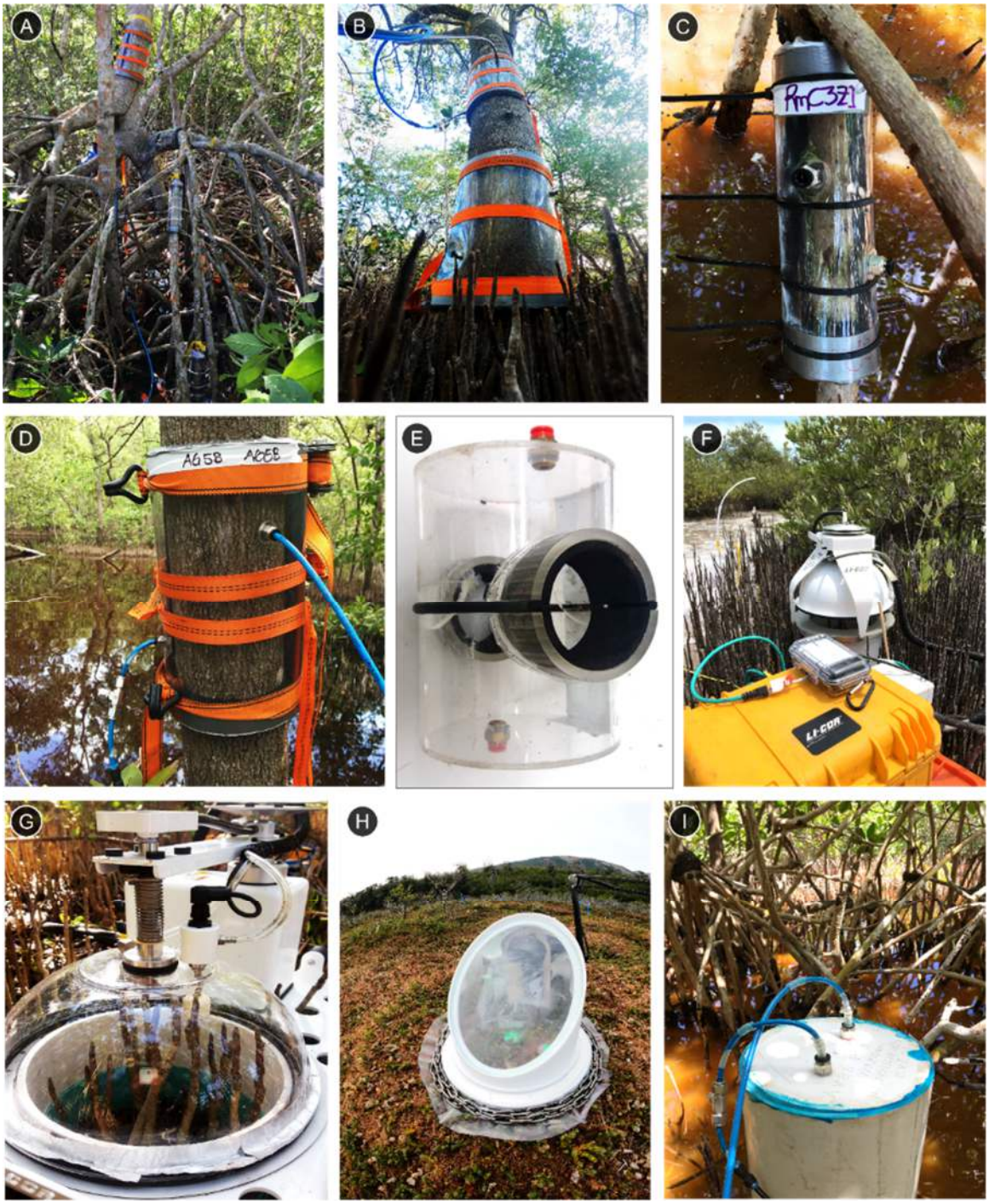

Figura 1.4. Cámaras para la medición de flujos de gases en suelos y compartimentos vegetales. **A–D.** Cámara semirrígida para la medición en tallos y zancos en árboles. **E.** Cámara rígida para medición en tallos. **F.G.** Cámara de sistema cerrado dinámico para medición en suelo y neumatóforos. **H.** Cámara 'skirt' de sistema abierto para medición en turberas (Thalasso *et al.,* 2023). **I.** Cámara de sistema cerrado para medición en la interfaz agua–aire.

1.2. JUSTIFICACIÓN

En los bosques de manglar, los suelos han recibido mayor atención en la cuantificación de las emisiones de CO_2 y CH_4 en comparación con los tallos y raíces. También es evidente que la mayoría de los estudios se han realizado en el Indo-Pacífico, con escasos trabajos en África y América. Sin embargo, en la península de Yucatán (y en México) no existe información sobre los flujos de moléculas de CO_2 y CH_4 en este ecosistema, a pesar de que esta región posee más del 60% de la cobertura de manglares del país y cuenta con diferentes tipos ecológicos de manglar, que varían en su estructura y composición de especies, así como en sus características hidrológicas, biogeoquímicas y microambientales. Por tanto, resulta imperativo 1) cuantificar correctamente las emisiones de CO_2 y CH_4 a través de tallos y raíces aéreas en especies de manglar; 2) conocer la variabilidad espacial y temporal de estos flujos en los diferentes tipos ecológicos; 3) determinar las características fisiológicas, morfo-anatómicas y fisicoquímicas que intervienen en los flujos de tallos y raíces. Esta información aumentará el entendimiento del balance de carbono, nutriendo los modelos actuales y redefiniendo nuestra línea base de emisiones. En el caso particular de la península de Yucatán, podrá sustentar la importancia de la restauración de este ecosistema no sólo por su aporte como almacén de carbono azul, sino también por evitar emisiones de GEI por degradación y deforestación, conociendo a los árboles desde su interior.

1.3. PREGUNTAS DE INVESTIGACIÓN

- ¿Cuál es el impacto, sólo y combinado, de las fugas y la acumulación de gases en la medición de los flujos de CO_2 y CH_4 en tallos?

- ¿Cuál es el rol de los neumatóforos en los flujos de CO_2 en las interfaces suelo-aire y agua-aire en bosques dominados por *Avicennia germinans* a lo largo de un gradiente de salinidad en Yucatán?

- ¿Qué relación tiene la anatomía de la corteza con el flujo radial CH_4 y CO_2 en tallos y zancos de árboles de *Rhizophora mangle* chaparro y de petén?

- ¿Cómo varían los flujos de CH_4 y CO_2 de los tallos de *Rhizophora mangle, Avicennia germinans* y *Laguncularia racemosa* durante las temporadas de lluvias y sequía en Yucatán?

1.4. HIPÓTESIS

- Las fugas y la acumulación de gas en los dispositivos experimentales (cámaras) utilizados para la determinación de las emisiones de GEI, conducen a una subestimación de las emisiones de GEI en árboles. Los cuales pueden ser resueltos con la consideración y cuantificación de las fugas y del gradiente de concentración entre la cámara y la atmósfera.

- Las magnitudes de los flujos de CO_2 serán mayores a mayores abundancias de neumatóforos debido a una mayor cantidad de tejido vivo que lleva a cabo la respiración, así como a una mayor movilización de gases producidos en suelos. Además, los flujos serán más altos en la interfaz sedimento-aire que en el agua-aire, ya que la primera incluye la respiración del suelo y la segunda es reducida por la barrera que ejerce la columna de agua al paso de gases. Del mismo modo, debido a la sensibilidad del flujo de CO_2 a la temperatura y la salinidad, se espera que estos flujos aumenten a temperaturas más altas y salinidades más bajas.

- En *Rhizophora mangle*, se encontrarán mayores flujos de CH_4 y CO_2 en los zancos en comparación con los tallos, ya que estos tejidos están más cerca de los sitios de producción de GEI en el suelo y tienen a su vez más aerénquima para movilizarlos.

- Debido a que *R. mangle* es más tolerante a la inundación que *A. germinans* y *L. racemosa*, se espera que esta especie emita proporcionalmente más GEI. Asimismo, se esperan mayores emisiones de CH_4 y menores de CO_2 en la estación lluviosa, ya que el tiempo de residencia del agua ejerce una barrera física a la difusión de ambos gases, pero también promueve la metanogénesis.

1.5. OBJETIVO GENERAL

Disminuir los errores en las estimaciones de CO_2 y CH_4 en manglares, considerando los efectos asociados al método de medición como al tipo de tejido medido. Asimismo, analizar la influencia de variables morfológicas, anatómicas y estructurales sobre los flujos de estas moléculas.

1.6. OBJETIVOS ESPECÍFICOS POR CAPÍTULO

Capítulo II

Evaluar el impacto de las fugas y la acumulación de concentración de gases sobre las estimaciones de gases de efecto invernadero (CH_4 y CO_2) en tallos de árboles mediante el método de cámara semirrígida cerrada en mediciones continuas.

Capítulo III

Evaluar la contribución de la estructura y la densidad de los neumatóforos al flujo de CO_2 en bosques de manglar chaparro, de cuenca y franja dominados por *Avicennia germinans* (L.) L. durante la temporada de lluvias y sequía.

Capítulo IV

Identificar la relación de atributos anatómicos de la corteza con el flujo radial de CH_4 en y CO_2 en tallos y raíces aéreas de *Rhizophora mangle* L. chaparro y de petén en Yucatán.

1.7. ESTRATEGIA EXPERIMENTAL

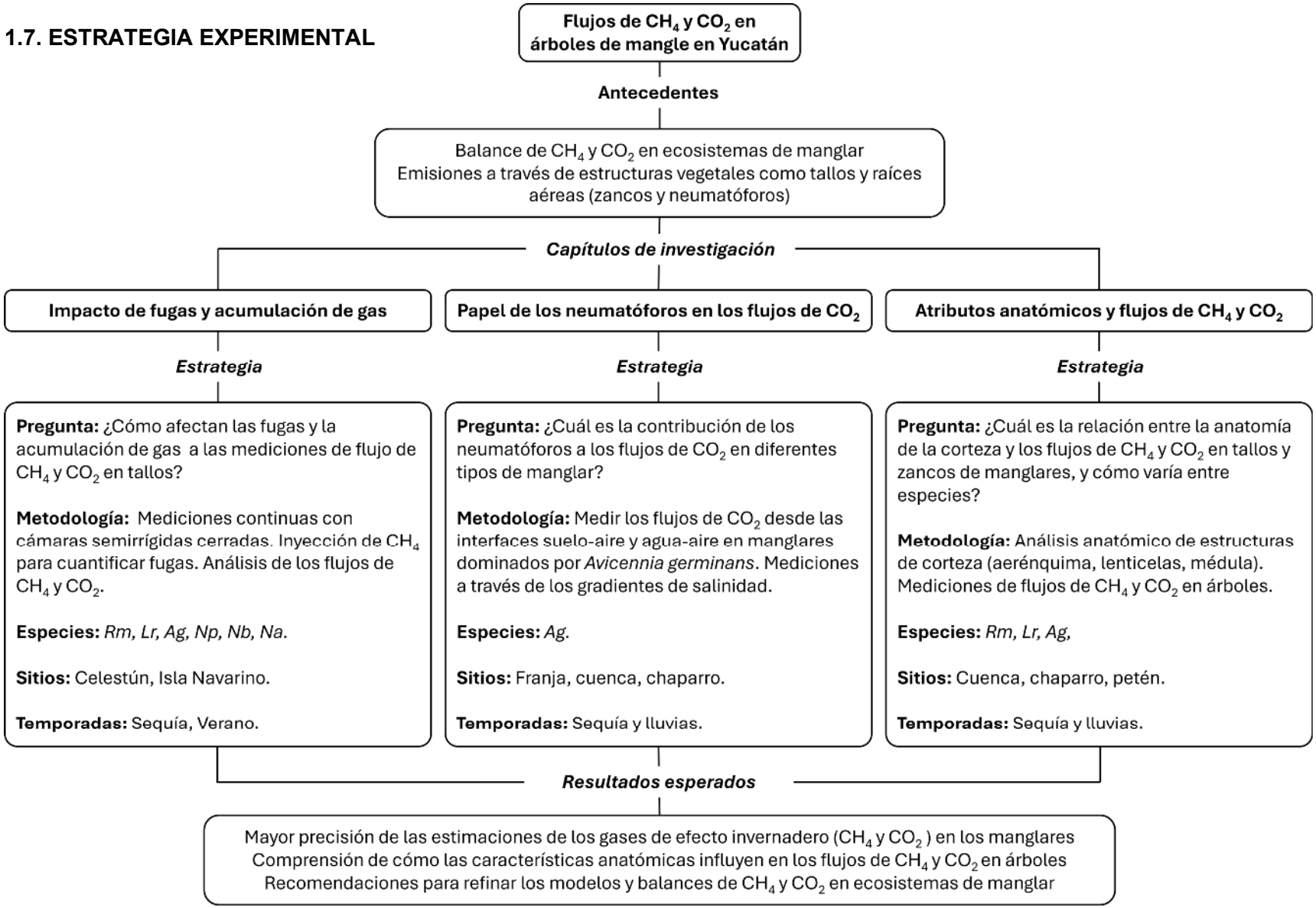

CAPÍTULO II.

IMPACTS OF LEAKS AND GAS ACCUMULATION ON CLOSED CHAMBER METHODS FOR MEASURING METHANE AND CARBON DIOXIDE FLUXES FROM TREE STEMS

Este capítulo fue publicado en la revista científica *Science of The Total Environment* y debe ser citado y referido de la siguiente manera:

Salas-Rabaza, J.A., Andrade, J.L., Us-Santamaría, R., Morales-Rico, P., Mayora, G., Aguirre, F.J., Fecci-Machuca, V., Gade-Palma, E.M., Thalasso, F., 2023. Impacts of leaks and gas accumulation on closed chamber methods for measuring methane and carbon dioxide fluxes from tree stems. Science of The Total Environment 904 (166358). https://doi.org/10.1016/j.scitotenv.2023.166358

RESUMEN

Los tallos de árboles emiten gases de efecto invernadero (GEI), por lo cual, es importante realizar mediciones precisas de los flujos de metano (CH_4) y dióxido de carbono (CO_2) para mejorar nuestra comprensión de la dinámica de GEI. Dentro de los métodos más comunes para este propósito se encuentran los sistemas de cámaras cerradas; sin embargo, las fugas entre la cámara y la atmósfera, así como la acumulación de la concentración de gas al interior de la cámara, pueden afectar significativamente las mediciones. Por tanto, en este estudio investigamos los impactos de la acumulación de concentración de gas y las fugas en el método de cámara cerrada semirrígida. Se realizaron mediciones de campo en seis especies de árboles, incluyendo tres especies de un ecosistema de manglar en México y tres especies de un bosque subantártico Magallánico. Las observaciones sistemáticas revelaron tasas de fugas significativas, las cuales oscilaron entre 0.00 y 465 L h^{-1}, con un valor medio de 1.25 ± 75.67 L h^{-1}. Se probó la eficacia del uso de aislantes para reducir las fugas, logrando una reducción de la tasa de fuga de gas del 46-98 % sin eliminarla por completo. Nuestro estudio también demostró un impacto claro y sustancial de la acumulación de concentración de gas en las mediciones de flujo de CH_4, mientras que las mediciones de flujo de CO_2 fueron relativamente menos afectadas en todas las especies de árboles estudiadas. Estos resultados muestran que los efectos combinados de las fugas y la acumulación de la concentración de gas pueden llevar a subestimar las emisiones de CH_4 en una media del 40 ± 20% y las emisiones de CO_2 en un 22 ± 22%, dependiendo de la rugosidad de la corteza. Con base en estos hallazgos, reevaluamos un método sencillo y efectivo para minimizar los errores experimentales asociados a estos dos efectos, previamente establecidos, y reiterados en el contexto actual, para calcular las emisiones tomando en cuenta los efectos de las fugas y la acumulación de concentración, pero eliminando al mismo tiempo la necesidad de determinar estos fenómenos por separado. En conclusión, nuestros resultados, combinados con una revisión de la literatura, sugieren que nuestras estimaciones actuales de los flujos de GEI proveniente de tallos de árboles están siendo subestimadas.

HIGHLIGHTS

- CH_4 and CO_2 fluxes from tree stems are significant and important to constrain
- Stem flux measurements can be affected by leaks and concentration buildup effects
- We studied these effects in six tree species from two contrasting forest ecosystems
- These effects led to an underestimation of 40% for CH_4 and 22% for CO_2 fluxes
- A simple method addresses both leaks and concentration buildup effects

Key words: mangrove, sub-Antarctic, forest, greenhouse gas, bark, roughness

ABSTRACT

Accurate measurements of methane (CH_4) and carbon dioxide (CO_2) fluxes from tree stems are important for understanding greenhouse gas emissions. Closed chamber methods are commonly employed for this purpose; however, leaks between the chamber and the atmosphere as well as gas accumulation, known as the concentration buildup effect, can impact flux measurements significantly. In this study, we investigated the impacts of concentration buildup and leaks on semi-rigid closed chamber methods. Field measurements were conducted on six tree species, including three species from a Mexican mangrove ecosystem and three species from a Magellanic sub-Antarctic forest. Systematic observations revealed significant leak flow rates, ranging from 0.00 to 465 L h^{-1}, with a median value of 1.25 ± 75.67 L h^{-1}. We tested the efficacy of using cement to reduce leaks, achieving a leak flow rate reduction of 46–98 % without complete elimination. Our study also demonstrates a clear and substantial impact of concentration buildup on CH_4 flux measurements, while CO_2 flux measurements were relatively less affected across all tree species studied. Our results show that the combined effects of leaks and concentration buildup can lead to an underestimation of CH_4 emissions by an average of 40 ± 20 % and CO_2 emissions by 22 ± 22 %, depending on the bark roughness. Based on these findings, we recall a straightforward yet effective method to minimize experimental errors associated with these phenomena, previously established, and reiterated in the current context, for calculating emissions that considers effects of leaks and concentration buildup, while eliminating the need for separate determinations of these phenomena. Overall, the results, combined with a literature review, suggest that our current estimates of GHG flux from tree stems are currently underestimated.

2.1. INTRODUCTION

In the context of climate change, understanding greenhouse gas (GHG) sources and sinks is of paramount importance. Forests are widely acknowledged as global sinks for methane (CH_4), where it is produced in the anaerobic deeper soil layer but oxidized in excess, within the aerobic upper layer. However, in flooded forests, like mangroves, water creates an oxygen barrier, turning forest soils into a net CH_4 source. Regardless of the specific forest type, it is well-established that trees play a pivotal role in the transport of CH_4 produced in forest soils (Barba *et al.,* 2019; Covey and Megonigal, 2019). The internal structure of tree stems facilitates the transport of soil CH_4 through both bark aerenchyma and xylem tissues (Yáñez-Espinosa and Ángeles, 2022; Vroom *et al.,* 2022; Bloemen *et al.,* 2013; Teskey *et al.,* 2008).

Tree-mediated emissions, therefore, represent a deviation from the standard CH_4 cycle in forest soils and can offset up to 46.5% of the soil CH_4 uptake (Machacova *et al.,* 2023). In fact, in the Amazon basin alone, approximately 21.2 ± 2.5 megatons (Mt) of CH_4 are emitted by trees annually, accounting for 10-13% of global wetland CH_4 emissions (Pangala *et al.,* 2017). On a broader scale, Covey and Megonigal (2019) reported CH_4 emission rates from tree stems ranging from -0.014 to 6.5 g m^{-2} d^{-1}. Regarding carbon dioxide, (CO_2), while forests significantly contribute to carbon dioxide (CO_2) sequestration, capturing about 11 gigatons (Gt) of CO_2 per year (Friedlingstein *et al.,* 2021), emissions from tree stems contribute to 5-38% of the total ecosystem respiration (Campioli *et al.,* 2016; Yang *et al.,* 2016). Though the contribution of CO_2 emissions from tree stems to the global CO_2 budget is relatively small, it remains relevant for studying tree physiology (Teskey *et al.,* 2017) throughout diurnal and/or seasonal cycles.

Measurement of GHG emissions from tree stems is therefore important, to constrain better our current estimates and to provide better inventories of GHG. Current methods for the determination of these emissions are mostly based on the use of chambers, temporarily fixed on tree stems in which the emitted gases are captured. Among several designs, semirigid chambers, as described by Siegenthaler *et al.,* (2016), are commonly used due to their ease of installation in the field. Regardless of the chamber design, chambers can be operated with continuous (dynamic) or discrete (static) sampling and measurement of the gas concentration. When a detector is used for dynamic measurement, it is usually connected to the chamber through a closed loop, and thus referred to as closed chambers.

In that case, fluxes are determined from the derivative of the gas concentration increase within the chamber. The same data processing strategy is generally used when discrete measurements are done.

Whatever the chamber design and the method used, flux measurements are challenging, mostly because they combine low flux magnitude, difficulties in hermetically coupling the chamber and the tree stems, and complex pneumatic behavior of the experimental setup, including the chamber and the pneumatic circuit connecting it to the gas analyzer. One of the challenges in flux measurements is to securely affix the chamber on tree stems avoiding leaks, i.e. gas exchange between the atmosphere and the internal volume of the chamber, that would bias the results. At least in some cases, the shape of tree stems or the natural bark roughness, which is highly variable among species, hinder hermetic sealing, and a common strategy is the use of different sealants (e.g., moldable cement, potting clays, non-caustic silicone, flexible putty adhesive, silicone rubber) to improve chamber's hermeticity (Bréchet *et al.,* 2021; Flanagan *et al.,* 2021; Jeffrey *et al.,* 2021; van Haren *et al.,* 2021). However, the use of sealants is not an absolute guarantee of sealing, at least in the case of very rough bark presenting deep channels, fractures, or irregular shapes. Moreover, even if the chamber is perfectly sealed, leaks might appear in the pneumatic circuit or within the detector, as exemplified by Wilkinson *et al.,* (2018). Leaks from different origins might therefore have a significant impact on the accuracy of emission measurements.

In addition to leaks, another potential challenge, is that during flux measurements an increase in concentration of the measured gases within the chamber is observed. This concentration buildup has the potential to reduce the gas partial pressure gradient between the tree stem and the atmosphere, which would otherwise be observed without a chamber. In turn, this phenomenon may result in underestimated fluxes, as suggested in aquatic ecosystems (Xiao *et al.,* 2016), soils (Juszczak, 2013; Kutzbach *et al.,* 2007; Welles *et al.,* 2001) and observed in trees (Bréchet *et al.,* 2021; Kohl *et al.,* 2021; van Haren *et al.,* 2021; Jeffrey *et al.,* 2020).

Lastly, while this has not been systematically studied, our interpretation is that, in dynamic chambers, the experimental setup forms a complex pneumatic circuit, which can also pose challenges in interpreting the measured concentration profile. Indeed, the gas within the chamber, exhibiting relatively good mixing, is pumped to the analyzer through tubing where plug-flow is observed. Subsequently, the gas passes through the sensor cavity of the

analyzer, with its own pneumatic behavior, before returning to the chamber, in the case of closed chambers. In consequence, during the starting period of the measurements, these phenomena can lead to delays, mixing effects, and potential concentration gradients, which hinder the interpretation of the gas concentration profiles observed. These effects have been previously identified and referred to as "dead band" by Siegenthaler *et al.,* (2016) and it is a common practice to discard data from the beginning of the measurements when continuous gas concentration is recorded (Fraser-McDonald *et al.,* 2022; Epron *et al.,* 2022; van Haren *et al.,* 2021; Pitz and Megonigal, 2017).

Overall, the impact of leaks and gas concentration buildup, along with the accurate interpretation of the pneumatic behavior in flux measurement setups, require a systematic and experimental analysis. This is the main objective of the present study. To achieve this goal, we established a mass balance of closed chambers and developed a method to quantify leaks and to analyze the effect of concentration buildup within the chamber headspace, with the hypothesis that by considering and quantifying leaks and analyzing the effect of concentration buildup, the accuracy of greenhouse gas (GHG) flux measurements from tree stems will be improved. The developed method was applied to six different tree species with distinct characteristics, from two contrasting ecosystems: a tropical flooded mangrove in Mexico and a subantarctic non-flooded forest in southern Chile. Through our findings, we quantified the potential errors associated with measuring GHG fluxes from tree stems and discussed various experimental procedures commonly documented in the literature.

2.2. MATERIALS AND METHODS

2.2.1. Chamber mass balance

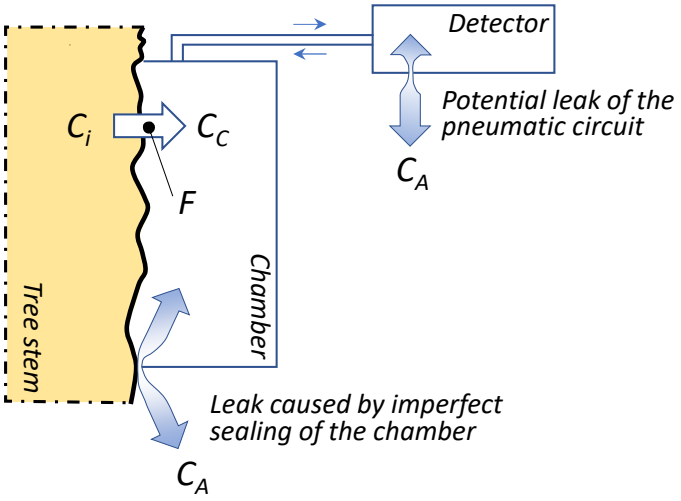

Figure 2.1. Conceptual scheme of the chamber mass balance. Where *F* is the flux from the tree stem, and C_C, C_A and C_i are the gas concentration within the chamber, the atmospheric gas concentration, and the tree internal gas concentration, respectively.

A detailed mass balance of the dynamic closed chamber and the corresponding equations are presented in Supplementary Material (Section S1.1). Briefly, the time derivative of the gas concentration within the chamber (C_C) can be summarized into fluxes from the tree stem and leaks between the atmosphere and the chamber headspace or the pneumatic circuit.

$$\frac{dC_C}{dt} = F \cdot \frac{A_C}{V_T} + k_L \cdot (C_A - C_C) \quad (1)$$

Where *F* is the observed flux; A_C is the chamber area in contact with the tree stem; V_T, is the total volume of the chamber, the detector and the pneumatic circuit; k_L is the leak constant (h^{-1}), which represents the frequency at which the gaseous content of the chamber and the pneumatic circuit is replaced by external air due to leakage; and C_A is the atmospheric gas concentration, observed during the measurements. It is worth noting that k_L is the ration between the leaks flow rate (Q_L) and V_T. Thus, leaks can be expressed, alternatively, by k_L, or by Q_L.

In Equation 1, F is the flux measured when the chamber is positioned on the tree stem. Thus, the surface of the bark is exposed to C_C, potentially different from the atmospheric concentration C_A. Hence, the actual flux (F^*), naturally occurring when the bark is exposed to C_A (no chamber) might be different from F. Since mass transfer is a lineal function of the concentration gradient, we can estimate that the measured flux is a function of the ration between the concentration gradient with and without a chamber:

$$F = F^* \cdot \frac{(C_i - C_C)}{(C_i - C_A)} \quad (2)$$

Where (C_i-C_C) and (C_i-C_A) are the concentration gradient observed during the chamber measurement and the gradient that would be otherwise observed in the absence of a chamber, respectively. Hereafter, Equation 2 will be referred to as "the concentration buildup effect", which bears similarity to equations commonly used in the study of aquatic ecosystems (Xiao et al., 2016) and wetlands (Juszczak, 2013; Kutzbach et al., 2007). Therefore, considering this concentration buildup effect, Equation 1 becomes:

$$\frac{dC_C}{dt} = F^* \cdot \frac{(C_i - C_C)}{(C_i - C_A)} \cdot \frac{A_C}{V_T} + k_L \cdot (C_A - C_C) \quad (3)$$

It is worth noting that, in an ideal case, at the onset of the measurement, just after chamber installation, C_C might be equal to C_A, and Equation 3 is greatly simplified, as follows:

$$\frac{dC_C}{dt} = F^* \cdot \frac{A_C}{V_T} \quad (4)$$

Equation 4 holds significant importance as it suggests that accurately measuring flux, free from the effects of leaks and concentration buildup, can be achieved by analyzing the initial slope of gas concentration within the chamber (Equation 4). However, in practice, measuring this initial slope, when C_C equals C_A, presents challenges for two primary reasons. Firstly, at the start of the measurement, there may be differences in gas concentration among the chamber, the pneumatic circuit, and the detector, leading to a transient period as the system

begins to operate. This is the main reason why it is a common practice to disregard data from the beginning of the measurements when calculating fluxes using continuous sampling (Pitz and Megonigal, 2017; Siegenthaler *et al.,* 2016). Secondly, during the installation of the chamber, gases may already accumulate within it or be influenced by the proximity of operators (often notable with CO_2 expelled by the operators), resulting in C_C being higher than C_A. Consequently, in real-case scenarios, even at the onset of the measurements, C_C often exceeds C_A and the observed concentration increase is influenced by multiple mechanisms beyond just the flux. Under these conditions, Equation 4 becomes inappropriate, and ideally, Equation 3 should be employed to accurately quantify the flux.

In Equation 3, if the time interval *dt* is sufficiently small, we can estimate the change in C_C over time ($C_{C,t}$), after the chamber has been installed and operated, by adding the rate of change (dC_C/dt) multiplied by the small-time interval (Δt) to the previous value of C_C ($C_{C,t-1}$). Mathematically, this approximation can be expressed as follows:

$$C_{C,t} = C_{C,t-1} + \left(F^* \cdot \frac{(C_i - C_{C,t-1})}{(C_i - C_A)} \cdot \frac{A_C}{V_T} + k_L \cdot \left(C_A - C_{C,t-1}\right) \right) \cdot \Delta t \qquad (5)$$

In Equation 5, the geometry of the chamber (A_C, V_T) is known, and C_A can be readily measured in the field. Therefore, if k_L is known, by calibrating Equation 5 to the experimental C_C time series, it becomes possible to determine F^* and C_i, effectively accounting for the effects of leaks and concentration buildup.

For the determination of k_L, we developed a method, that is described in detail in the Supplementary Material (Section S1.2). Briefly, the method involves inducing a transient state by injecting a pulse of CH_4 into the chamber, artificially creating a relatively high concentration of CH_4. Following this injection, any leakage would result in an asymptotic decrease in the CH_4 concentration, until the system reaches a new steady state. Assuming a well-mixed behavior of the gas phase within the chamber, this asymptotic decrease could be described by Equation 6, where $C_{C,0}$ and $C_{C,f}$ are the CH_4 chamber concentration at time zero (shortly after pulse injection) and after the chamber reaches steady state (details provided in Section S1.2).

$$C_{C,t} = C_{C,0} + (C_{C,0} - C_{C,f}) \cdot (1 - exp(-k_L \cdot t)) \quad (6)$$

By calibrating Equation 6 to the experimental C_C time series, it is possible to determine $C_{C,f}$ and k_L, with the latter being the parameter of primary interest. However, it is important to note that for this purpose, $C_{C,0}$ must be sufficiently high, typically a few hundreds of ppm, to ensure a subsequent decrease in $C_{C,t}$ over time. Furthermore, in the Supplementary Material, we demonstrate that while Equation 6 is correct, it does not fully capture the intricate pneumatic behavior observed in certain cases (Fig. S2). Although we have mathematically described this complex behavior, it falls outside the primary scope of the present study, which is centered around evaluating the impact of leaks on emissions. Therefore, we have included these findings in the Supplementary Material, Section S1, provided for those readers who are interested in exploring this aspect further.

2.2.2. Fluxes, leaks and C_i determination

In the present work, fluxes of CH_4 and CO_2 (F^*_{CH4}, and F^*_{CO2}, respectively), were determined according to the following 4-step protocol (materials being described in Section 2.3). Step 1, semi-rigid chambers were tidily fixed on the tree stem using 3 to 4 nylon straps. Step 2, the air content of the chamber where CH_4 or CO_2 potentially accumulated during chamber installation, was replaced by fresh ambient air over 2 minutes, with a portable external air pump (Flextailgear Tiny Pump, Mexico). Step 3, the chamber was immediately connected, in a closed loop, to a laser ultraportable greenhouse analyzer (i.e. UGGA, model 915-0011-1000, Los Gatos Research, ABB, USA). Step 4, the CH_4 and CO_2 concentration within the chamber was measured for 10-15 minutes. Step 5, k_L was determined from the injection of 1 mL of CH_4 into the chamber. Pulse injection and k_L determination was done after flux measurement, to avoid any potential effect of increasing artificially CH_4 concentration to much higher levels than standardly observed during flux determination. Specifically, k_L was determined from Equation 6 calibration (details provided in Section S1.2). Step 6, C_C dataset measured during step 4, was used to calibrate Equation 5, which was adjusted to the experimental data, using Ci and F^* as adjustment parameters, and where k_L was determined during step 5.

2.2.3. Experimental setup

Depending on the size of the tree, we used four different sizes of semi-rigid chambers (#1, 0.50 × 0.30; #2, 0.30 × 0.24; #3 0.24 × 0.18; #4, 0.15 × 0.10 m), all of them composed of a 0.7 mm thick impermeable polyethylene terephthalate (PET) plastic sheet glued along its entire perimeter to a 20 × 30 mm closed cell neoprene foam (Seals+Direct Ltd, Hamphshire, UK), as described in Siegenthaler *et al.,* (2016). The distance between the tree stem and the PET plastic sheet, which determined the chamber volume, was 20 mm. The chambers were connected in a closed loop to the UGGA, with two 6 mm external diameter (4 mm internal diameter) flexible polyurethane tubing (PUN-6X1-DUO-BS, Festo, Mexico). To reduce the volume of the pneumatic circuit and improve the recirculation rate between the chamber and the detector, the length of this tubing was as short as possible (about 2 m) in dry ecosystems, but of up to 12 m long in the mangrove ecosystem, to ensure that the detector was placed in a dry and safe place. It should be noted that, in contrast to the relatively heavy UGGA model used in the present work (16 kg plus batteries), the current trend is towards lightweight and backpack portable GHG detectors, making their deployment in close vicinity of the chamber easier. The volume of the semi-rigid chambers used is an important parameter, which is required for flux determination (Equation 3). Compared to rigid chamber, which have an approximately constant volume, the volume of semi-rigid chambers depends on the deformation of the chamber around the tree stem. The volume of the chambers was determined according to Siegenthaler *et al.,* (2016), and ranged 0.22−2.9 L. On the contrary to several previous reports, in the present work, the relatively low thickness of the chambers used impeded the use of an internal fan to homogenize the chamber headspace. However, the relatively small chamber volume and the UGGA flow rate (1.2 L min^{-1}) ensured a relatively good mixing of the chamber volume. In some experiments, the impact of moldable cements (Play-Doh, purchased in toy stores, México) was used as leak repressor. In each case, flux and leak measurements were done according to the standard method described above.

2.2.4. Sites description and campaigns

The method was applied to two contrasting forest ecosystems; a mangrove forest located in Celestun, in the Yucatan Peninsula (Mexico; 20.855, -90.374) and a sub-Antarctic forest

located in Puerto Williams, in the Navarino Island (Chile; -54.949, -67.660). Celestun is characterized by a hot and semi-arid climate with a marked rainfall season (Orellana *et al.,* 2010), an annual mean rainfall of 746.7 mm (mean monthly range from 8.2 to 144.0 mm) and an annual mean temperature of 26.4 °C (mean monthly range from 23.2 to 28.5 °C) (CONAGUA, 2023). In turn, Puerto Williams has a tundra and oceanic climate with an annual mean rainfall of 822 mm (mean monthly range from 51 to 131 mm) and an annual mean temperature of 6.1 °C (mean monthly range from -2.8 to 7.2 °C) (DMC, 2023; Aguirre *et al.,* 2020). In the mangrove ecosystem, we measured flux and leaks on the stem of the tree dominant species; “red mangrove” (Rm; *Rhizophora mangle*), “black mangrove” (Ag; *Avicennia germinans*), and “white mangrove” (Lr; *Laguncularia racemosa*). In Navarino Island, we also characterized the three dominant species; “low deciduous beech” (Na; *Nothofagus antarctica*), “high deciduous beech” (Np; *Nothofagus pumilio*), and “evergreen beech” (Nb; *Nothofagus betuloides*). It is worth mentioning that, in each ecosystem, the bark of the trees was drastically different among species (Fig. S3 and S4), offering a good model to evaluate the impact of leaks. For each species, nine to thirteen trees were selected with a range of diameter at breast height (DBH) from 3.8 to 56.6 cm. Then flux, leaks and bark roughness were determined in each tree at two stem heights, at 0.25 m and 1.4 m (up to 26 measurements by species). In the case of Rm, characterized by stilt roots, all measurements were made at 0.25 m above the last stilt root. According to the stem diameter, chambers #1 and #2 were used for larger diameters mostly at a tree height of 0.25 m, chambers #2 or #3 were used for medium diameters at both tree heights, and chambers #3 and #4 were used for smaller diameters (see Table S2 for further details). The diameter of the trees was measured using a sewing measuring tape (Singer 50003 ProSeries) which was calibrated with a caliper (Mitutoyo 530-101). As the objective of the present work was to quantify leaks and the effects of concentration buildup, rather than focusing on reporting emissions, we determined fluxes during the daytime only, typically from 10 am to 4 pm. The field campaign in México took place from September 6th to September 18th, 2021, while the Navarino campaign took place from February 20th to March 3rd, 2022. During these campaigns, the mean temperature was 30.5 ± 2.0 °C and 8.9 ± 3.1 °C for Celestun and Puerto Williams, respectively. While the mean wind speed was 1.2 ± 0.5 km h^{-1} and 6.8 ± 4.5 km h^{-1} for Celestun and Puerto Williams, respectively. Weather data were obtained from public data of nearby stations, namely, from the Celestun weather station (#31040; CONAGUA, 2023) located 2800 m west of the mangrove location, and from Puerto Williams airport station

(#550001; DMC, 2023), located 3200 m northeast from the forest where measurements were taken.

2.2.5. Bark roughness determination

In order to correlate leaks to bark roughness, which is on first approximation a governing parameter of leaks, we developed our own method, founded on our field experience. The method is based on a 0.2 m contour gauge (6″ Contour Gauge, General Tools & Instruments, Mexico) that was firmly pressed against the tree bark at the same height where chamber was placed. We defined bark roughness (*R*; Figure 2.2) as the relative difference between the length of the bark contour (*L′*) and its equivalent smooth length (L; Equation 7). In each case, *L′* was determined from a scaled photograph of the gauge taken in the field, and analyzed with ImageJ (Schneider *et al.,* 2012).

$$R = \frac{(\mathrm{L}' - \mathrm{L})}{L} \cdot 100 \quad (7)$$

Since the bark geometry of the tree stems differs along both axes, we distinguished axial and radial roughness, as follows. Axial roughness ($R_{A\%}$) was defined as illustrated in Figure 2.2A and Equation 8:

$$R_{A\%} = \frac{(\mathrm{L}'_A - \mathrm{L}_A)}{\mathrm{L}_A} \cdot 100 \quad (8)$$

In turn, radial roughness ($R_{R\%}$) was defined as the perimeter section of the bark contour (L'_R) and the section of a smooth circle of the same tree radius (L_R), as shown in Equation 9 and Figure 2.2B.

$$R_{R\%} = \frac{(\mathrm{L}'_R - \mathrm{L}_R)}{\mathrm{L}_R} \cdot 100 \quad (9)$$

In Equation 9, L_R can be determined, as follows, where angles are expressed in radians;

$$L_R = \frac{2\beta}{2\pi} \cdot 2\pi R = 2\beta R \quad (10)$$

$$Sin(\beta) = \frac{r}{\mathrm{R}}; \quad \beta = \arcsin\left(\frac{r}{\mathrm{R}}\right) \quad (11)$$

$$L_R = 2 \cdot R \cdot \arcsin\left(\frac{r}{\mathrm{R}}\right) \quad (12)$$

For each measurement, $R_{A\%}$ was taken from both lateral sides of the chamber and $R_{R\%}$ was taken from upper and lower sides of the chamber. For each position, a single mean bark roughness percentage ($R_{\%}$) was determined, using a weighted average (Equation 13), where H_C and W_C are the height and width of the chamber used.

$$R_{\%} = \frac{R_{A\%} \cdot H_C + R_{R\%} \cdot W_C}{H_C + W_C} \quad (13)$$

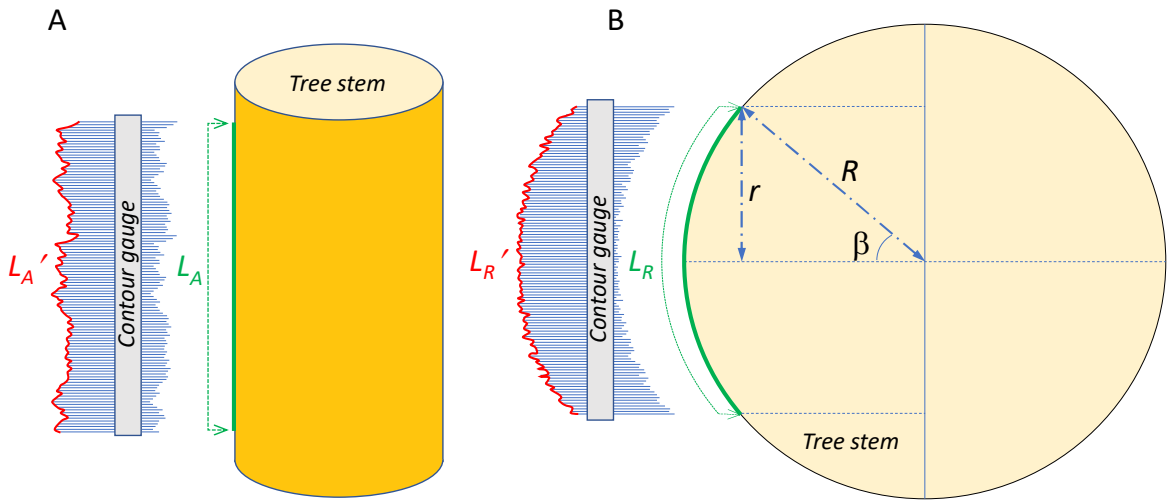

Figure 2.2. Conceptual scheme of bark roughness for both axial (A) and radial (B) determination in a longitudinal and cross sections, respectively.

2.2.6. Data treatment and statistics

Equations 5 and S8 were calibrated to experimental data using a Generalized Reduced Gradient (GRG) non-linear tool and minimizing the root-mean-square error (RMSE) between experimental data and models. Normality (Shapiro-Wilk) and homoscedasticity (Levene) were tested prior to statistical analysis. Then, two-way ANOVA were performed. Most variables had a positive skew, which were log-transformed to achieve normality. If normality was not achieved, then a Kruskal-Wallis test was applied instead. Statistical differences among tree species, chamber designs, and ecosystems, were determined according to Tukey's post-hoc tests. All statistical analysis were performed in R language version 2023.03.1.446 (Posit team, 2023) or with Origin(Pro) software (OriginLab Corporation, 2016). In the present work, results are usually presented in term of the median ± one standard deviation, unless specified. Boxplots in Section 3 and Supplementary Material display the first quartile (Q1), median (Q2), and third quartile (Q3) as boxes, with whiskers extending to the minimum and maximum values. Outliers are represented as individual data points beyond the whiskers.

2.3. RESULTS AND DISCUSSION

2.3.1. Leaks characterization

Fluxes and leaks were determined 153 times in different trees and under different configurations. Overall k_L ranged 0.00−284 h^{-1}, with a median of 1.25 ± 46.9 h^{-1}, which corresponded to leaks flow rates (Q_L) from 0.00 to 465 L h^{-1}, with a median of 1.25 ± 75.67 L h^{-1}. Thus, the chambers were far from being well sealed, and significant gas exchanges occurred between the chamber headspaces and the atmosphere. It is worth noting that the leak flow rates reported here are not exclusively caused by the chamber sealing, but include all components of the measurement setup, including the UGGA leak flow rate of 0.27 ± 0.05 L h^{-1}, reported in Section S1.3. Compared to the total leak flow rate, the UGGA's leak represented, on average, about 8.8% of the total leaks.

No significant difference of leaks was observed among tree species, except Na, which were significantly higher than those observed with Rm, Ag, Lr, and Np ($P < 0.05$; Fig. 2.3A). The

notable difference in leaks between Na and the other tested species was most certainly due to bark roughness, as $R_{\%}$ of Na (51.1 ± 16.8 %) was significantly higher than all other species ($P < 0.05$; Fig. S4). It is important to mention that there were no differences between the roughness measured at two stem heights within each species (Table S1). To further characterize possible correlations between bark roughness and leaks, $R_{\%}$ of the measured trees was compared to k_L. A positive exponential correlation was observed between $R_{\%}$ and k_L ($P < 0.05$: Fig. S5). On the contrary, no significant difference was observed among k_L measured in the same trees, but with different chambers (p=0.66), which is not surprising because k_L is a specific parameter, i.e. where Q_L is proportional to V_T, (Fig. S6).

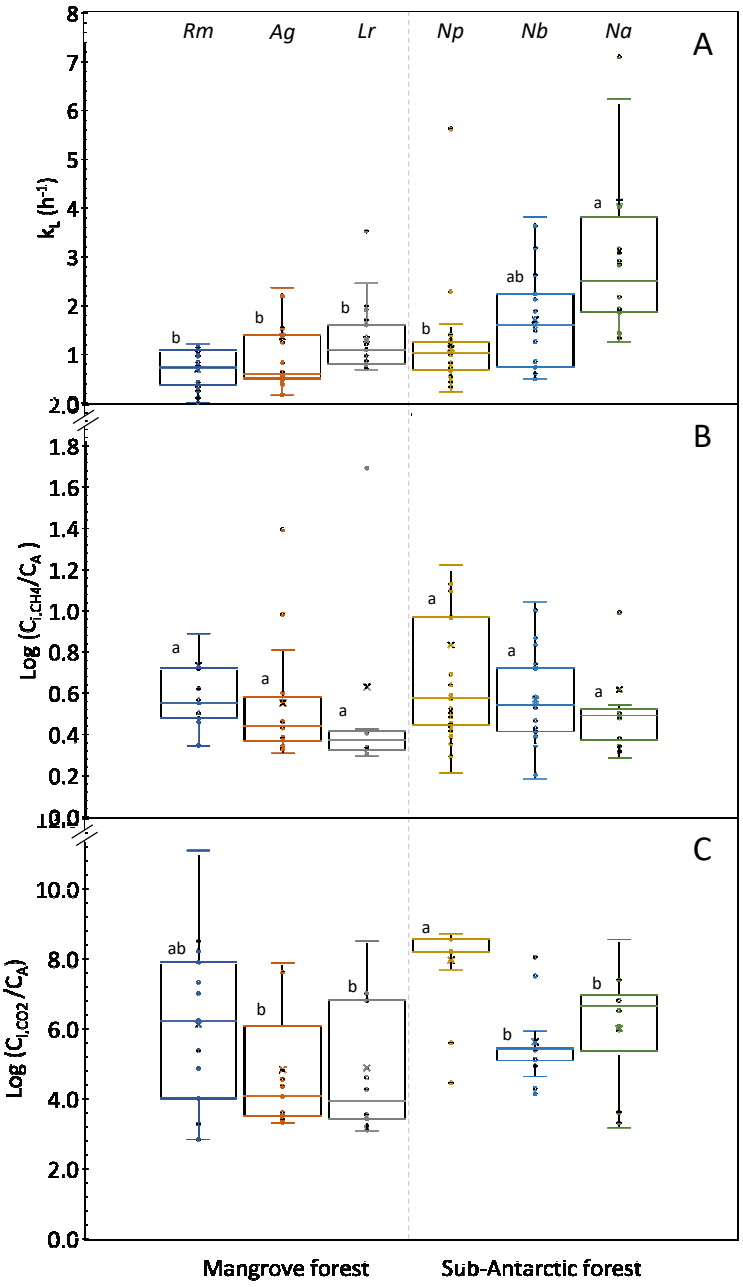

Figure 2.3. Leaks, expressed as k_L, among the different tree species (A); ratio between C_i and C_A, for CH_4 (B) and CO_2 (C).

Leaks between the chamber and the atmosphere might be dependent on the weather conditions, and particularly on the wind speed, which might alter the gas exchange between the chamber and the atmosphere, leading to flux measurement errors or artifacts (Jiang *et al.,* 2023; Maier *et al.,* 2019; Bain *et al.,* 2005). To check for the latter, in another set of experiments, 6 replicates of k_L, were determined over two hours, in two trees; one presenting

a moderate roughness (Np; $R_{\%}$ = 4.10) and one presenting a high roughness (Na; $R_{\%}$ = 88.58). This test was done on a day with variable winds, i.e., 18.7 ± 6.0 km h^{-1} with gusts at 39 km h^{-1}. In the case of Np, the mean k_L was equal to 0.86 ± 0.02 h^{-1}, with a coefficient of variation of 2.0%, which suggest that the variable wind had little effects on leak determination. This was confirmed by a generally good adjustment of the leak model (Equation S8) to the experimental data, with a mean R^2 of 0.999 ± 0.001. On the contrary, in the case of Na, the mean k_L was 16.8 ± 6.2 h^{-1} (coefficient of variation of 37%), and with a poorer model fitting (R^2 of 0.951 ± 0.109). Therefore, the wind conditions had a major impact on leak detection in the tree with high roughness, and it would be advisable, in these cases, to determine fluxes during stable and moderate wind conditions or to use cement to reduce k_L.

2.3.2. Impact of moldable cement

The most common strategy to avoid or reduce leaks is using cement. To evaluate the impact of cement, another set of measurements was done with and without moldable cement on trees where significant leaks were previously detected. Overall, the use of cement reduced the leak flow rates by 46−98%, with a mean of 92 ± 20% (n=20), which corresponded to a reduction of k_L by 92 ± 27%. Thus, leaks were not completely avoided by cement, but they were reduced to a large extent (data not shown).

2.3.3. Fluxes and C_i determination

As expected from Equation 5, an asymptotic trend of C_C was almost systematically observed, more clearly marked for $C_{C,CH4}$ than for $C_{C,CO2}$, as exemplified on Figure 2.4. Notably, at the onset of the measurements, and despite the chamber ventilation performed to allow for equilibration of the experimental setup, an instability that lasted 2-3 minutes was standardly observed (Fig. 2.4). Therefore, calibration of Equation 5 was done discarding this initial period. Overall, F^*_{CH4} ranged 0−2.05 mg m^{-2} h^{-1} with a mean of 0.17 ± 0.29 mg m^{-2} h^{-1}. These emissions are in accordance with the literature, i.e. -0.06 to 271.68 mg m^{-2} h^{-1} (Covey and Megonigal, 2019), with an estimated mean from these reported values of 22.16 ± 53.40 mg m^{-2} h^{-1}. Regarding CO_2, F^*_{CO2} ranged 32−2851 mg m^{-2} h^{-1} with a mean of 358 ± 378 mg m^{-2} h^{-1}. This range of F_{CO2} range is also in accordance with the literature, i.e. 0.33 to 406.05 mg m^{-2} h^{-1} (Salomón *et al.,* 2017; Campioli *et al.,* 2016; Yang *et al.,* 2016), with an estimated

mean from these reported values of 112.55 ± 100.38 mg m^{-2} h^{-1}. In the case of mangrove trees, the mean stem CH_4 flux was 0.10 ± 0.17 mg m^{-2} h^{-1}, which is slightly greater than the mean stem CH_4 flux of 0.04 ± 0.05 mg m^{-2} h^{-1} previously reported for mangroves of the same genera (Dušek *et al.,* 2021; Gao *et al.,* 2021; He *et al.,* 2019; Jeffrey *et al.,* 2019; Zhang *et al.,* 2019). Concerning the *Nothofagus* species measured on Navarino Island, the mean stem CH_4 flux was 0.06 ± 0.15 mg m^{-2} h^{-1}, with no previous reports yet.

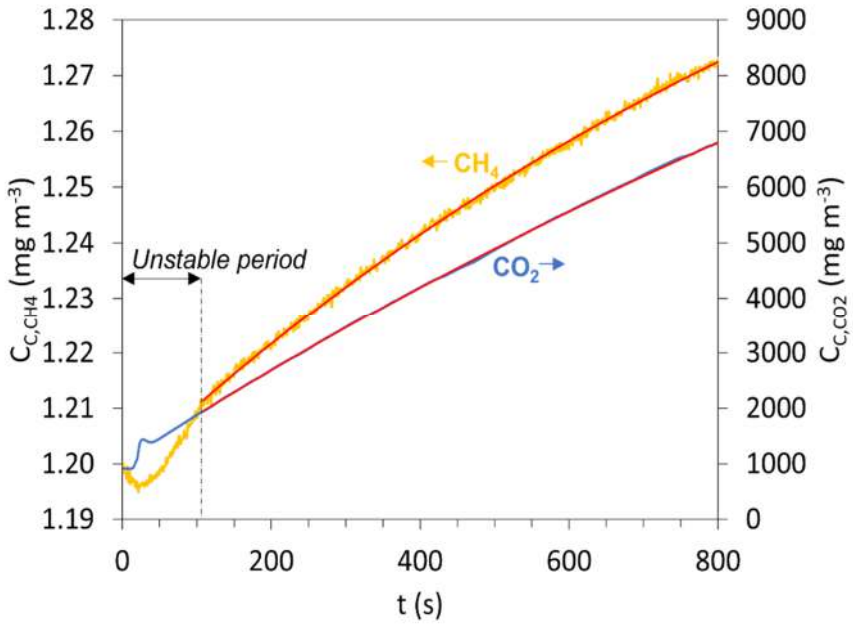

Figure 2.4. Example of C_C measurement and model fitting (Eq. 5; red continuous lines).

By model calibration, we observed that $C_{i,CH4}$ was varying largely and was relatively close to the atmospheric concentration. To reflect the latter more evidently, we expressed the closeness of C_i to C_A by the ratio between them. The $C_{i,CH4}/C_{A,CH4}$ ratio was 3.2 ± 11.5 (median ± one standard deviation; Fig. 2.3B). The latter indicate that the CH_4 fluxes measured were highly sensitive to the concentration buildup phenomenon, and that this observed behavior was shared by the six tested tree species, with no significant difference (Fig. 2.3B). The same approach with CO_2 provided a very distinct behavior, with a median $C_{i,CO2}/C_{A,CO2}$ ration of 337×10^3 ± 19×10^3 (Fig. 2.3C), suggesting that, in most cases, no significant effect of CO_2 concentration buildup within the chamber was observed. Although Np was characterized by a $C_{i,CO2}$ significantly higher than those of the other tree species, all

species exhibited a $C_{i,CO2}/C_{A,CO2}$ several order of magnitude above $C_{i,CH4}/C_{A,CH4}$ (Fig. 2.3B and 3C).

To further visualize the segregated impact of leaks and concentration buildup during flux measurements, Figure 2.5 shows the CH_4 and CO_2 concentration profiles in a chamber, established numerically, from the mean results obtained in the present work, i.e. median A_C, V_T, F^*, k_L and C_i. It can be observed that, compared to the linear increase of C_C expected in an ideal system, the presence of leaks and the effects of concentration buildup, whether separately or combined, resulted in a similar curvature in the C_C trends. However, the contribution of both effects is drastically different among CH_4 and CO_2 trends. In the case of CH_4, most of the curvature effect is caused by the concentration buildup, while in the case of CO_2, the effect of C_i appears insignificant. Overall, 76% of the deviation from linear $C_{C,CH4}$ increase was explained by the effect of concentration buildup, and 24% was explained by leaks. The same exercise for CO_2, indicated that 3% of the deviation to the linear $C_{C,CO2}$ increase was explained by the effect of concentration buildup, and 97% was explained by leaks (k_L). Therefore, the relative weight of both mechanisms is drastically different among gases.

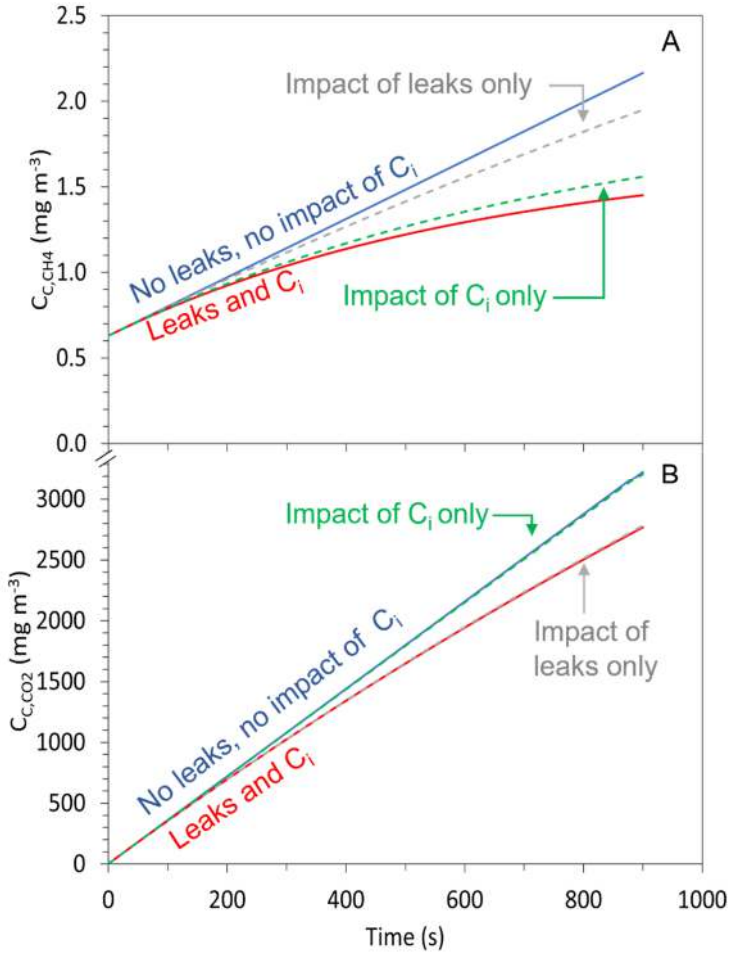

Figure 2.5. Theoretical profiles of $C_{C,CH4}$ (A) and $C_{C,CO2}$ (B) that are expected during chamber deployment, from median A_C, V_T, F^*, k_L and C_i, without considering leaks and the effect of C_i (ideal and linear profile), considering the effect of leaks only (median k_L), considering only the concentration buildup (median C_i), and considering both median k_L and C_i.

2.3.4. Errors in F determination

At the beginning of the measurements, when the chamber has been properly ventilated with atmospheric air and if C_C is equal to C_A, the initial slope of C_C accurately reflects the actual flux, independent of k_L and C_i. Therefore, one common error in determining F would be to assume that the initial linear slope is correct, because independent of leaks and concentration buildup effects. This would be an error, because disregarding potential gas accumulation during chamber installation or any other influences in the early stages of measurement. To estimate this potential error, we conducted a numerical analysis to determine the range of errors in flux determination, considering a delay between the start of

chamber operation (t = 0, C_C equals C_A) and the actual acquisition of C_C data. In this exercise, we focused exclusively on the effect of gas accumulation resulting from tree emissions during chamber deployment, as other potential effects are stochastic and challenging to quantify. Based on the mean, second, and third quartiles of k_L, F^*, and C_i complete dataset, we compared the slope of C_C observed after a delay time with the theoretical slope at time zero (Equation 3). Figure 2.6A shows that even a short delay of three minutes can result in an underestimation ranging 7−37% in F_{CH4} determination and 5−15% in F_{CO2} determination.

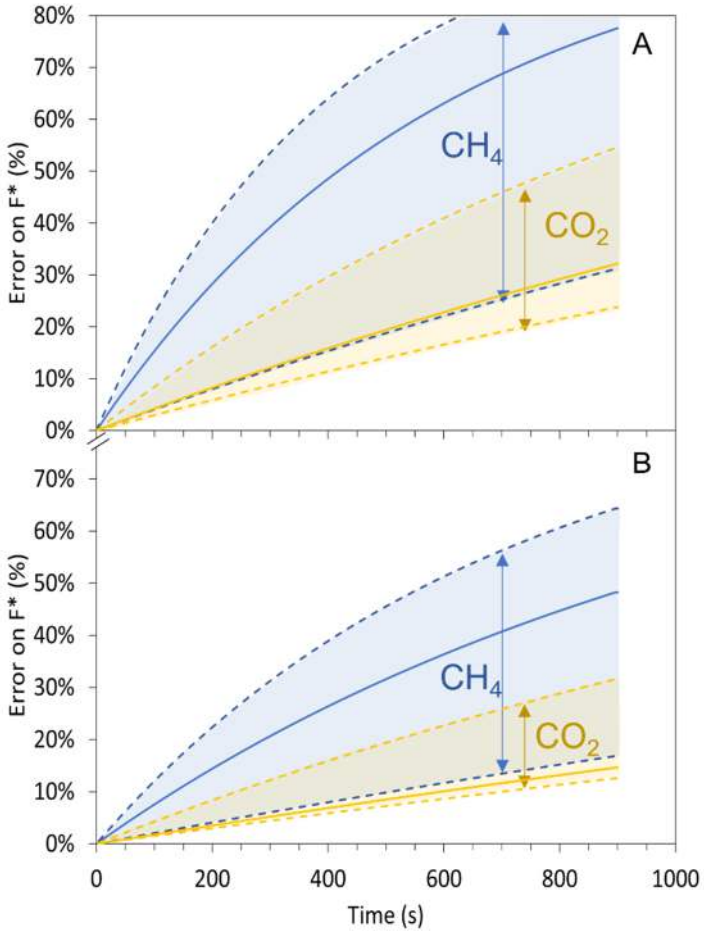

Figure 2.6. Range of error theoretically committed when discarding delay in starting measurements of C_C (A) and as a function of the duration of the measurements (B), for CH_4 (light blue area) and for CO_2 (light yellow area). Continuous lines show the error considering the median k_L, F^*, and C_i data observed in the present work, while dashed lines shows the limit between the second and third quartile of these parameters.

A second, more obvious error in determining F^* would be to neglect the effects of leaks and concentration buildup and to assume that the slope between the initial C_C value and C_C at any time adequately reflects the flux. This error would occur when using a discrete sampling strategy or employing linear regression for dynamic C_C measurements. To assess the magnitude of this error, in this case too, we calculated the error range using the second and third quartiles of our complete dataset of k_L, F^*, and C_i. The results (Fig. 2.6B) are that, for instance, a short 3-minutes measurement would result in an underestimation ranging from 4−20% for F_{CH4} and from 3−8% for F_{CO2} determination. It is important to note that the error presented in Figure 2.6B does not account for the delay-induced error shown in Figure 2.6A, which further emphasizes the magnitude of errors, when combined. Moreover, Figure 2.6B highlights that the errors resulting from discrete measurements over extended durations reach magnitudes that potentially exceed an acceptable threshold. For instance, a 15-minute measurement may result in a range of underestimation from 17% to 64% for F^*_{CH4}, not to mention the potential errors when there are several hours between measurements, as sometimes reported.

To estimate the experimental error, combining the errors caused by delay and experimental duration, we determined fluxes in each C_C profile measured in the present work, discarding effects of leaks and concentration buildup, and considering in each case only the first three minutes of measurement, after the initial instable period. Under these conditions, the error committed on F^*_{CH4} was an underestimation by 1.3−92% with a median of 40 ± 20%, and an underestimation by 0−91% with a median of 22 ± 22%, regarding F^*_{CO2}, similar to the 33% underestimation in CH_4 fluxes from soils found by Pihlatie *et al.,* (2013) in static chambers.

2.3.5. Practical Considerations

The chamber model and the results obtained indicate that leaks and concentration buildup during flux measurements have an important impact on the estimation of greenhouse gas (GHG) emissions from tree stems. Leaks are difficult to eradicate, even when using moldable cement, and the effects of concentration gradients are highly variable among gases. Based on this analysis, it is advisable to consider both phenomena. However, this implies determining k_L and C_i, which would require relatively long and tedious fieldwork. However, the determination of leaks and C_i, as performed in the present study for

explanatory purposes, is not mandatory. Data can be corrected using a simple analytical solution previously suggested (see below), although it is not commonly employed.

During the deployment of the chamber, it is observed that the concentration of C_C follows an asymptotic curve from an initial value $C_{C,1}$ to a final value $C_{C,2}$, as the chamber reaches a steady-state condition and C_C becomes independent of time, as discussed by Welles et al., (2001) for soil CO_2 fluxes. This concentration trend can be described by a standard exponential equation that has been previously described by several authors (Pihlatie et al., 2013; Pedersen et al., 2010; Hutchinson and Mosier, 1981), similar to Equation 6 (Equation 14; specific details provided in Section S1.4).

$$C_{C,t} = C_{C,2} - (C_{C,2} - C_{C,1}) \cdot \exp(-k_t \cdot t) \quad (14)$$

Where k_t is a kinetic constant which include all kinetic parameters of flux and leaks. Equation 14 is numerically equivalent to Equation 6, and can be used instead, without requiring the determination of k_L and C_i. Equation 14 can be easily calibrated using any experimental C_C segment of the measurement series, using $C_{C,2}$ and kt as adjustment parameters. After determining these parameters, F^* can be numerically determined, assuming $C_C = C_A$, as follows:

$$F^* = \left(\frac{dC_C}{dt}\right)_{t=0} \cdot \frac{V_T}{A_C} = k_t \cdot (C_{C,2} - C_A) \cdot \frac{V_T}{A_C} \quad (15)$$

Equation 15, can be used in all cases, in substitution to Equation 5, without requiring the identification of k_L and C_i.

Regarding the implications of our findings on the methods used for the determination of GHG emissions from tree stems, the dynamic closed chamber, i.e., continuous measurement of C_C in a closed chamber, is certainly the best method, as it would allow calibration of Equation 14 with a large dataset. Discrete sampling in a closed chamber (static

chamber method) could also be applied using this approach, but only if several samples are taken, to allow for Equation 14 calibration.

In all cases, it is highly advisable to proceed to a good ventilation of the chamber prior to any measurement (Hutchinson and Livingston, 2001), in order to reach initial condition where C_C is as close as possible to C_A. The results obtained in the present work and the experimental strategy suggested indicate that the use of cement is not a requirement, although it would certainly provide better data quality in trees with severe roughness, i.e., reducing experimental noise. It is also advisable, in order to reduce noise at the onset of measurements, to use a pneumatic circuit as short as possible by placing the detector as close as possible to the chamber and to consider detectors with an internal pump flow rate as high as possible or even to consider an additional external recirculation pump. These recommendations are favorable to a short gas residence time within the pneumatic circuit, thus allowing a rapid equilibration between the chamber and the detector, producing better data quality at the onset of the measurement.

2.4. CONCLUSION

The effects of leaks and of concentration buildup severely impair flux measurements from tree stems and must be considered. After conducting a comprehensive literature review on CH_4 fluxes from tree stems over the past decade (69 items, Table S3), we observed that linear adjustment was consistently used in 75% of the reports, while the choice of asymptotic-like data adjustment for flux calculation was only utilized in approximately 9% of the cases. Consequently, the use of asymptotic fitting is not a common practice and remains limited, despite its ability to effectively handle data with or without significant curvature. Additionally, among the reports that employed linear adjustment, 42% were based on discrete sampling methods, which complicates the accurate determination of potential data curvature over time caused by leaks and/or concentration buildup. By separately analyzing the impacts of leaks and concentration buildup, our study underscores the importance of both factors in accurately measuring CH_4 fluxes, and leaks having a dominant effect on CO_2 flux determination. Overall, this study serves as a reminder of the key findings highlighted in previous reports: the precise assessment of greenhouse gas emissions from tree stems necessitates the consideration of both leaks and concentration buildup, with the utilization of asymptotic data adjustment methods. These results, combined with the literature review, also suggest that our current estimates of GHG flux from tree stems are currently underestimated.

CAPÍTULO III.

PNEUMATOPHORE CO_2 EFFLUXES DECREASE WITH INCREASED SALINITY IN MANGROVE FORESTS OF YUCATAN, MEXICO

Este capítulo fue publicado en la revista científica Scientific Reports y debe ser citado y referido de la siguiente manera:

Salas-Rabaza JA, Yáñez-Espinosa L, Cejudo E, Cerón-Aguilera SG, Us-Santamaría R and Andrade JL. 2024. Pneumatophores CO_2 effluxes decrease with increased salinity in mangrove forests of Yucatan, Mexico. Sci Rep 14: 18449. https://doi.org/10.1038/s41598-024-68822-9

RESUMEN

Si bien, los bosques de manglar son grandes sumideros de carbono, también liberan dióxido de carbono (CO_2) a través de los suelos, las plantas y el agua, debido a diferentes procesos como la respiración. La mayoría de los estudios se han centrado en los flujos de CO_2 provenientes del suelo; dejando de lado el papel que tienen ciertas estructuras biogénicas como los neumatóforos sobre estos flujos. Por tanto, los flujos de CO_2 de neumatóforos fueron cuantificados en las interfaces sedimento–aire y agua–aire a lo largo de un gradiente de salinidad considerando tres tipos de manglar (de franja, chaparro y cuenca) dominados por *Avicennia germinans*, durante la estación lluviosa y de sequía en Yucatán, México. La abundancia de neumatóforos explicó hasta el 91% de los flujos de CO_2 en el manglar chaparro, el 87% para el manglar de franja y el 83% para el manglar de cuenca en la interfaz agua–aire. Hubo una correlación inversa entre los flujos de CO_2 con la temperatura y la salinidad. Los mayores flujos de CO_2 ocurrieron en el manglar de franja y las menores tasas en el manglar chaparro. La inundación redujo las emisiones de CO_2 de la estación de sequía a la lluviosa en todos los tipos de bosque. Estos resultados destacan la contribución de los neumatóforos a la respiración de los manglares, y la necesidad de incluirlos en nuestros balances y modelos de carbono actuales, enfatizando en la inclusión de diferentes interfaces de intercambio de materia, estaciones del año y tipos de manglar.

ABSTRACT

Although mangrove forests are great carbon sinks, they also release carbon dioxide (CO_2) from soil, plants, and water through respiration. Many studies have focused on CO_2 effluxes only from soils, but the role of biogenic structures such as pneumatophore roots has been poorly studied. Hence, CO_2 effluxes from pneumatophores were quantified at sediment-air (non-flooded sediment) and water-air (flooded sediment) interfaces along a salinity gradient in three mangrove types (fringe, scrub, and basin) dominated by *Avicennia germinans* during the dry and rainy seasons in Yucatan, Mexico. Pneumatophore abundance explained up to 91% of CO_2 effluxes for scrub, 87% for fringe, and 83% for basin mangrove forests at the water-air interface. Overall, CO_2 effluxes were inversely correlated with temperature and salinity. The highest CO_2 effluxes were in the fringe and the lowest were in the scrub mangrove forests. Flooding decreased CO2 effluxes from the dry to the rainy season in all mangrove forests. These results highlight the contribution of pneumatophores to mangrove respiration, and the need to include them in our current carbon budgets and models, but considering different exchange interfaces, seasons, and mangrove ecotypes.

Keywords: *Avicennia germinans*, Carbon dioxide, Interface, Respiration, Roots

3.1. INTRODUCTION

Mangrove forests are highly productive ecosystems with a great potential as a blue carbon reservoir, particularly in the soil (Donato *et al.,* 2011; Bouilon *et al.,* 2008). This is a reason why these forests have been recognized as nature-based allies in climate change mitigation (Friess et al., 2022; Leal et al., 2022). In soils, roots and microorganisms' respiration contributes to the main carbon output, as carbon dioxide (CO_2) efflux of forest ecosystems (Leon *et al.,* 2014; Lopes de Gerenyu *et al.,* 2011).

Plants, through respiration, utilize stored energy for growing and completing their lifecycle. Therefore, assessing plant respiration can deepen understanding of mangrove tree physiology and their contribution to the ecosystem carbon budget. In mangrove soils, several factors influencing CO_2 effluxes have been documented, such as temperature, salinity, and flooding (Akhand *et al.,* 2019; Chen *et al.,* 2012; Poungparn *et al.,* 2009; Lovelock, 2008). However, many studies have focused on the quantification of soil CO_2 fluxes only and a few have considered biogenic structures such as pneumatophores (root snorkels) and crab burrows, which could potentially increase CO_2 (Nie *et al.,* 2023; Kristensen *et al.,* 2022; Troxler *et al.,* 2015; Penha-Lopes *et al.,* 2010; Kristensen *et al.,* 2008) and methane emissions (Zhang *et al.,* 2022; Sheng *et al.,* 2021; Lin *et al.,* 2021; Krithika *et al.,* 2008; Purjava *et al.,* 2004). Pneumatophores have an internal pathway for gas flow, or aerenchyma (Yánez-Espinosa, L. and Ángeles, 2022; Purnobasuki *et al.,* 2017; Purnobasuki and Suzuki, 2005), through which soil-produced gases can be emitted. Because of the presence of photosynthetic tissues and microalgae, they can carry out photosynthesis (Kitaya *et al.,* 2002; Aiga *et al.,* 1995), which can lead to an additional source of oxygen for the anoxic soils. Pneumatophores represent a very important component of the carbon budget in mangrove forests and their contribution to greenhouse gases emissions has already been reported (Nie *et al.,* 2023; Lin *et al.,* 2021; Lin *et al.,* 2020; Purjava *et al.,* 2004).

Although mangrove forests are flooded at different times depending on regional seasonality and tidal regimes, CO_2 efflux at the water-air interface has been estimated in some cases (Jacotot *et al.,* 2018; Troxler *et al.,* 2015), indicating that CO_2 effluxes are no negligible especially during receding tides. Studies on these below-canopy CO_2 emissions should also consider the different mangrove ecological types, which vary in their structure, composition, and carbon storage capacity. Also, because salinity and hydroperiod are the main drivers of mangrove zonation (Herrera-Silveira *et al.,* 2020; Adame *et al.,* 2014; Zaldívar-Jiménez *et al.,* 2010; Lugo and Snedaker, 1974), high salinities and long inundation decrease organic matter decomposition,

which can ultimately be reduced by root respiration. In this study, we proposed quantifying CO_2 fluxes from soils and waters, with pneumatophores, along a salinity gradient in three different mangrove ecotypes (fringe, scrub, and basin) dominated by the black mangrove *Avicennia germinans* (L.) L. in the Yucatan Peninsula (Fig. 3.1), a region that has 60% of the total mangrove area in Mexico (Velázquez-Salazar *et al.,* 2021) and represents about 62% of all mangrove carbon stored in this country (Herrera-Silveira *et al.,* 2020). We hypothesized that CO_2 efflux magnitudes would be greater at high pneumatophore abundance because of the increased amount of living tissue that carry out respiration and of the aerenchyma that mobilize the gases produced in soils. Also, effluxes would be higher at the sediment-air than at the water-air interface exchange, because in the former, aerobic microorganism respiration is also contained and, in the latter, the water column exerts a physical barrier for gas diffusion from the sediment. Similarly, due to the sensitivity of CO_2 efflux to temperature and salinity (Lambers and Oliveira, 2019; Luo and Zhou, 2006), these CO_2 effluxes would be expected to increase at higher temperatures and lower salinities.

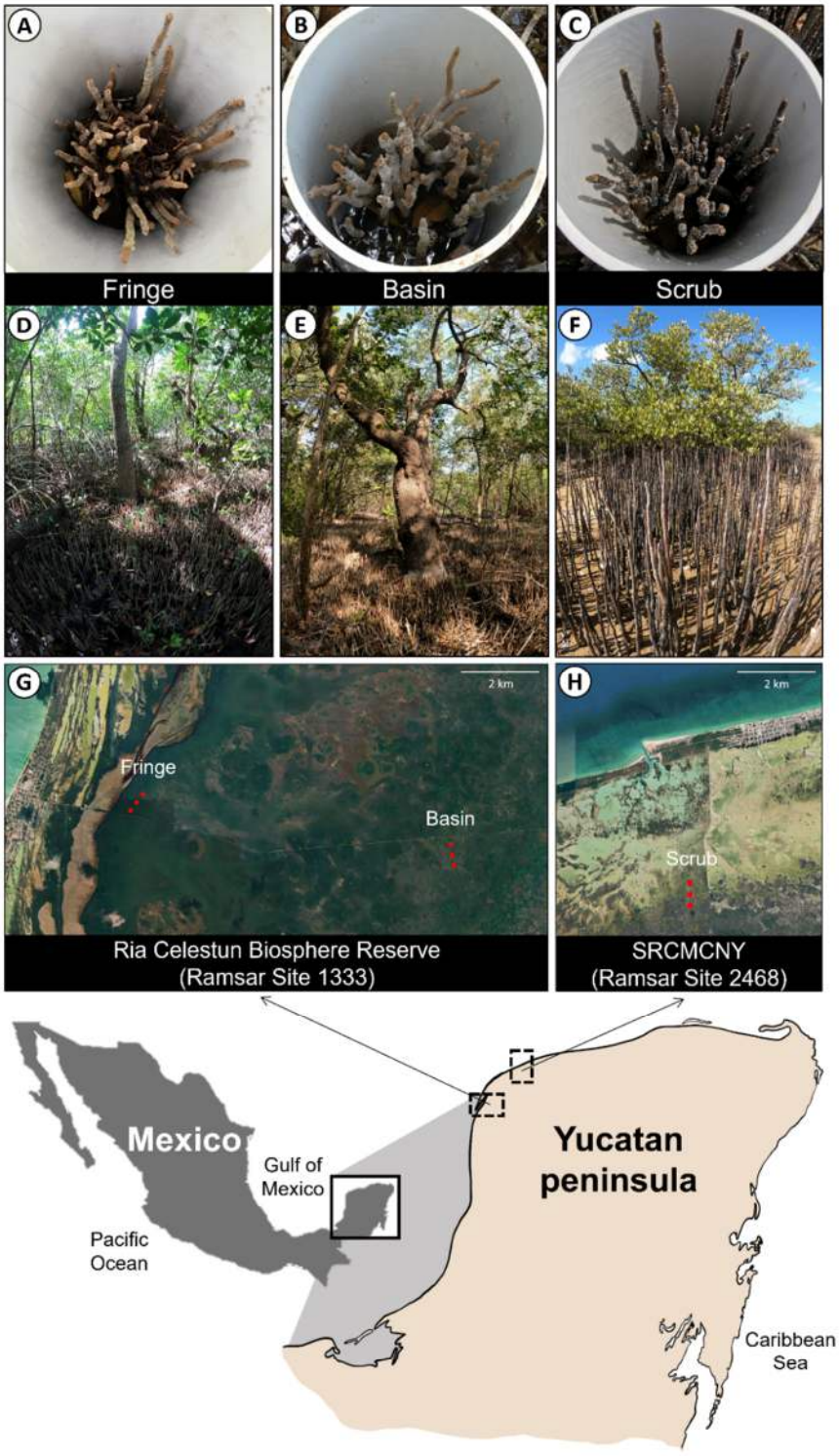

Figure 3.1. Location of the study sites in Yucatan. PVC tubes with pneumatophores where CO_2 efflux measurements were carried out (A-C), Mangrove ecotypes (D-F), and location of the mangrove ecotypes within the Ramsar sites (G-H). SRCMCNY = State Reserve Ciénagas y Manglares de la Costa Norte de Yucatán. Satellite images were obtained from Google Earth Pro 7.3 (https://earth.google.com) and maps were generated using Procreate Raster Graphics Program 5.3.9 (Savage Interactive Pty Ltd., https://procreate.com/procreate).

3.2. MATERIALS AND METHODS

3.2.1. Study sites and field measurements

Three mangrove ecotypes, dominated by Avicennia germinans (L.) L. were chosen in the northwestern coast of Yucatan: fringe and basin mangroves in the Ria Celestun Biosphere Reserve (20° 51' 27.4" N, - 90°22'33.9"W; 20° 51' 03.6" N, -90° 17' 42.5" W, respectively; Ramsar Site 1333; Fig. 3.1) and scrub mangrove in the State Reserve Cienagas y Manglares de la Costa Norte de Yucatán (21°13' 17.7" N, -89° 49' 49.4" W; Ramsar Site 2468; Fig. 3.1). Field measurements were made in May 2021 and in September 2021 for the dry and rainy seasons, respectively. Sediment-air and/or water-air interfaces were considered depending on the inundation state of each mangrove ecotype on the day of measurements. When possible, both interfaces were measured. Sediment-air interface was measured for all mangrove ecotypes during the dry season and only for scrub mangrove forest during the rainy season. The water-air interface was evaluated for all mangrove ecotypes during the rainy season, and for basin and scrub mangroves during the dry season.

3.2.2. Physicochemical measurements

Air temperature and relative humidity were recorded with a 12-bit Temp/RH Smart Sensor (S-THB-M002, Onset Computer Corporation, Bourne, MA) every 10 s and 10-min averages were stored with a data acquisition system (HOBO U30-NRC Weather Station, Onset) at each mangrove ecotype during the fieldwork in both seasons. Porewater samples were taken at 30 cm soil depth adjacent to each CO_2 efflux tube, then porewater salinity was measured. When sediment was flooded, surface water salinity, surface water temperature and flooding level were taken. Both porewater and surface water parameters were obtained with a portable conductivity meter (YSI, Model Pro2030, Yellow Springs, OH). Porewater salinity was measured in all cases for both sediment-air and water-air CO_2 efflux measurements. Sediment temperature (Type “T” Omega Soil Temperature Probe, Omega Engineering Inc., Stamford, CT) and volumetric water content (Theta Probe ML2x, The Macaulay Land Use Research Institute and Delta T Devices, Cambridge, UK) were recorded at 0.1 m depth of the sediment next to each PVC tube at the same time as CO_2 efflux was being measured for non-flooded conditions, while surface water temperature was measured for flooded conditions. During the dry season, we also measured pneumatophore temperature (Table 3.1).

3.2.3. Pneumatophores characterization

At each mangrove ecotype and season, 32-37 plots (0.5 m^2 each; divided in 4 subplots) were randomly chosen for pneumatophores counting to estimate the mean pneumatophore abundance per unit area (pneu m^{-2}; Table 3.1). Within each plot a polyvinyl chloride (PVC) tube (0.2 m diameter, and 0.30 ± 0.08 m height) was inserted 0.03 m into the sediment. PVC tubes were placed at each site before CO_2 efflux measurements were taken. To represent different pneumatophore abundances, PVC tubes were placed enclosing from 3 to 72 pneumatophores each, which cover pneumatophore abundances ranging from 95 to 2292 pneu m^{-2} (Fig. 3.3). Additionally, distance from the PVC tube to the nearest tree was also taken. After CO_2 efflux measurements, five pneumatophores per PVC tube were characterized in the field measuring total height, basal diameter, top diameter, and distance between the top diameter and apex of the pneumatophores. Three pneumatophores per PVC tube were taken to the laboratory to obtain pneumatophore dried biomass (g). Then, pneumatophore basal area (cm^2), lateral area (cm^2), total volume (cm^3), and density (g cm^{-3}) were calculated.

3.2.4. CO_2 efflux measurements

CO_2 efflux rates from pneumatophores or sediment-air and water-air were quantified using a dynamic-closed chamber system (0.2 m in diameter: 8200-103 Smart Chamber, LI-COR Biosciences; Lincoln, NE) connected to an infrared gas analyzer (LI-8100A, LI-COR). For each sampling point, chambers were placed on PVC tubes previously installed (one week before), then CO_2 efflux was recorded for 7 minutes. At each season, CO_2 efflux measurements were made from 8:30 h to 12:30 h. The CO_2 efflux data were first analyzed using the SoilFlux Pro-4.2.1 software (LI-COR Biosciences) to recognize possible leaks or disturbances inside the chamber during measurements. Then, effluxes were re-computerized using asymptotic fits, previously employed for soils, plants and waters to reduce underestimations (Salas-Rabaza *et al.,* 2023; Pihlatie *et al.,* 2013; Pedersen *et al.,* 2010). Only fits with a $R^2 \geq 0.95$ were chosen (n = 171).

3.2.5. Data analysis and representation

Normality (Shapiro-Wilk) and homoscedasticity (Levene) were tested for all data prior parametric analysis. Then, simple regressions were run to elucidate the relationship between pneumatophores abundance and CO_2 effluxes by mangrove ecotype, season, interface, and its interactions (Fig. 3.3; see Supplementary Table S1). Kruskal-Wallis (or one-way ANOVA on ranks) analyses were performed to find differences among mangrove ecotypes within each

interface or season, then reported as H-values (Table 3.1; Fig. 3.2; Fig. 3.7). Also, Mann-Whitney-Wilcoxon were performed to test two groups' differences for ecotype or season, then reported as W-values (Fig. 3.7). For pairwise multiple comparisons either Dunn's or Tukey's procedures with or without Bonferroni or Holm adjustments were used. Figures 3.1-3.2 and Tables 3.1-S1 were analyzed from raw field data (n=171). A multi-comparison matrix using Spearman's correlation was performed to elucidate the role of biophysical variables. To account for the contribution of physicochemical and biological variables to the CO_2 efflux and the differentiation of mangrove ecotypes, a Canonical Correspondence Analysis (CCA) was used. Models from Table S1 and Figure 3.3 were applied to the pneumatophore abundance dataset (from characterization), then it was unified with the CO_2 efflux dataset containing only CO_2 effluxes from the mean pneumatophore abundance observed at each mangrove ecotype, to exclude outliers. This new dataset from observed and predicted data was used for Figure 3.7 (totaling n=850). All statistical analyses were performed using R language version 2023.03.1.446 (Posit Team, 2023). Results are usually presented in terms of the mean ± standard error, unless specified.

3.3. RESULTS

3.3.1. Air and pneumatophores characterization

Mean air temperature was slightly higher during the dry season for all mangrove forests ($H = 97.64$; $P < 0.001$), but the greatest was for the scrub ecotype (dry, 31.98 ± 1.59 °C; rainy, 31.61 ± 2.26 °C; $P < 0.001$), which also had the highest temperatures of pneumatophores during the dry season (Table 3.1). Also, pneumatophores' dimensions (height, volume, and biomass) were slightly higher for the rainy than for the dry seasons for all mangrove types (Table 3.1).

3.3.2. Physicochemical variables

Flooding level for the basin mangrove was always higher than for the scrub and fringe mangroves (dry season, $H = 56.30$; $P < 0.001$; rainy season, $H = 48.32$; $P < 0.001$; Fig. 3.2A). For the fringe mangrove, the flooding level was significantly higher during the rainy season than during the dry season (Fig. 3.2A; $P < 0.001$).

Table 3.1. Microenvironment and morphology of pneumatophores (pneu.) from different mangrove ecotypes in Yucatan during the dry and rainy season. Data are means ± standard deviation. Letters denote significant differences between mangrove ecotypes-season combinations as resulted from the one-way ANOVA on ranks (H-values). Asterisks denote $P < 0.001$, and n.m. = not measured.

Variables	Basin		Fringe		Scrub		H-value
	Dry	*Rainy*	*Dry*	*Rainy*	*Dry*	*Rainy*	
Air temperature (°C)	29.53 ± 1.73^{b}	29.07 ± 1.87^{b}	28.69 ± 3.36^{bc}	26.96 ± 2.46^{c}	31.61 ± 2.26^{a}	31.98 ± 1.59^{a}	97.64*
Volumetric water content (m^3 H_2O m^{-3})	0.52 ± 0.01^{b}	0.55 ± 0.01^{a}	0.54 ± 0.01^{ab}	0.52 ± 0.01^{b}	0.56 ± 0.01^{a}	0.55 ± 0.01^{a}	110.49*
Surface water salinity (‰)	5.93 ± 1.33^{b}	1.9 ± 0.31^{c}	n.m.	4.53 ± 0.54^{b}	36.39 ± 20.01^{a}	20 ± 13.13^{a}	62.75*
Pneu. Abundance (pneu m^{-2})	256.01 ± 146.71^{a}	255.31 ± 144.58^{a}	255.3 ± 164.11^{a}	253.36 ± 162.12^{a}	224.31 ± 171.32^{a}	215.16 ± 173.23^{a}	27.59
Pneu. Height (cm)	31.59 ± 9.98^{a}	33.68 ± 5.55^{a}	23.76 ± 3.87^{c}	27.1 ± 4.37^{bc}	27.47 ± 6.50^{ab}	34.22 ± 8.58^{a}	43.13*
Pneu. Volume (cm^3)	11.69 ± 4.54^{a}	12.17 ± 2.94^{a}	7.88 ± 2.00^{b}	8.89 ± 1.95^{ab}	8.87 ± 3.63^{ab}	12.66 ± 4.44^{a}	38.4*
Pneu. Biomass (g)	3.74 ± 1.81^{ab}	4.73 ± 1.27^{a}	2.37 ± 0.76^{b}	3.34 ± 0.81^{ab}	4.34 ± 2.56^{a}	4.98 ± 1.90^{a}	39.2*
Nearest tree distance (m)	1.9 ± 0.91^{a}	2.3 ± 2.19^{a}	2.96 ± 2.15^{a}	2.34 ± 1.38^{a}	1.9 ± 1.26^{a}	2.44 ± 2.19^{a}	4.17
Pneu. Temperature (°C)	29.97 ± 1.85^{b}	n.m.	30.01 ± 1.72^{b}	n.m.	34.54 ± 3.23^{a}	n.m.	44.06*

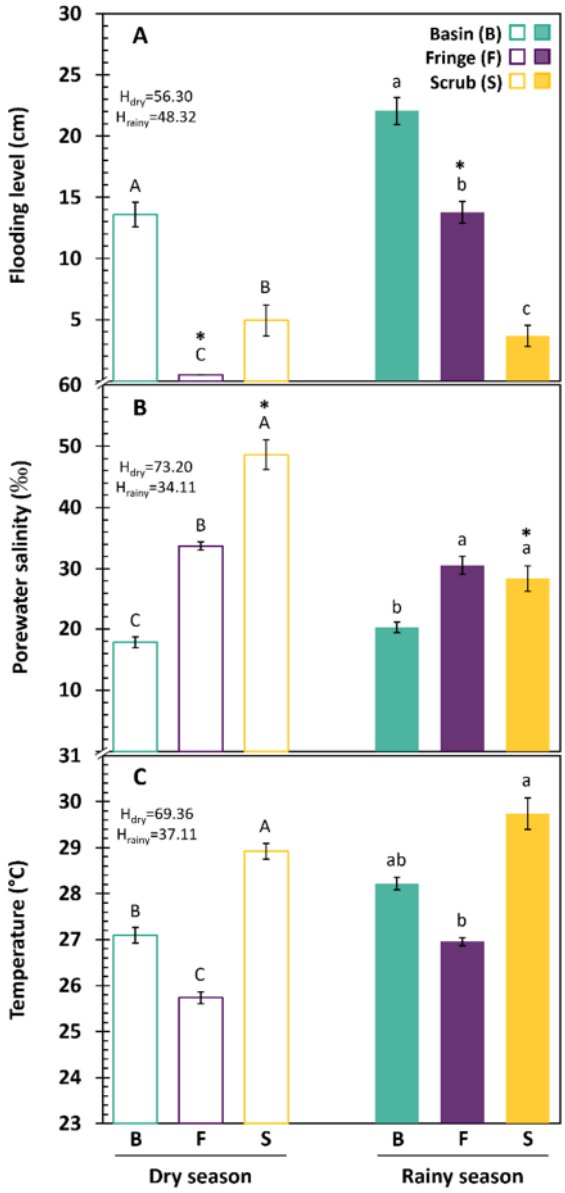

Figure 3.2. Flooding level (A), sediment porewater salinity (B), and temperature (C) of sediment (dry season) or surface water (rainy season) in the three mangrove ecotypes for the dry (open bars) and rainy (filled bars) season in Yucatan, Mexico. Data are means ± SE. Letters denote differences among mangrove ecotypes within each season (capital letters for dry and lowercase for rainy); and asterisks denote differences between seasons within mangrove ecotypes (P < 0.001). H-values for the Kruskal Wallis tests are given for dry (H_{dry}) and rainy

During the dry season, the scrub mangrove had the highest mean porewater salinity (48.61 ± 2.43 ‰; H = 73.20; P < 0.001), followed by the fringe (33.69 ± 0.65 ‰) and the basin (17.82 ± 0.91 ‰) mangroves (Fig. 3.2B). Surface water salinity was about seven-fold higher in scrub (36.39 ± 20.01 ‰; H = 62.75; P < 0.001) than in fringe (4.53 ± 0.54 ‰) and in basin (5.93 ± 1.33 ‰) mangrove ecotypes. Porewater and surface water salinities had significant differences in basin (t = -16.31; P < 0.001) and fringe (t = -33.69; P < 0.001), but slight in scrub (t = -2.75; P = 0.020) mangrove ecotypes.

In the rainy season, porewater and surface water salinities at the basin mangrove ecotype were significantly lower than for the fringe and the scrub mangrove ecotypes (porewater, H = 34.11; water, H = 62.75; P < 0.001; Fig. 3.2B; Table 3.1). However, no differences in salinity were found between seasons for the basin and fringe mangroves; it only decreased significantly for the scrub mangrove in the rainy season (Fig. 3.2B; P < 0.001).

Mean temperature of the sediment was higher for the scrub mangrove than for the basin and fringe mangrove ecotypes (dry season, H = 69.36; P < 0.001; rainy season, H = 37.11; P < 0.001). This temperature was also significantly higher during the rainy season than during the dry season in the fringe mangrove ecotype (Fig. 3.2C; P < 0.001).

3.3.3. Pneumatophores CO_2 effluxes

Pneumatophore abundance explained up to 91% of the variation in CO_2 effluxes for the scrub, 87% for the fringe and 83% for the basin mangrove ecotypes (Fig. 3.3; Table S1) during the rainy season at the water-air interface. During the dry season, when measurements were also done for the sediment-air interface, pneumatophore abundance explained up to 83% of the variation in CO_2 effluxes for scrub, 77% for basin and 65% for fringe mangrove forests (Fig. 3.3; Table S1). The slope of these relationships, which denote the individual contribution of pneumatophores, were also related to the mangrove ecotype, where the steepest slopes were recorded at the fringe mangrove for sediment-air (4.51×10^{-3}) and the scrub mangrove for water-air (4.78×10^{-3}) interfaces as compared to the lower contribution of pneumatophores in basin mangrove for sediment-air (3.04×10^{-3}) and water-air (2.34×10^{-3}) interfaces (Fig. 3.3; Table S1). This effect was greater in the dry season (4.30×10^{-3}) than in the rainy season (3.49×10^{-3}) as well as in the sediment-air (4.54×10^{-3}) than in the water-air (3.20×10^{-3}) interface (Table S1). Overall, the highest contribution of pneumatophores to CO_2 effluxes was found in the fringe mangrove (6.24×10^{-3}; Table S1).

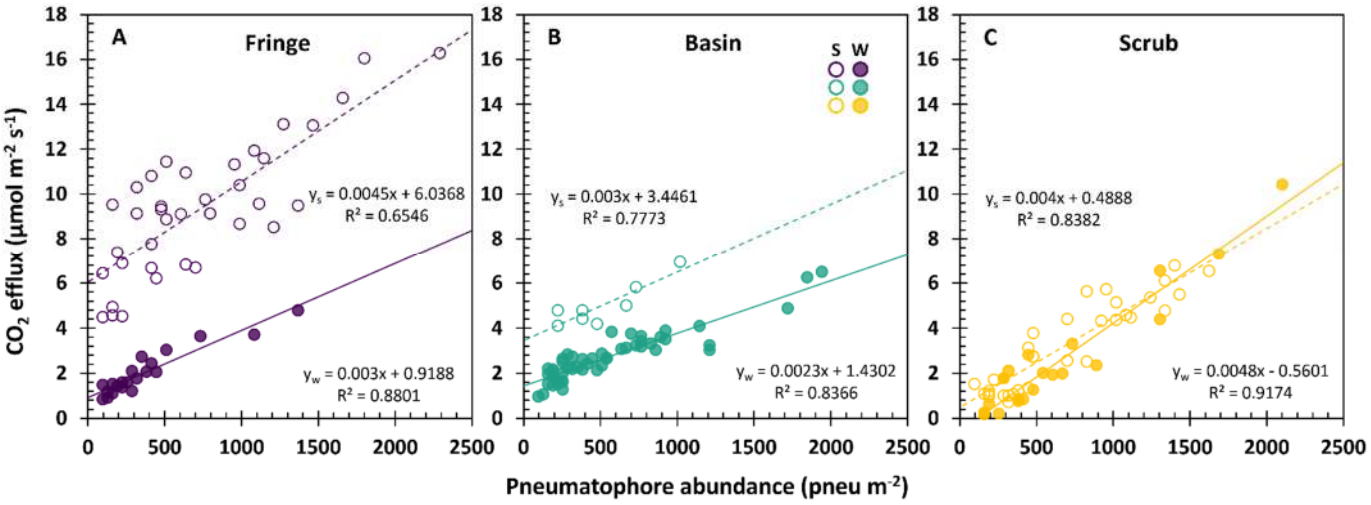

Figure 3.3. Linear relationships of CO_2 effluxes and pneumatophore abundance for fringe (A), basin (B) and scrub (C) mangrove ecotypes at sediment-air (S, open circles) and water-air (W, filled circles) interfaces.

3.3.4. Biophysical associations

The CO_2 efflux at the sediment-air was mainly correlated with sediment temperature (ρ = -0.73), porewater salinity (ρ = -0.45), and pneumatophore abundance (ρ = 0.49; Fig. 3.4-top). Instead, CO2 efflux at the water-air interface was related to pneumatophore abundance (ρ = 0.82) and pneumatophore height (ρ = 0.32; Fig. 3.4-bottom). Because normality's assumption was not satisfied for our data, Spearman's correlations were more convenient.

We performed a Canonical Correlation Analysis (CCA; Fig. 3.5) to look up for the contribution of physicochemical and biological variables to the CO_2 effluxes in the three mangrove ecotypes evaluated. As categories we used mangrove ecotype and as objects the variables measured, including the CO_2 efflux. Mangrove ecotypes were distinguished by salinity, temperature, and flood height. Surface water salinity (F2 contribution 47.36%), porewater salinity (F2 contribution 13.00%) and sediment temperature (F1 contribution 14.41%) separated scrub mangrove; flooding conditions (F1 contribution 36.90%) segregated basin mangrove; and CO_2 effluxes (F2 contribution 11.37%) separated fringe mangrove.

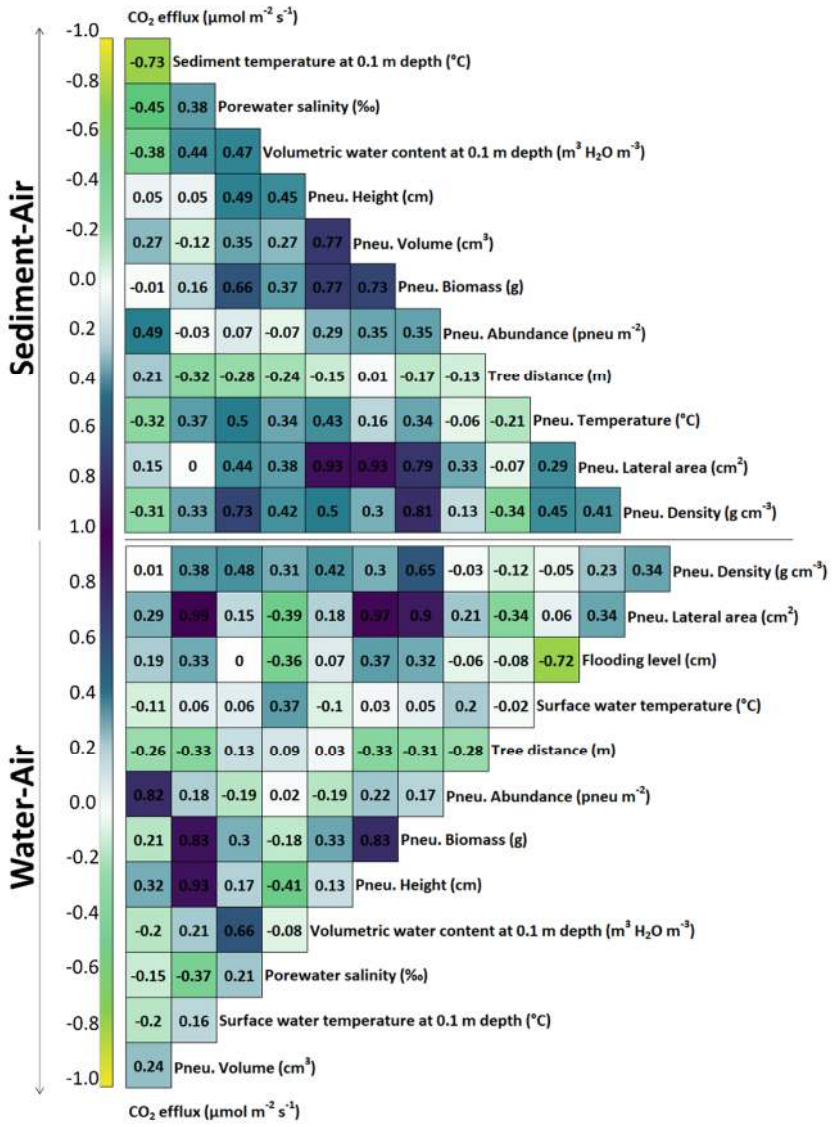

Figure 3.4. Correlation matrix for pair correlation of all variables using the Spearman's rank method for the sediment-air (top) and water-air (bottom) interfaces. Pneu. = Pneumatophore Some variables are not shared in both interfaces due to the absence of measurements.

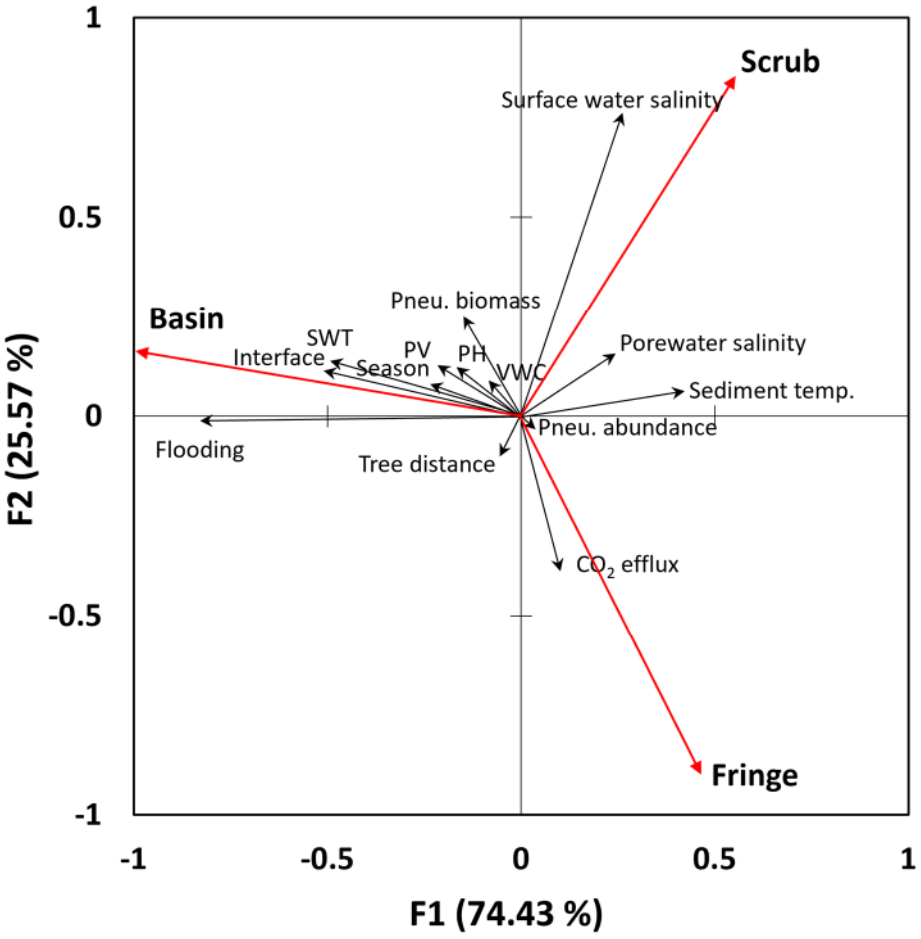

Figure 3.5. Canonical Correlation Analysis (CCA) of physicochemical and biological variables related to the CO_2 efflux and mangrove ecotype. Surface water temperature (SWT), pneumatophore volume (PV) and height (PH), volumetric water content (VWC).

3.3.5. Temperature and salinity effects

The CO_2 effluxes were inversely correlated with sediment or water temperature (Fig. 3.6A) and with porewater or water salinities at the sediment-air and water-air interface, respectively (Fig. 3.6B). Sediment temperature was positively correlated with porewater salinity ($\rho = 0.38$; Fig. 3.4-top) which ultimately differentiated the mangrove ecotypes (Fig. 3.5). Higher temperatures were found in saline sites exposed to higher solar radiation (scrub mangrove) and lower temperatures in sites with medium to low salinities below the canopy (fringe and basin mangroves; Fig. 3.2B-C). Likewise, magnitudes of sediment-air CO_2 effluxes in scrub mangrove did not differ from those from the water-air interface (Fig. 3.3C).

This mangrove ecotype was also the only one where flooding was less variable during measurements (Fig. 3.2A). Indeed, temperature and salinity decreased the CO_2 effluxes from pneumatophores in the three mangrove types studied.

Figure 3.6 shows the relationship between CO_2 efflux with salinity and temperature for each exchange interface. Both sediment and surface water temperatures decreased CO_2 efflux from sediment-air and water-air interfaces (Fig. 3.6A-B). A similar pattern is observed for porewater and surface water salinity (Fig. 3.6C-D). Indeed, CO_2 effluxes decreased from fringe to scrub mangroves, similarly to the groups formed when porewater salinity and both sediment and surface water temperatures are plotted (Fig. S2).

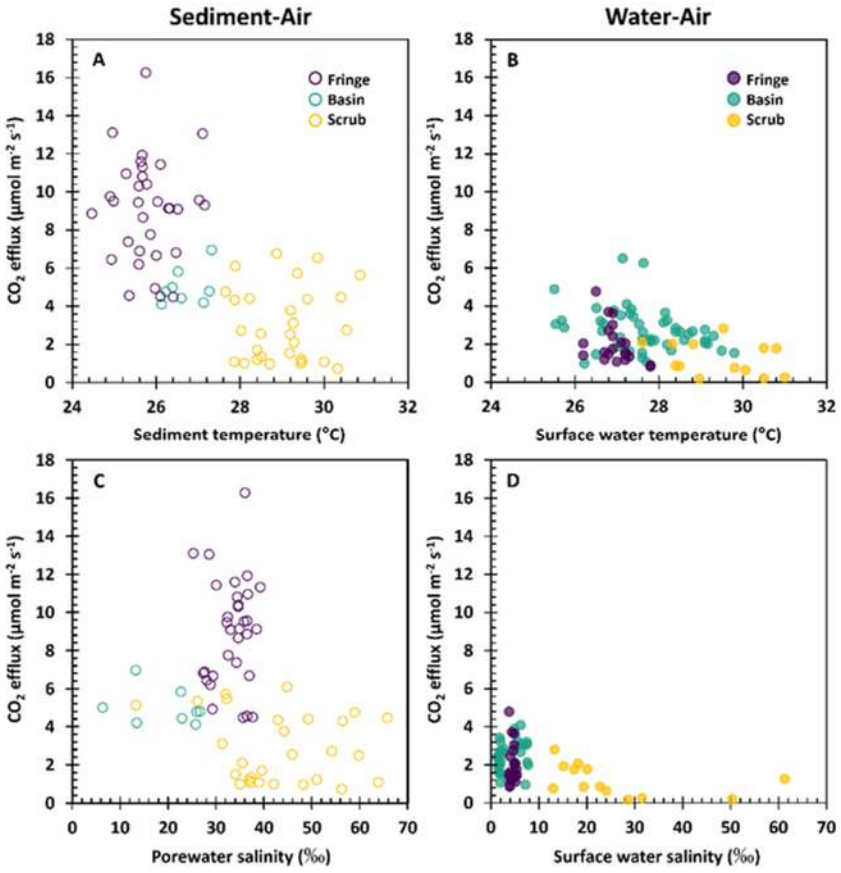

Figure 3.6. Relationships between pneumatophore CO_2 effluxes and sediment temperature (A), surface water temperature (B), porewater salinity (C) and surface water salinity (D) from both sediment-air (open circles, left panels) and water-air (filled circles, right panels) interfaces.

3.3.6. Interface and seasonal effects on CO_2 effluxes

Although no differences were found among mean pneumatophore abundance and mangrove ecotypes and seasons, mean CO_2 efflux varied with mangrove ecotype, interface, and season (Fig. 3.7). Mean pneumatophore abundance was 255.65 ± 145.37 pneu m^{-2} for basin, 254.32 ± 162.79 pneu m^{-2} for fringe and 218.41 ± 172.40 pneu m^{-2} for scrub during all measurements (Table 3.1). Differences of mean CO_2 efflux among mangrove ecotypes were given by differences in mean porewater salinity (dry season for sediment-air interface, $H = 218.46$; $P < 0.001$; rainy season for water-air interface, $H = 251.41$; $P < 0.001$). However, mean CO_2 efflux decreased either from dry to rainy season or from sediment-air to water-air due to increasing flooding level (Fig. 3.2A; Fig. 3.7A-B). For the sediment-air interface, the highest CO_2 efflux was for the fringe mangrove (7.19 ± 0.74 µmol m^{-2} s^{-1}) and the lowest was for the scrub mangrove (1.28 ± 0.74 µmol m^{-2} s^{-1}), both during the dry season (Fig. 3.7A). For the water-air interface, the highest CO_2 efflux was for the basin mangrove (2.14 ± 0.24 µmol m^{-2} s^{-1}) and the lowest CO_2 efflux was for the scrub mangrove during both the dry (0.28 ± 0.83 µmol m^{-2} s^{-1}) and the rainy (0.59 ± 0.80 µmol m^{-2} s^{-1}) seasons (Fig 3.7B). There was a slight increase of CO_2 efflux in the scrub mangrove from the dry to the rainy seasons in both sediment-air and water-air interfaces (Fig. 3.7A-B).

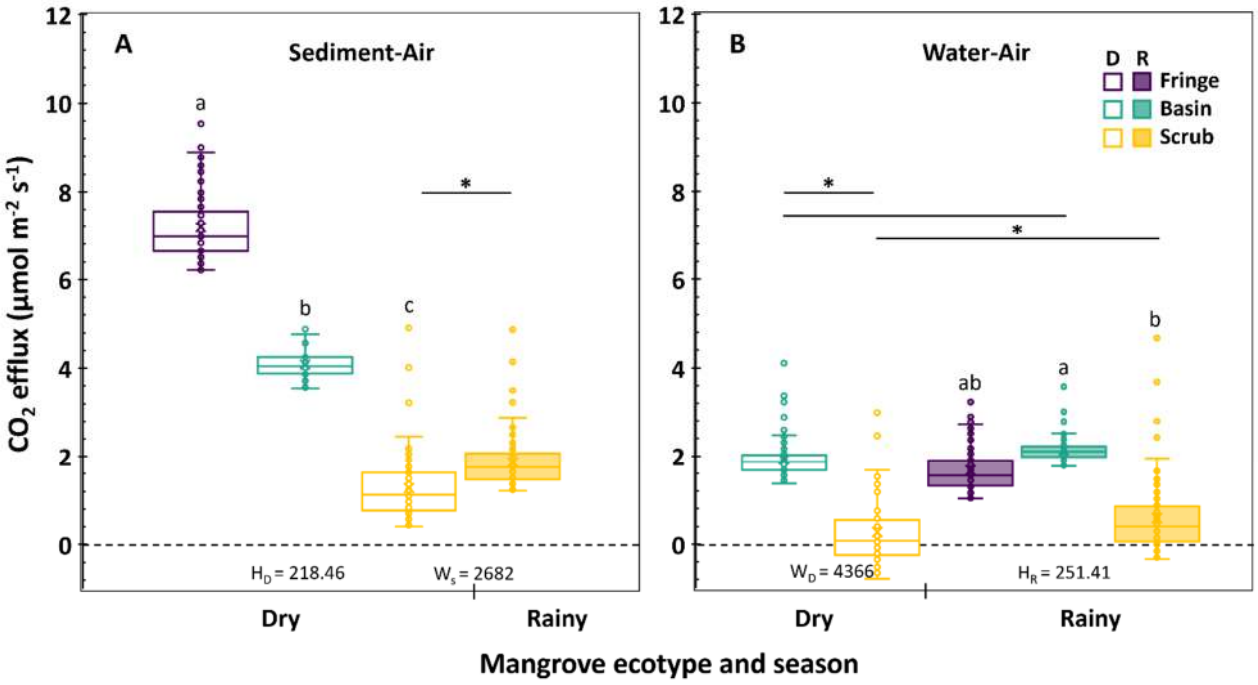

Figure 3.7. Median CO_2 effluxes from three different mangrove ecotypes during the dry (open boxes) and rainy (filled boxes) seasons at the sediment-air (A) and water-air (B) interfaces. Boxes correspond from first to third quartiles; letters denote significant differences among mangrove ecotypes, capital letters for sediment-air and lowercase for water-air interfaces. Lines and asterisks denote differences between seasons for the same mangrove ecotype (A) or between mangrove ecotypes within seasons (B; $P < 0.01$).

3.4. DISCUSSION

Although CO_2 efflux from soils and pneumatophores of mangrove forest dominated by trees of the genus *Avicennia* has been documented (Kristensen *et al.,* 2022; Troxler *et al.,* 2015; Penha-Lopes *et al.,* 2010; Kristensen *et al.,* 2008), but only one reports both pneumatophore abundance and mangrove ecotype (Kristensen *et al.,* 2022). These studies reported lower CO_2 effluxes than those in the present study. We found mean CO_2 effluxes rates of 1.61 to 7.19 µmol m^{-2} s^{-1} (with a mean pneumatophore abundance from 224.31 to 256.01 pneu m^{-2}) at the sediment-air interface, which is comparable to the mean CO_2 effluxes from mangrove soils throughout the world reported by Akhand et al.[10] (-0.37 to 8.73 µmol m^{-2} s^{-1}). Data from creeks and estuaries surrounding mangrove forests (Akhand *et al.,* 2019; Jacotot *et al.,* 2018; Call *et al.,* 2015) show a large range of data, from -0.01 to 7.28 µmol m^{-2} s^{-1}, but our data from water-air interfaces, in the presence of pneumatophores, has a small range (0.51 – 2.05 µmol m^{-2} s^{-1}). However, the use of different methods for CO_2

measurements, as well as the large variation between mangrove ecotypes and climate conditions, do not allow us to make direct comparisons.

Even though we did not carry out measurements of sediment or water only, from the regression intercepts of Fig. 3.3 we can obtain basal respirations of 6.04 μmol m^{-2} s^{-1} for fringe, 3.45 μmol m^{-2} s^{-1} for basin, and 0.49 μmol m^{-2} s^{-1} for scrub mangrove ecotypes at the sediment-air interface; and 0.92, 1.43 and -0.56 μmol m^{-2} s^{-1} from fringe, basin, and scrub mangroves, respectively, at the water-air interface. Then, we can consider that the proportion of aerial autotrophic respiration can be comparable to those CO_2 effluxes from sediments or water with pneumatophores minus that basal efflux. Autotrophic respiration is supposed to represent 48.60% of the total soil respiration in forests (Hanson *et al.,* 2000). In our study, this proportion would be of 15.62 – 69.69% and 30.15 – 209.13% for sediment-air and water-air, respectively, and taking into consideration the CO_2 release driven by pneumatophores only. Yet, although *Avicennia* is one of the most widely distributed mangrove genera and can have more than 10,000 pneumatophores per tree (Tomlinson, 2016; Chen, 2016), pneumatophore CO_2 effluxes are not being reported as a distinct form of carbon loss in mangroves (Adame *et al.,* 2024a).

As predicted, CO_2 effluxes were greater at high pneumatophore abundance, which is related to a high plant biomass. When soils are flooded, pneumatophore respiration is supposed to be the main source of CO_2 effluxes, because gas diffusion in the water column is limited. Additionally, the individual contribution of the pneumatophores is represented by the slope value of the relationships between CO_2 efflux and pneumatophore abundance, allowing comparisons between mangrove ecotypes or tree ages. Pneumatophore CO_2 effluxes were greater at the sediment-air than at the water-air interface exchange for the fringe and basin mangrove ecotypes. For the scrub mangrove, such regressions showed data points overlapping from both interfaces (Fig. 3.3C), but mean CO_2 effluxes were higher at the sediment-air than at the water-air interface for both seasons (Fig. 3.7A-B; Fig. S3). Hydrodynamics in mangrove forests depends on the duration, level, and frequency of flooding, and it is known that CO_2 increases during ebb and spring tides and decreases during flow and neap tides (Jacotot *et al.,* 2018). In our study, we only tested the presence (level) or absence of the water column and found that passing from sediment-air to water-air conditions, the CO_2 efflux rates decreased 76.77 %, 49.75 % and 68.32 % for fringe, basin, and scrub mangrove ecotypes. These results can help adjust our current CO_2 models in mangrove forests considering their hydrology.

Under sunlight, flooding can also reduce CO_2 fixation by photosynthetic layers of pneumatophores in *Avicennia marina* (Aiga et al., 1995). We have found, in preliminary studies, 35.36 ± 28.22 % of the respired CO_2 is offset by pneumatophore photosynthesis (unpublished data), like the 49.58 ± 13.35 % observed in *A. officinalis* and *Sonneratia alba* (Yabuki, 2004). Thus, pneumatophore photosynthesis can represent a source of oxygen and carbon when leaf stomata are closed at high vapor pressure deficit especially for the scrub mangrove ecotype, allowing survival during the dry season.

Few studies have reported CO_2 effluxes as a function of salinity variability within the same mangrove ecotype (Akhand *et al.,* 2019; Troxler *et al.,* 2015). It is well known that salinity decreases photosynthesis and respiration in plants (Lambers and Oliveira, 2019; Krauss *et al.,* 2008; Luo and Zhou, 2006; Medina, 1999; Kozlowski, 1997), accordingly, the site with the highest salinities, the scrub mangrove, showed the lowest CO_2 effluxes, despite having the highest sediment and surface water temperatures, which was not expected as temperature increases respiration in many plant species (Lambers and Oliveira, 2019). Indeed, this scrub mangrove ecotype also had lower CO_2 efflux in the dry than in the rainy season (Fig. 3.7), indicating that high salinity also decreases soil respiration. In fact, in our study, the CO_2 efflux was the result of the effect of salinity, temperature, and flooding that differed between mangrove ecotypes (Fig. 3.2, 3.6; Fig. S2). Although the basin mangrove had the lowest porewater salinities, it showed low CO_2 effluxes because it had the highest flooding level; however, during the dry season in non-flooded places, CO_2 effluxes were high (Table S1, Fig. 3.7). Also, during the dry season, flooding level was inversely correlated with sediment temperature and pneumatophore temperature, which reduced CO_2 efflux. In studies conducted in soils of different forests, a positive relationship between CO_2 effluxes and soil temperature has been found (Poungparn *et al.,* 2009; Lovelock, 2008), because high temperatures favor microbial activity in the soil (Luo and Zhou, 2006). However, in our study, an interaction between high temperatures and high salinities led to a lower CO_2 efflux in the scrub mangrove forest for both seasons and both exchange interfaces.

Mangrove soils that are rich in carbon, organic matter, and nutrient availability (*e.g.,* N, P and Fe) favor CO_2 efflux (Chen *et al.,* 2012; Chen et al., 2010). In some mangrove flooded soils, the enzyme that regulates phosphorus (P) cycling (alkaline phosphatase) is strongly related to CO_2 effluxes, but no relationship between the enzyme that regulates nitrogen (N) cycling (β-N-acetylglucosaminidase) and CO_2 efflux was found (Chambers *et al.,* 2016)[45]. Lower CO_2 effluxes in the scrub mangrove forest could then indicate that this site is P-limited,

because previous reports assign the stature of this mangrove forests to P deficiency in soils (Medina *et al.,* 2010; Lovelock *et al.,* 2004; Feller *et al.,* 2003), although this is still controversial (Cisneros-de la Cruz *et al.,* 2018). In our study, the CO_2 effluxes in flooded soils of scrub mangrove were like those in non-flooded soils and, in some cases, these were very low or even negatives values (Fig. 3.2C; Fig. 3.6). Further research on salinity and P availability would also be needed in arid regions, where scrub mangroves are dominated by *Avicennia germinans* (Adame *et al.,* 2021).

During the rainy season, we found the tallest pneumatophores in all mangrove forests because of a higher level and frequency in flooding events (Zaldívar-Jiménez *et al.,* 2010) and confirmed with a positive correlation between pneumatophore height and flooding level ($\rho = 0.48$; Fig. 3.3). Pneumatophore height has also been positively correlated to flooding level in several studies (Al-Khayat and Alatalo, 2021; Dahdouh-Guebas *et al.,* 2007; Toma *et al.,* 1991), and both pneumatophore height and density have been reported as indicators of soil conditions and the hydrodynamics in mangroves (Al-Khayat and Alatalo, 2021; Tomlinson, 2016). Pneumatophores of *Avicennia* spp. are supposed to be up to 30 cm height (Chen, 2016), but, in our study, pneumatophores were up to 48 cm height in the scrub mangrove ecotype. This pneumatophore extreme length can be related to the increase in water level due to the heavy rain caused by four tropical storms in 2020 in the Yucatan Peninsula (Romero and León-Cruz, 2024).

The average CO_2 effluxes from *A. germinans* pneumatophores in our study sites, at the water-air and sediment-air interfaces, were comparable to those reported in several studies (Nóbrega *et al., 2016*; Penha-Lopes *et al.,* 2012; Kristensen *et al.,* 2008a; Kristensen *et al.,* 2008b). The highest CO_2 effluxes in this study were even higher than those from other forest ecosystems around the world (Arellano-Martín *et al.,* 2022; Maher *et al.,* 2015; Krauss *et al.,* 2012; Litton *et al.,* 2011; Katayama *et al.,* 2009), reflecting the high productivity of the mangrove ecosystems. Our findings question the current understanding of the carbon budget in mangrove forests and highlight the importance of unifying carbon-based studies considering tree physiology in a more dynamic way. Indeed, we propose that further studies on CO_2 (or other greenhouse gases) effluxes should also consider other mangrove tissues, such as stilts, stems, and even leaves, to evaluate their contribution to ecosystem respiration under different global change scenarios.

CAPÍTULO IV.

BARK AERENCHYMA ENHANCES METHANE AND CARBON DIOXIDE EMISSIONS FROM TREE STEMS AND STILT ROOTS OF MANGROVES

Este capítulo será enviado para su evaluación inicial a la revista científica *New Phytologist*, por tanto, debe ser citado y referido según los lineamientos vigentes de la revista final de publicación. Por el momento:

Salas-Rabaza JA, Thalasso F, Yáñez-Espinosa L, Cejudo E, Cerón-Aguilera SG, Us-Santamaría R and Andrade JL. (En preparación). Bark aerenchyma enhances methane and carbon dioxide emissions from tree stems and stilt roots of mangroves.

RESUMEN

- Los manglares son reconocidos por su capacidad de retener el carbono atmosférico, pero también pueden contribuir significativamente a las emisiones de gases de efecto invernadero de diferentes tejidos vegetales.

- Este estudio evalúa los flujos de CH_4 y CO_2 de tallos y zancos de *Rhizophora mangle*, *Avicennia germinans* y *Laguncularia racemosa* en diferentes ecotipos de manglar (cuenca, chaparro y petén) durante las estaciones de lluvias y sequía en Yucatán, México.

- Investigamos la relación entre los rasgos anatómicos de la corteza, el el aerénquima y los flujos de GEI. Los resultados muestran que los zancos (con más aerénquima y densidad de lenticelas) emiten más CH_4 y CO_2 en comparación con los tallos, con mayores emisiones observadas en *R. mangle* chaparro. Además, las emisiones de CH_4 son mayores durante la estación de lluvias.

- Una mayor proporción de aerénquima en la corteza de las raíces y tallos de *R. mangle* facilita el intercambio de gases, contribuyendo a emisiones importantes de GEI. Estos resultados sugieren la incorporación de rasgos anatómicos en los modelos de GEI, a fin de mejorar las estimaciones actuales en los humedales tropicales.

SUMMARY

- Mangroves are recognized for their capacity to sequester atmospheric carbon but can also contribute significantly to greenhouse gas emissions from their tree surfaces.

- This study evaluates CH_4 and CO_2 fluxes from stems and stilt roots of *Rhizophora mangle*, *Avicennia germinans*, and *Laguncularia racemosa* across different mangrove ecotypes (basin, scrub and hammock) during the rainy and dry seasons in Yucatán, Mexico.

- We investigated the relationship between bark anatomical traits, aerenchyma development, and GHG fluxes. Results show that stilt roots (with more bark aerenchyma and lenticel density) emit more CH_4 and CO_2 compared to stems, with higher emissions observed in scrub *R. mangle*. Also, higher CH_4 emissions occur during the rainy season.

- The enhanced aerenchyma in the bark of stilt roots and stems facilitates gas exchange, contributing to significant GHG emissions. These findings emphasize the need to incorporate tree anatomy into models for more accurate GHG estimates in tropical wetlands.

Key Words: *Aerenchyma, Avicennia germinans, Bark anatomy, CH_4 emission, CO_2 flux, Greenhouse gases, Laguncularia racemosa, Rhizophora mangle*

4.1. INTRODUCTION

Mangroves have been recognized as great carbon sinks, providing critical ecosystem services such as pulling carbon dioxide (CO_2), from the atmosphere and storing it as blue carbon. These forests have also a role in the greenhouse gas (GHG) dynamics, particularly methane (CH_4) and CO_2, which are potent contributors to global climate change (Alongi, 2014). While the role of mangrove soils in GHG emissions has been well-documented, the contribution of mangrove trees, particularly through their stems and roots, remains poorly explored (Zhang et al., 2022; Barba *et al.,* 2019a; Jeffrey *et al.,* 2021a).

Trees can mediate the greenhouse gases produced in soils, either by transporting these gases through their tissues (Jeffrey *et al.,* 2019; Covey and Megonigal, 2019) or by hosting methanogens – microorganisms that produce methane – within their woody tissues (Feng et al., 2021; Li *et al.,* 2020; Wang *et al.,* 2016). However, the mechanisms driving these emissions, including diffusion through the bark, pressurized flow, and transpiration-driven flow, are not yet fully understood (Anttila et al., 2024; Vroom *et al.,* 2022; Barba *et al.,* 2019a). The limited understanding of these processes poses challenges to accurately quantifying the role of trees in the global GHG budget. In upland species, CH_4 fluxes from tree stems have been associated with CH_4 concentration in internal tissues such as heartwood or sapwood (Moisan *et al.,* 2024; Wu *et al.,* 2024; Wang *et al.,* 2021; Wang *et al.,* 2017), suggesting that xylem sap flow and bark anatomy exerts barriers to axial and radial diffusion of CH_4 (Jeffrey *et al.,* 2024; Anttila *et al.,* 2024). In wetland species, such as mangroves, trees species exhibit a range of adaptations that allow them to thrive in flooded environments which can in turn increase GHG emissions to the atmosphere. Among these, the development of specialized root structures, such as stilt roots, and pneumatophores, plays a crucial role in gas exchange.

Stilt roots, characteristic of *Rhizophora* species, and pneumatophores, found in *Avicennia* genus and some *Laguncularia* species, are particularly well-adapted for gas exchange due to their extensive development of aerenchyma —spongy tissue that facilitates the diffusion of gases— in the cortex (Tomlinson, 2016; Takahashi *et al.,* 2014; Evans, 2004; Colmer, 2003; Ángeles et *al.,* 2002). In fact, aerenchyma can constitute up to 70% of the tissue in these roots, creating an efficient pathway for the escape of gases produced in the anaerobic soil (Yáñez-Espinosa and Angeles, 2022; Purnobasuki *et al.,* 2017; Evans *et al.,* 2005).

Beyond these aerial roots, the stem bark of mangrove trees also plays a critical role in gas exchange, as an effect of prolonged flooding (Yáñez-Espinosa and Flores, 2011; Yáñez-Espinosa *et al.,* 2008). Stem and roots are often equipped with lenticels—small openings—that facilitate gas movement between the internal tissues and the external environment. These lenticels, in combination with the extensive aerenchyma in the bark, allow for both axial and radial diffusion of gases (Sorrell and Brix, 2013; Youssef and Saenger, 1996). This gas transport can occurs bypassing the xylem and directly influencing the exchange of gases between the bark and the atmosphere, as shown in other species (Jeffrey et al., 2024; Moisan et al., 2024; Wu et al., 2024; Ge et al., 2024; Beckett et al., 2023; Rosner and Morris, 2022). While these adaptations are primarily geared towards enhancing oxygen supply to submerged roots, they also create pathways for the release of GHG into the atmosphere, impacting GHG exchange at both the ecosystem and global scales (Ward and Megonigal, 2024; Bastviken *et al.,* 2023).

The formation of aerenchyma is a critical adaptation not only in wetlands but also in other species, such as maize (*Zea mays*), which develop this tissue in response to hypoxic conditions. Aerenchyma can form through two main processes: lysigeny, where cells break down to create air spaces, and schizogeny, where spaces are created by the separation of cells (Takahashi *et al.,* 2014; Yamauchi *et al.,* 2013; Evans, 2004). The presence of aerenchyma in both roots and stems enhances the plant's ability to transport gases under flooded conditions, making it a key feature in wetland species globally.

In mangroves, the interaction between macro and microstructures creates a complex system for gas exchange that is influenced by a variety of environmental factors, including hydroperiod (level, duration and frequency of flood events), soil composition, and seasonal changes. Understanding these interactions is essential for accurately modeling the contribution of mangroves to global GHG emissions. Previous studies have demonstrated that CH_4 and CO_2 emissions from mangrove trees can vary significantly depending on the species, environmental conditions, and functional traits of the stems and pneumatophores (Salas-Rabaza *et al.,* 2024; Liao *et al.,* 2024; Yong *et al.,* 2024; Epron *et al.,* 2023; Zhang et al., 2022; Gao *et al.,* 2021; Dušek *et al.,* 2020; Jeffrey *et al.,* 2019; He *et al.,* 2019; Zhang *et al.,* 2019). However, *Rhizophora mangle* and *Avicennia germinans* species have not been reported yet. Also, to the best of our knowledge, stilt roots have only been considered in one study of CO_2 fluxes (Troxler *et al.,* 2015).

The objective of the current study was to evaluate the relationship between the bark anatomical traits of mangrove trees and their GHG fluxes, focusing on CH_4 and CO_2 emissions from the stems and stilt roots of the red mangrove (*R. mangle*) in scrub and hammock ecotypes during the rainy and dry seasons in Yucatán, Mexico. We also measured CH_4 and CO_2 fluxes from the stems of black (*A. germinans*) and white (*L. racemosa*) mangroves in the basin ecotype. We hypothesized that higher GHG fluxes would be observed in the stilt roots of *R. mangle* compared to its stems due to the proximity of these roots to soil production sites and their higher aerenchyma content. Additionally, we expected *R. mangle* to exhibit greater GHG emissions than *A. germinans* and *L. racemosa*, given its higher tolerance to inundation. Finally, we anticipated that CH_4 emissions would peak during the rainy season, while CO_2 emissions would be higher in the dry season, influenced by flooding conditions, which can act as a barrier to gas diffusion and simultaneously enhance methanogenesis.

4.2. MATERIALS AND METHODS

4.2.1. Site sampling and tree structure

Fieldwork was conducted in the Ria Celestun Biosphere Reserve, Yucatán, México (Lat. 20° 51’ 03.6” N, Long. -90° 17’ 42.5” W; Ramsar Site 1333), during two measurement campaigns corresponding to the rainy (September 2021) and dry (April 2022) seasons. Sampling was carried out on the three mangrove species within three ecological types: *Rhizophora mangle* in the scrub and hammock ecotypes, and both A*vicennia germinans* and *Laguncularia racemosa* in the basin ecotype. Nine trees per species were chosen for flux measurements. Trees were structurally characterized following the standardized methodology of Howard *et al.,* (2014) and Kauffman and Donato (2012). Additionally, *R. mangle* trees were measured as follows (Fig. S4.1): major diameter (D_s) and minor diameter (d_s) of the main stem at 0.30 m on the last stilt root for hammock mangroves and at 0.10 cm for scrub mangrove. The total length of the main stem (L_s) in scrub trees and first branching stem height (H_f) in tall trees were estimated with a laser hypsometer (Vertex, Haglöf Sweden AB), as well as the total height (H_t). For stilt roots, diameters (D_r and d_r), lengths (L_r), and heights (H_r) were also recorded.

4.2.2. Microenvironment, physico-chemical of water and porewater

Air temperature (°C), relative humidity (RH, %) and photosynthetic photon flux (PPF, µmol m^{-2} s^{-1}) were measured using a Temp Smart Sensor (TMB-M003, Onset) and a Quantum Smart Sensor (Photosynthetic Light, S-LIA-M003, Onset, USA). Both sensors were recorded in a portable weather station (U30-NRC Weather Station Starter Kit, Onset), during the flux measurement times at each site. The vapor pressure deficit (VPD) was calculated using the formula from Jones (2014). Additionally, porewater salinity (in ppm) at 30 cm below the ground, surface salinity (ppm), surface water temperature (°C) and flood level (cm) were measured using a portable conductivity meter (YSI, Model Pro2030, Yellow Springs, OH).

4.2.3. Tree CH_4 and CO_2 determination

Methane and carbon dioxide fluxes were quantified at 0.10-0.25 m above the main stem for *R. mangle* trees and at 0.20-0.40 m and 1.20-1.40 m for both *A. germinans* and *L. racemosa* stems. Stilt roots measurements were performed at the 5-10 cm of the lower portion of each root. Fluxes were measured using a static chamber method, together with leaks detection and quantification, according to the method previously described by Salas-Rabaza et al., (2023). Briefly, depending on the stem/root size, we used four different sizes of semi-rigid chambers (0.50 × 0.30; 0.30 × 0.24; 0.24 × 0.18; 0.15 × 0.10 m) in order to fit most of the stem or stilt. Semi-rigid chambers were made of a 0.7 mm thick impermeable polyethylene terephthalate (PET) plastic sheet glued to a 20 x 30 mm closed cell neoprene foam (SealsCDirect Ltd, Hamphshire, UK) according to Siegenthaler *et al.,* (2016). CH_4 and CO_2 measurements were performed *in situ* using the integrated cavity laser spectroscopy (OA-ICOS) method. Chambers were connected in a closed loop of flexible polyurethane tubing (PUN-6X1-DUO-BS, Festo, Mexico) to an ultra-portable greenhouse gas analyzer (UGGA, model 915-0011-1000, Los Gatos Research, ABB, USA). Air chamber was replaced with ambient air by an external air pump (Flextailgear Tiny Pump, Mexico) to minimize the impact of chamber installation. Then, CH_4 and CO_2 concentration within the chamber was measured for 10-15 minutes followed by the injection of 1 mL of CH_4 to determine the leak constant (k_L) of the circuit. Fluxes were determined according to the following modified formula from Salas-Rabaza *et al.,* 2023:

$$F = \left(\frac{dC_C}{dt}\right)_{t=0} \cdot \frac{V_T}{A_C} = k_t \cdot \left(C_{C,2} - C_A\right) \cdot \frac{V_T}{A_C}$$

Where F is the gas flux (mg m^{-2} h^{-1}), dC_C is the gas concentration change between chamber and atmosphere (C_A) at a time interval (dt), V_T is total volume and A_c is the chamber area. k_t is a kinetic constant which include all kinetic parameters of flux and leaks, $C_{C,2}$ is the final value of the chamber concentration (C_C) when the chamber reaches a steady-state condition from an asymptotic curve.

4.2.4. Bark and anatomical characterization

Macroscopic observations of the bark were made on stems and stilt roots. Photographs were then taken using grids of 5 x 5 cm for stems and 2 x 3 cm for stilt roots at each measurement height. The photographs were used to calculate the number, size (mm^2) and density of lenticels (lenticels cm^2) using the ImageJ Program (Schneider *et al.,* 2012). Stems/roots were marked to identify them after the last greenhouse gas quantification campaign. Wood core samples were then collected from the middle of the stem's measurement height with an increment borer (Haglöf, Längsele, Sweden) of 5.5 mm diameter for wood density and 12 mm diameter for anatomical analysis. Stem cores were obtained at 0.30 m and 1.30 m for both *A. germinans* and *L. racemosa*, and at 0.15 m for hammock's *R. mangle*. Two cross samples (5 cm each) of stilt roots and stems of scrub *R. mangle* were collected with a hacksaw. From the collected samples, the wood specific density was calculated based on its oven-dry mass (at 100°C for 48 h) and its green volume, which was measured by the water displacement method (Archimedes principle). Photographs of *R. mangle*'s cross sections were analyzed using ImageJ Program (Schneider *et al.,* 2012) to measure the bark, xylem and pith areas and proportions. Bark was considered as all the tissues outside of the vascular cambium, including the cortex or cortical parenchyma, and the outer bark (periderm and epidermis). Tree cores and cross sections were immediately fixed in FAA (formaldehyde-alcohol-water-glacial acetic acid) for 24 h. Subsequently, samples were washed with running water and preserved in GAA (glycerin-alcohol-water) for 6 months until its processing. In the laboratory, 3 x 2 x 2 cm subsamples were taken, of which transverse sections of 4-20 µm thick were obtained with a sliding microtome (GSL-1, Swiss Federal Research Institute WSL, SW). These slides were bleached with sodium hypochlorite, dehydrated in absolute alcohol, and dyed with safranin and fast O green for microscope observation. Aerenchyma's intercellular space area (ISA, in μm^2) and intercellular spaces per 100 μm^2 were measured manually or using the binary/threshold tool in ImageJ.

Intercellular space proportion (%) was calculated as the ratio of the total ISA : total area of the I- and Y-shaped cells. Also, the roundness shape function (ImageJ) was used.

4.2.5. Data analysis

Fluxes and aerenchyma data did not meet the assumptions of the Shapiro-Wilk normality test or Levene's test for homoscedasticity. Therefore, non-parametric tests were used to assess differences between species, stilt root order, ecotype, organ, or season. Wilcoxon tests were applied to evaluate differences between seasons or ecotypes within the same group, while Kruskal-Wallis tests for comparisons among multiple groups (such as species or stilt root order), and Wilcoxon-Mann Whitney or Welch test for two-sample comparisons, depending on the normality/homoscedasticity. Dunn test was applied as post-hoc test. For tissue proportion data, the assumptions of normality and homoscedasticity were met, so two-way ANOVAs were conducted to examine differences between organs and ecotypes, followed by Tukey's post-hoc tests. Regression models were selected based on the best fit and R^2, reducing the RSME. All analyses were conducted using R Studio version 2023.03.1.446 (Posit Team, 2023). Results are typically presented as the median ± one standard deviation unless otherwise specified.

4.3. RESULTS

4.3.1. Methane and carbon dioxide fluxes

Methane fluxes from stems varied significantly among species during dry ($H = 22.53$; $P < 0.001$) and rainy seasons ($H = 18.42$; $P < 0.001$), but no difference between lower and upper levels of the stem were found for both *A. germinans* and *L. racemosa*. In both, *Ag* and *Lr*, CH_4 fluxes remained low, showing no significant seasonal differences (Ag, $t = -1.02$; $P = 0.32$; Lr, $t = -2.38$; $P = 0.02$) between dry (Ag, 0.50 ± 1.25; Lr, 0.27 ± 1.61 mg CH_4 m^{-2} d^{-1}) and rainy seasons (Ag, 0.71 ± 1.66; Lr, 1.10 ± 1.75 mg CH_4 m^{-2} d^{-1}; Fig. 4.1A). In contrast, *R. mangle* (*Rm*) exhibited clearly higher fluxes but no differences between seasons ($t = 0.86$; $P = 0.40$). Notably, the scrub ecotype (*RmS*) showed an increase in CH_4 flux during the rainy season (8.45 ± 5.90 mg CH_4 m^{-2} d^{-1}) compared to the dry season (3.02 ± 7.65 mg CH_4 m^{-2} d^{-1}). Rm in the hammock ecotype (*RmH*) showed no differences ($t = 0.33$; $P = 0.74$) for rainy (0.27 ± 0.37 mg CH_4 m^{-2} d^{-1}) and dry seasons (0.22 ± 0.86 mg m^2 d^{-1}), though with lower absolute emissions than *RmS* (Fig. 4.1A). Methane emissions from stilt roots also varied by stilt order during the dry ($H = 30.96$; $P < 0.001$) and rainy seasons ($H = 28.92$; $P < 0.001$)

but not between seasons. In both scrub and hammock ecotypes, emissions increased significantly with stilt root (Fig. 4.1B), particularly in third-order stilt roots during the rainy season for *RmS*$_3$ (11.95 ± 11.80 mg CH_4 m^{-2} d^{-1}) and *RmH*$_3$ (7.94 ± 4.19 mg CH_4 m^{-2} d^{-1}). Root emissions were higher in *RmS* than *RmH* and higher during the rainy season compared to the dry season.

Regarding the stem CO_2 fluxes, they were more variable than CH_4 fluxes. *Lr* showed the highest fluxes, particularly during the rainy season (362.12 ± 142.14 mg CO_2 m^{-2} h^{-1}), followed by *Ag* (207.91 ± 218.04 mg CO_2 m^{-2} h^{-1}), whereas *RmH* had lower CO_2 emissions, with no significant seasonal differences (rainy, 128.09 ± 36.11; dry, 153.93 ± 71.40 mg CO_2 m^{-2} h^{-1}; Fig. 4.1C). The range of CO_2 emissions from stems across species suggests variation in stem respiration rates and gas transport capabilities. CO_2 emissions from stilt roots showed significant seasonal variation, with higher rates during the dry season in comparison to the rainy season. Third-order roots exhibited the highest emissions during the dry season in both *RmH*$_3$ (590.94 ± 367.55 mg CO_2 m^{-2} h^{-1}) and *RmS*$_3$ (652.79 ± 503.45 mg CO_2 m^{-2} h^{-1}; Fig. 4.1D), but they were highly variable.

Overall, GHG emissions varied significantly between organs for both CH_4 (scrub, $H = 9.58$; $P < 0.01$; hammock, $H = 29.88$; $P < 0.001$) and CO_2 (scrub, $H = 27.23$; $P < 0.001$; hammock, $H = 31.88$; $P < 0.001$). CH_4 and CO_2 fluxes were consistently higher in the stilt 3 of *R. mangle* in scrub (CH_4, 14.90 ± 14.16 mg CH_4 m^{-2} d^{-1}; CO_2, 504.99 ± 451.08 mg CO_2 m^{-2} h^{-1}) and hammock (CH_4, 7.15 ± 4.04 mg CH_4 m^{-2} d^{-1}; CO_2, 448.07 ± 323.10 mg CO_2 m^{-2} h^{-1}), with scrub exhibiting the higher emissions (Fig. 4.2A-B). On the other hand, the intercellular space area of the aerenchyma followed a similar pattern, with stilt 3 showing higher areas for both scrub (62.94 ± 37.05 μm^2) and hammock (39.03 ± 20.02 μm^2), though with more variable values (Fig. 4.2C). These aerenchyma were significantly variable by organs for scrub ($H = 336.86$; $P < 0.001$) and hammock ($H = 379.46$; $P < 0.001$) with larger intercellular space areas in stilt 3 than in the stem by a factor of 9.46 for scrub and 6.66 for hammock, which may explain their enhanced capacity for gas exchange.

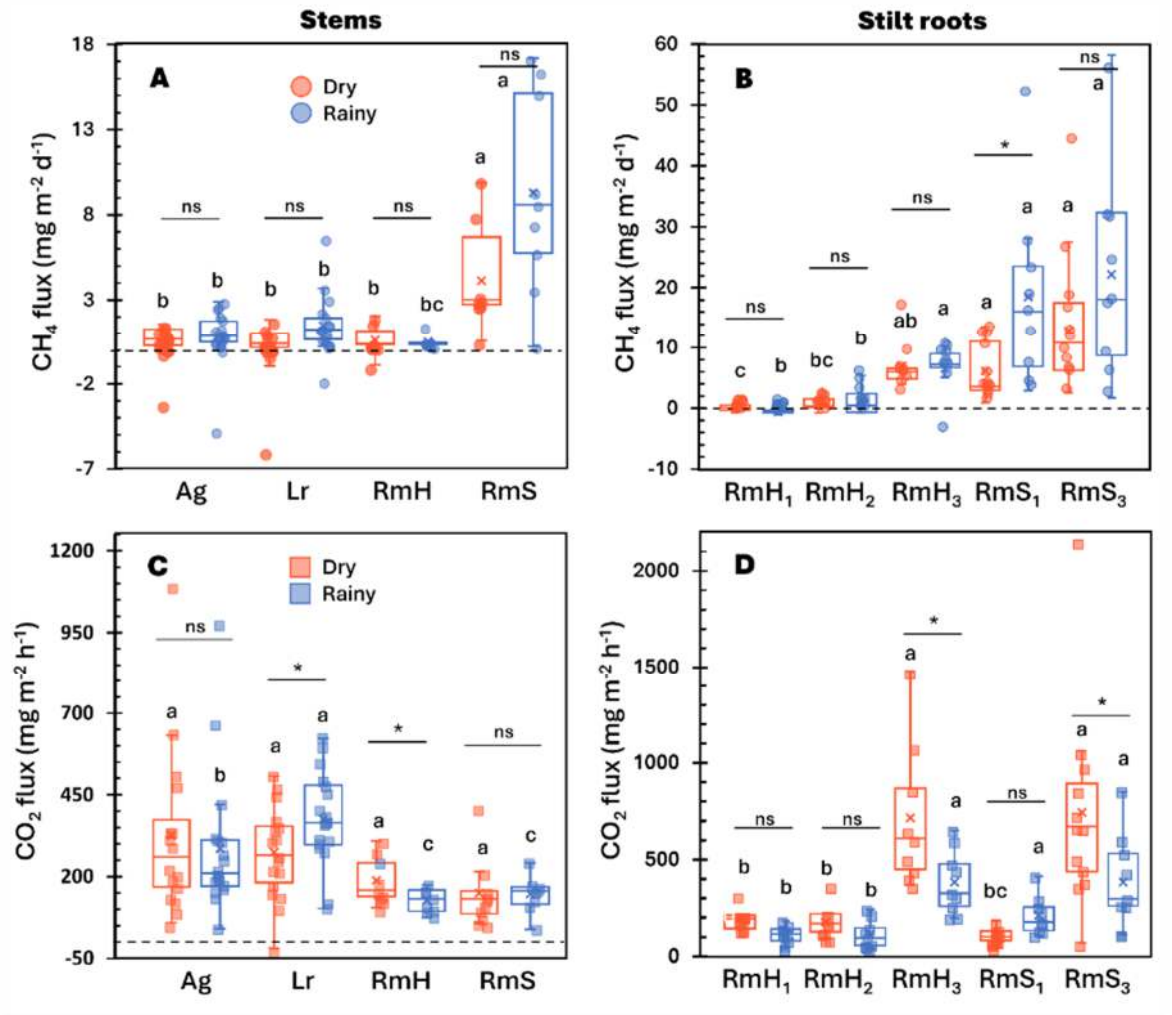

Figure 4.1. Tree methane (A, B) and carbon dioxide (C, D) fluxes from stems (left) and stilt roots (right) of different mangrove species (*Ag* = *Avicennia germinans*; *Lr* = *Laguncularia racemosa*; *Rm* = *Rhizophora mangle*) and mangrove ecotypes (*RmS* = scrub *R. mangle*; *RmH* = hammock *R. mangle*), during the rainy (blue) and dry (orange) seasons. The subscript number denotes the order of the *R. mangle*'s stilt root in scrub and hammock. Letters indicate differences between species within seasons. Asterisks denote differences between seasons for each species.

4.3.2. Bark morpho-anatomical traits

Stem and stilt 3 exhibited evident differences between the proportions of bark ($F = 94.39$; $P < 0.001$) and xylem tissues ($F = 56.58$; $P < 0.001$; Fig. 4.3A-B). The tissue composition analysis showed that bark comprised the largest proportion of the tissues in stilt 3 for scrub (Fig. 4.3C), while xylem proportion was higher in stems (59.00 ± 19.43 %). The pith proportion showed a slight increase from stems to stilt 3, even if no significant differences were found ($F = 47.79$; $P = 0.04$). The bark proportion was notably higher in scrub than

hammock for stem (37.80 ± 16.45%; 19.82 ± 7.00%; P < 0.01) and stilt 1 (59.02 ± 8.75%; 37.53 ± 8.78%; P < 0.001), but no for stilt 3 (75.72 ± 6.85%; 69.66 ± 8.24%; P = 0.75).

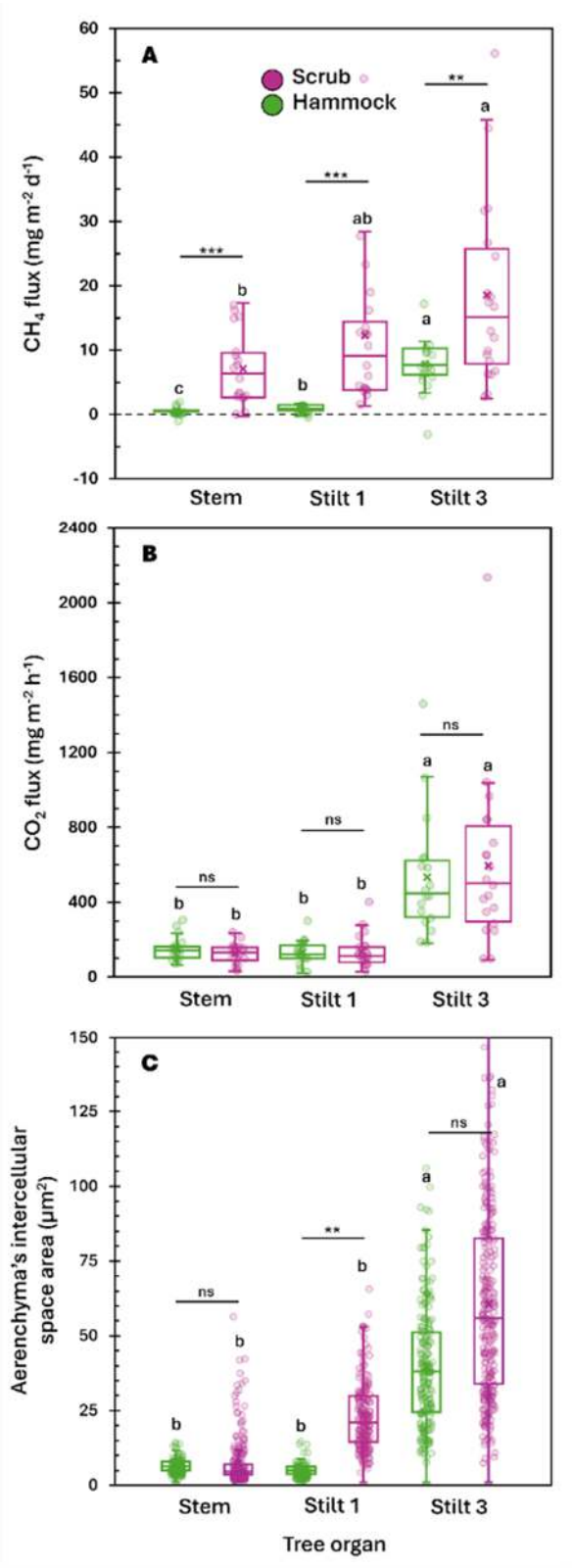

Figure 4.2. Methane fluxes (A), carbon dioxide fluxes (B), and aerenchyma's intercellular space area (C) from stem and stilt root of *Rhizophora mangle* in scrub (purple) and hammock (green) ecotypes. Letters denote differences between tree organs within each ecotype. Asterisks indicate differences between ecotypes. ns = no significative

Additionally, more intercellular spaces per 100 μm^2 were found in stilt 1 (7.30 ± 0.63) and stilt 3 (5.86 ± 0.30) of hammock, followed by stems of scrub (5.05 ± 4.53) and hammock (4.23 ± 1.26). The percentage of air intercellular spaces was higher in third-order stilt root sections (scrub, 51.63 ± 3.22%; hammock, 44.84 ± 5.86%) and lower in stems (scrub, 23.95 ± 8.91%; hammock, 25.17 ± 8.33%), consistent with the bark proportion, even if the total bark area was lower in stilt 1 (scrub, 6.33 ± 2.91 cm^2; hammock, 12.96 ± 15.28 cm^2) and stilt 3 (scrub, 7.09 ± 2.43 cm^2; hammock, 7.51 ± 3.85 cm^2) than stem (scrub, 8.36 ± 5.63 cm^2; hammock, 54.57 ± 31.64 cm^2).

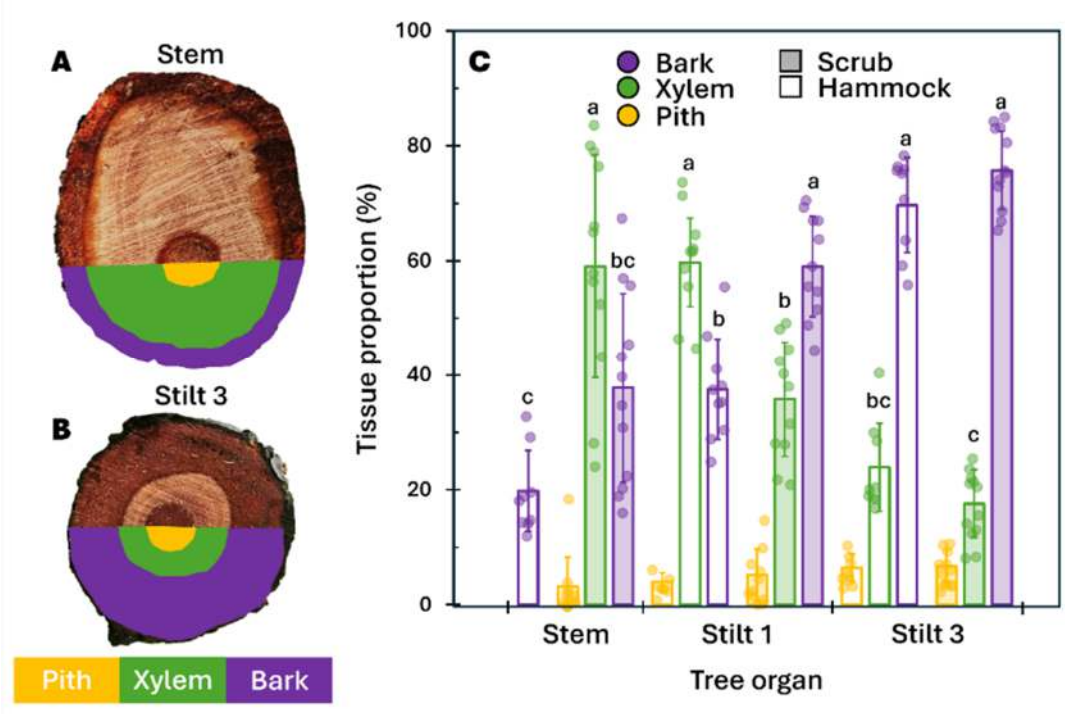

Figure 4.3. Photographs of the stem (A) and stilt 3 (B) showing the proportion of the main three tissue measured. Mean ± standard deviation of the tissue proportion (C) for each tree organ at scrub (filled bars) and hammock (open bars) ecotypes. Letters denote differences between tree organs and ecotype.

Transverse sections of the stem bark structure in *R. mangle* of the scrub ecotype revealed distinct anatomical features. Near the vascular tissue, axial parenchyma alternated with sieve tube elements, and ray cells exhibited abundant druses and crystals (Fig. 4.4A). In the outer cortex, a honeycomb-like structure, formed by both Y- and I-shaped aerenchyma cells, defined large polygonal intercellular spaces of schizogenic origin, presenting pit thickening and druses (Fig. 4.4B). In the pith region (Fig. 4.4C), a well-developed aerenchyma with

polygonal intercellular spaces, bordered by rounded cells with pits and druses, was observed, surrounded by protoxylem. The periderm consisted of multiple layers of phellem cells (Fig. 4.4D), followed by 5-7 layers of phelloderm. The phelloderm gave way to the formation of cortical aerenchyma including both axial and radial parenchyma. An innermost cortex delimited by a band of sclereids, included also aerenchymatous tissues with the presence of large groups of brachysclereids, druses and H-trichosclereids.

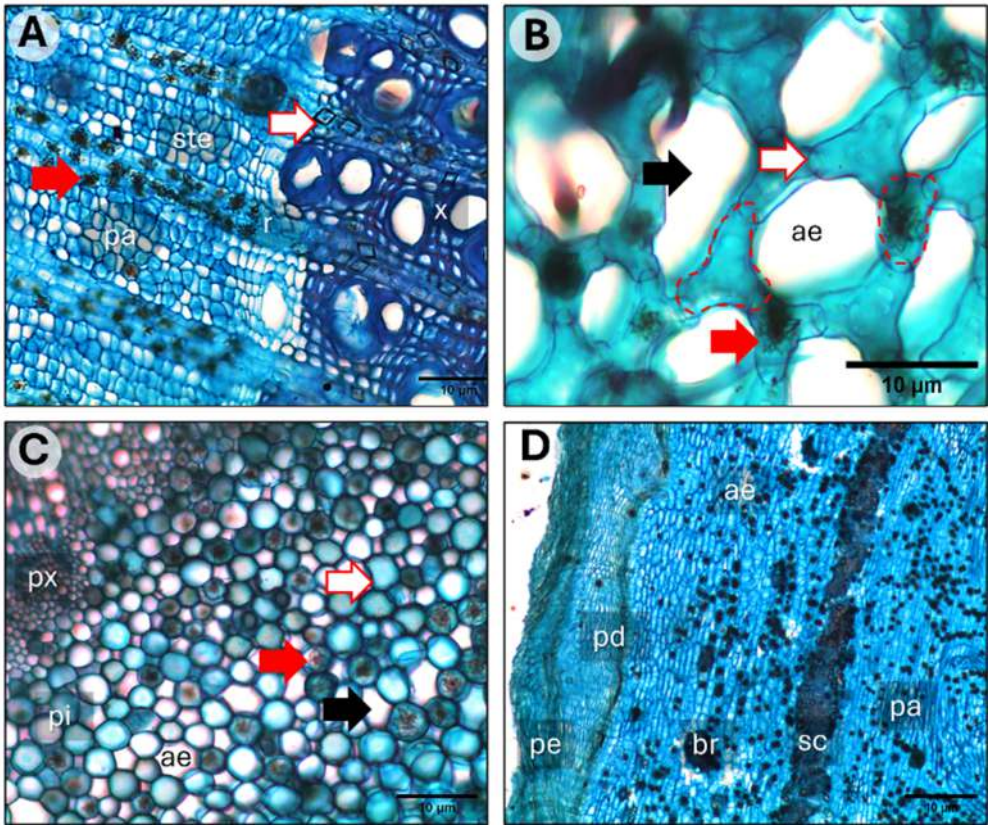

Figure 4.4. Transverse sections of the stem bark structure in scrub Rhizophora mangle. **A.** Axial parenchyma close to the xylem alternating with sieve tube elements, and ray cells showing abundant druses (red arrow) and crystals (hollow arrow). **B.** Honeycomb-like structure formed of Y- and I-shaped cells (dotted line) with large pits (hollow arrow) and druses (red arrow) creating polygonal intercellular spaces (black arrow). **C.** Pith region showing an extensive aerenchyma with polygonal intercellular spaces (black arrow) formed of 5-7 round-shaped cells with pits (hollow arrow) and druses (red arrow), surrounded by protoxylem. **D.** Periderm with multiple layers of cells, and aerenchyma formed by axial and radial parenchyma cells, with a band of sclereids and abundant brachysclereids. *ae* aerenchyma, *br* brachysclereids, *pa* axial parenchyma, *pd* phelloderm, *pe* periderm, *pi* pith, *px* protoxylem, *r* phloem rays, *sc* sclereids, *ste* sieve tube element, *x* xylem.

The bark structure of first-order stilt roots from both scrub and hammock exhibited similar anatomical features than stems (Fig. 4.5). In both ecotypes, dilation of axial and radial parenchyma was present bordered by a sclerenchyma band and associated with ray cells containing abundant druses (Fig. 4.5A, H). Large polygonal intercellular spaces formed schizogenously by rounded and Y-shaped aerenchyma cells with large pits and druses were prominent, forming honeycomb-like structures (Fig. 4.5B, E). The periderm consisted of multiple compact layers of phellem, surrounding internal aerenchyma in the secondary cortex with abundant H-trichosclereids and druses (Fig. 4.5C, F). The perimedullary region displayed protoxylem bundles rich in tannins and abundant pith aerenchyma (Fig. 4.5D, G, I).

In the third-order stilt roots of *R. mangle*, extensive well-developed aerenchyma of schizogenic origin was also present. In both ecotypes, axial and radial parenchyma presented abundant druses and were delimited by a sclerenchyma band. The ray cells display notable dilatation, and extensive aerenchyma was observed, characterized by abundant druses, large brachysclereids, and H-trichosclereids (Fig. 4.6A, E). In the perimedullary region, bundles of protoxylem are evident, along with a well-developed pith aerenchyma containing druses and H-trichosclereids (Fig. 4.6B, F). The schizogenous aerenchyma formed a honeycomb-like structure, composed of I- and Y-shaped cells, with phi thickening around the radial cells, with abundant H-trichosclereids, and druses, contributing to the formation of polygonal intercellular spaces (Fig. 4.6C, H, I). The pith aerenchyma was comprised of rounded cells forming polygonal intercellular spaces (Fig. 4.6D). Additionally, the aerenchyma of the secondary cortex was also rich in H-trichosclereids and druses and delimited by layers of porous phelloderm (Fig. 4.6G).

4.3.3. Relationships between GHG fluxes and bark traits

Methane fluxes from scrub trees increased exponentially with bark proportion during both dry ($R^2 = 0.36$; $P < 0.01$) and rainy seasons ($R^2 = 0.45$; $P < 0.001$). This relationship was stronger in the rainy season, with fluxes reaching up to 50 mg m^2 d^{-1} at more of 80% bark proportion (Fig. 4.7A). In case of CH_4 from hammock trees, the best fit was a linear relationship for dry ($R^2 = 0.58$; $P < 0.001$) and rainy ($R^2 = 0.64$; $P < 0.001$), with differences between seasons. While CH_4 emissions were higher in the rainy season, the overall fluxes were lower compared to scrub (Fig. 4.7B). Both results suggesting that bark aerenchyma plays a critical role in facilitating CH_4 transport.

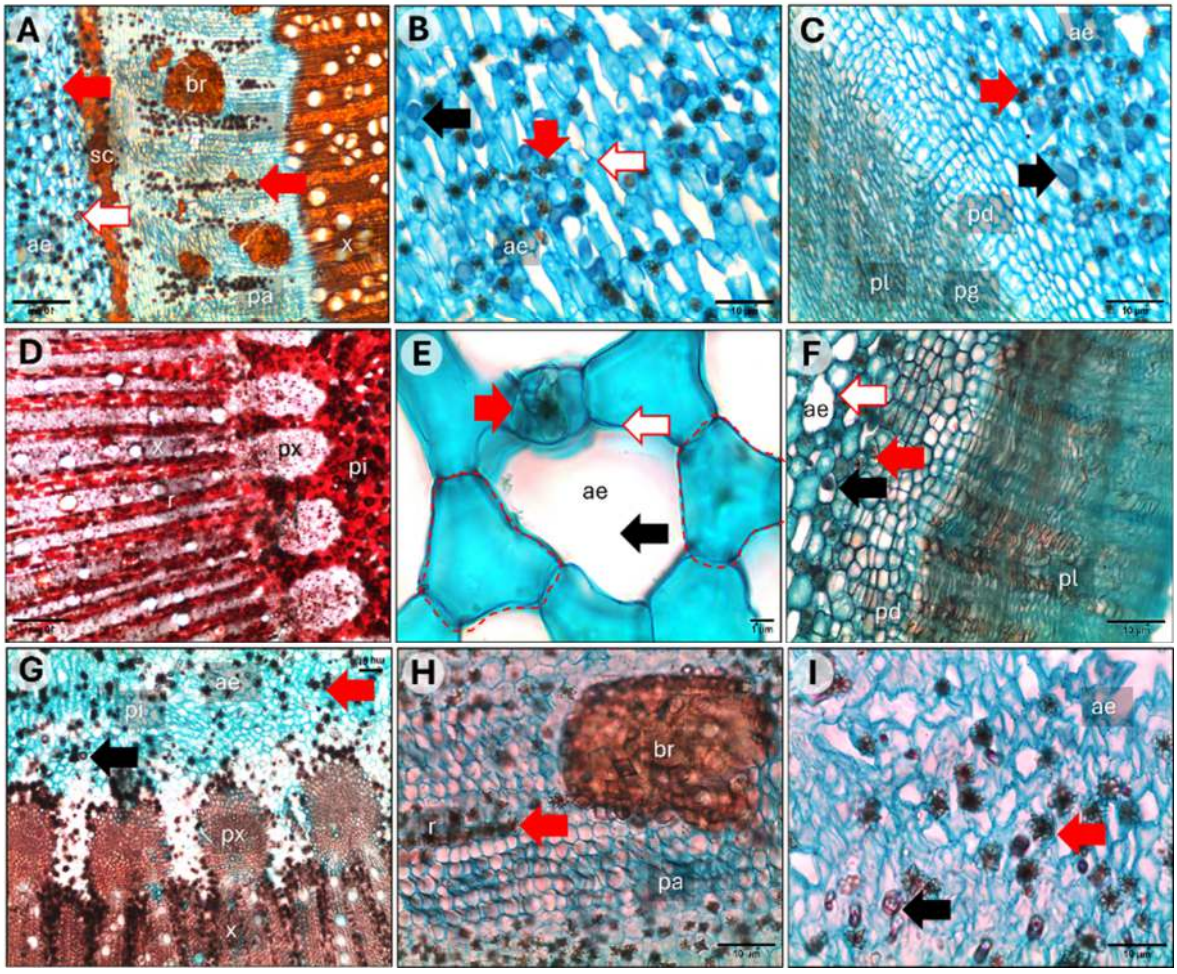

Figure 4.5. Transverse sections of the stilt 1 bark structure in scrub (A-F) and hammock (G-I) *Rhizophora mangle*. **A.** Axial parenchyma surrounding the xylem delimited by a sclerenchyma band, showing ray cells and an extensive aerenchyma with abundant druses (red arrow), large brachysclereids, and H-trichosclereids (black arrow). **B.** Polygonal intercellular spaces formed by rounded and enlarged aerenchyma cells with large pits (hollow arrow), druses (red arrow) and H-trichosclereids (black arrow). **C.** Periderm with multiple layers of compact phellem cells and phellogen, delimited by 7 layers of porous phelloderm, surrounding inner aerenchyma with abundant H-trichosclereids (black arrow) and druses (red arrow). **D.** Pith, xylem and perimedullary region with bundles of protoxylem, with abundant tannins. **E.** Honeycomb-like structure formed by rounded and Y-shaped aerenchyma cells (dotted line) with large pits (hollow arrow) and druses (red arrow) creating polygonal intercellular spaces (black arrow). **F.** Periderm with stratified compact phellem and porous phelloderm formed of few layers of cells, near to the aerenchyma with pits (hollow arrow), H-trrichosclereids (black arrow) and druses (red arrow). **G.** Perimedullary region with bundles of protoxylem, and pith aerenchyma with abundant druses (red arrow) and H-trichosclereids (black arrow). **H.** Axial parenchyma and ray cells with abundant druses (red arrow) and large brachysclereids. **I.** Pith aerenchyma intercellular spaces with abundant druses (red arrow) and H-trichosclereids (black arrow). *ae* aerenchyma, *br* brachysclereids, *pa* axial parenchyma, *pd* phelloderm, *pg* phellogen, *pe* periderm, *pi* pith, *px* protoxylem, *r* phloem rays, *sc* sclereids, *x* xylem.

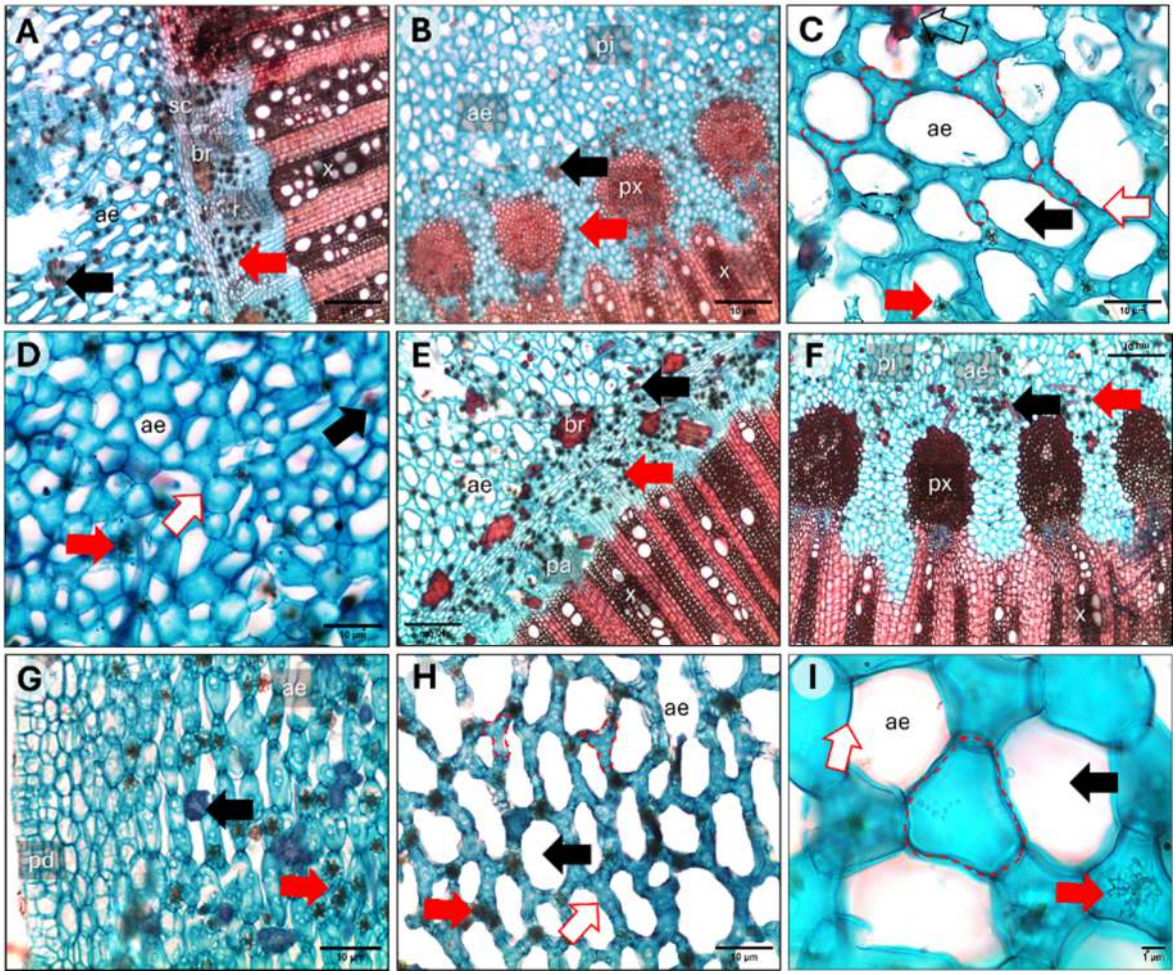

Figure 4.6. Transverse sections of the stilt 3 bark structure in scrub (A-D) and hammock (E-I) *Rhizophora mangle*. **A,E.** Axial parenchyma surrounding the xylem delimited by a sclerenchyma band, showing dilatation of ray cells and an extensive aerenchyma both with abundant druses (red arrow), large brachysclereids, and H-trichosclereids (black arrow). **B,F.** Perimedullary region with bundles of protoxylem, and pith aerenchyma with abundant druses (red arrow) and H-trichosclereids (black arrow). **C,H,I.** Honeycomb-like structure formed by I- and Y-shaped aerenchyma cells (dotted line) with large pits (hollow arrow), H-trichosclereids (black hollow arrow) and druses (red arrow) creating polygonal intercellular spaces (black arrow). **D.** Pith aerenchyma formed by rounded cells with large pits (hollow arrow), druses (red arrow) and H-trichosclereids (black arrow). **G.** Aerenchyma formed by polygonal intercellular spaces with abundant H-trichosclereids (black arrow) and druses (red arrow), delimited by layers of porous phelloderm. *ae* aerenchyma, *br* brachysclereids, *pa* axial parenchyma, *pd* phelloderm, *pi* pith, *px* protoxylem, *r* phloem rays, *sc* sclereids, *x* xylem.

The relationship between CO_2 flux and bark proportion in *Rm* scrub was less pronounced than for CH_4 ($R^2 = 0.28$ in dry; $P < 0.05$, $R^2 = 0.20$ in rainy; $P > 0.05$). Although CO_2 emissions increased with bark proportion, the response was more variable, especially during the rainy season (Fig. 4.7C). In *Rm* hammock, CO_2 flux also increased with bark proportion but showed a stronger relationship during the dry season ($R^2 = 0.64$, $P < 0.01$) (Fig. 4.7D). This suggests that bark proportion may have a greater effect on CO_2 release in drier conditions, potentially due to increased respiratory activity in response to stress.

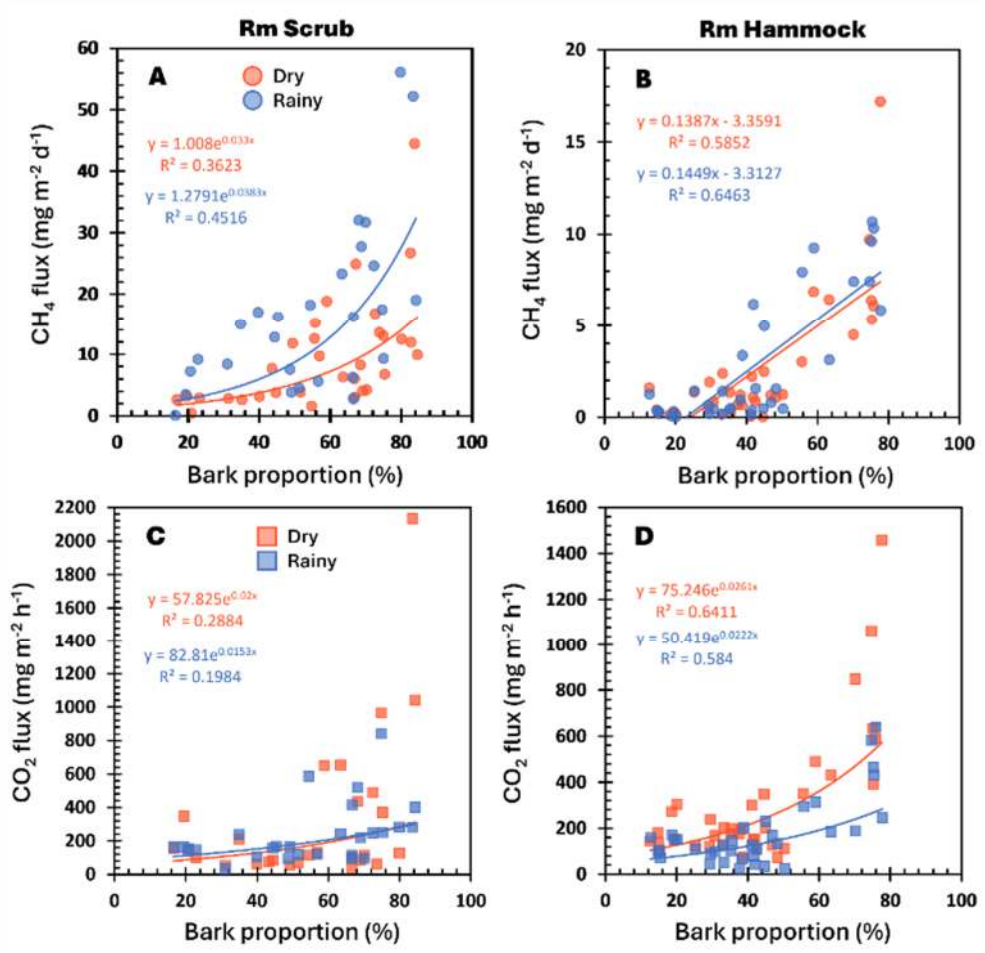

Figure 4.7. Relationship between bark proportion and CH_4 (circles) or CO_2 (squares) fluxes in *R. mangle* of scrub (A, C) and hammock (B, D) ecotypes during the dry (orange) and rainy (blue) season.

CH_4 increased with higher lenticel densities in both scrub and hammock ecotypes, and during both dry and rainy seasons (Fig. 4.8A-B). The positive linear relationships observed suggest that lenticels play a significant role in facilitating CH_4 emissions. Specifically, in the

scrub (Fig. 4.8A), the slopes of the regressions for the dry and rainy seasons were 10.50 and 16.23, respectively. The hammock ecotype (Fig. 4.8B) showed a similar trend, with slightly lower slopes of 4.05 and 4.74 for the dry and rainy seasons, respectively. These results indicate a stronger influence of lenticel density on CH_4 fluxes in scrub compared to hammock in order of two-to-three-fold. CO_2 fluxes also exhibited a positive relationship with lenticel density, though the patterns were less consistent than for CH_4. In the scrub ecotype (Fig. 4.8C), fluxes were substantially higher during the dry season (slope = 427.29; compared to the rainy season (slope = 121.87), indicating that other factors modulate CO_2 emissions beyond lenticel density alone. Similarly, in the hammock ecotype (Fig. 4.8D), CO_2 fluxes showed a marked seasonality, with a steeper slope during the dry season (slope = 251.15).

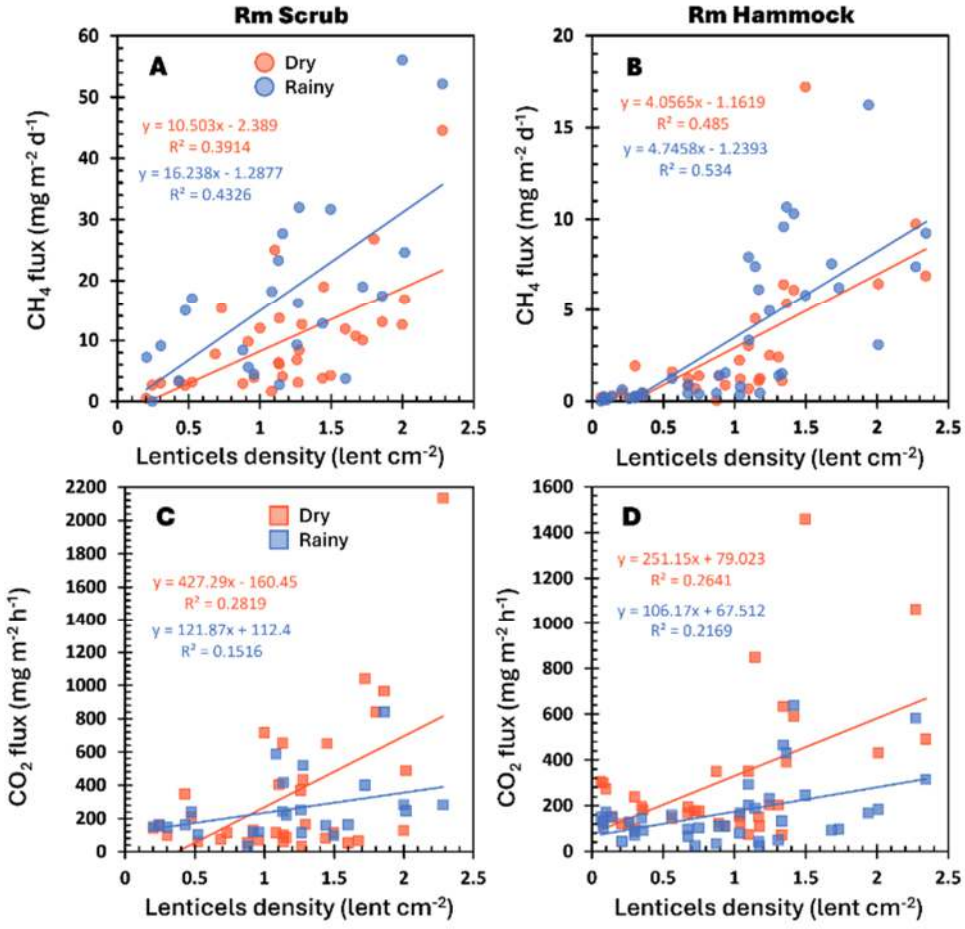

Figure 4.8. Relationship between lenticels density and CH_4 (circles) or CO_2 (squares) fluxes in *R. mangle* of scrub (A, C) and hammock (B, D) ecotypes during the dry (orange) and rainy (blue) seasons.

4.4. DISCUSSION

4.4.1. The bark side of mangrove greenhouse gas emissions

To the best of our knowledge this is the first time that both CH_4 and CO_2 fluxes from stems of *L. racemosa*, *A. germinans* and *R. mangle* are reported in their natural areas of distribution, which made this study valuable for the Americas region. Stem CH_4 emissions were highly variable inter- and intra-species in the mangrove ecotypes studied. Here we reported fluxes as the median ± one standard deviation due to the non-normality of the data, but the magnitudes (mean ± standard error) of these emissions were comparable to the species of the same genera already reported in the literature. For instance, during all seasons, CH_4 from stems of *L. racemosa* and *A. germinans* exhibited fluxes of 0.73 ± 0.30 and 0.63 ± 0.25 mg m^{-2} d^{-1}, respectively, which are in concordance with emissions from exotic *L. racemosa* in China (0.34 ± 0.31 mg m^{-2} d^{-1}; He *et al.,* 2019) and *Avicennia* genera in the Indo-Pacific (0.90 ± 1.30 mg m^{-2} d^{-1}; Yong *et al.,* 2024; Zhang *et al.,* 2022; Gao *et al.,* 2021; Dušek *et al.,* 2020; Jeffrey *et al.,* 2019). Regarding *R. mangle*, CH_4 fluxes from stems of scrub and hammock ecotypes were 8.12 ± 1.55 and 0.38 ± 0.15 mg m^{-2} d^{-1}, respectively. Methane emissions of *R. mangle* in hammock was between the range of *R. apiculata* in Vietnam (0.04 to 0.90 mg m^{-2} d^{-1}; Dušek *et al.,* 2020), while stems of *R. mangle* in scrub emitted more CH_4 than the species listed before and other mangrove genera worldwide such as *Aegiceras*, *Kandelia*, *Sonneratia*, and *Bruguiera* (-2.18 to 4.64 mg m^{-2} d^{-1}; Liao *et al.,* 2024; Yong *et al.,* 2024; Epron *et al.,* 2023; Zhang *et al.,* 2022; Gao *et al.,* 2021; He *et al.,* 2019; Zhang *et al.,* 2019), but less than *Aegiceras corniculatum* in China (16.23 mg m^{-2} d^{-1}; Gao *et al.,* 2021).

In the case of CO_2, mean fluxes ± standard error were similar for stems of *A. germinans* and *L. racemosa* (329.93 ± 47.96 and 323.26 ± 24.96 mg m^{-2} h^{-1}; respectively) during all periods, but in order of two-fold higher than *R. mangle* in both scrub (144.15 ± 18.63 mg m^{-2} h^{-1}) and hammock (154.11 ± 14.85 mg m^{-2} h^{-1}). CO_2 fluxes from mangrove stems are also scared measured worldwide, but our findings were comparable with some of them. For instance, CO_2 emissions from *A. germinans* was higher than the range of CO_2 emissions reported in *A. alba* (37.50 to 210.83 mg m^{-2} h^{-1}; Dušek *et al.,* 2020) but lower than those found in *A. marina* (625.82 ± 361.32 mg m^{-2} h^{-1}; Yong *et al.,* 2024). *R. mangle* CO_2 emissions from both scrub and hammock were lower than these of *R. apiculata* (196.95 to 406.90 mg m^{-2} h^{-1}; Vinh et *al.,* 2019). Also, the three species studied here were comparable to the range of CO_2

emissions in other mangrove species such as *Kandelia obovata* and *Sonneratia apetala* (-59.77 to 332.9 mg m^{-2} h^{-1}; Liao *et al.,* 2024; Yong *et al.,* 2024).

We did not find significative differences in CH_4 and CO_2 fluxes with increasing stem height, which is a common pattern in tree stem GHG dynamics in both tropical (Sjögersten *et al.,* 2020; Jeffrey *et al.,* 2019; Pangala *et al.,* 2017) and temperate (Schindler *et al.,* 2021; Martínez and Ardón, 2021; Pitz *et al.,* 2018) wetland species. This suggest that the flow of gases through the lower an upper portion of the stem can be improved by the internal pathways of the bark which exert less resistance to the axial diffusion of gases, as has been reported for *R. mangle* and *A. germinans* species (Yáñez-Espinosa and Ángeles, 2022). Additionally, other bark features can affect the GHG emissions from the tree stems. One of the variables associated to stem CH_4 fluxes is the wood specific density, as an indicator of the wood properties, which has been negatively related to these fluxes (Pangala *et al.,* 2015; Pangala *et al.,* 2013). Wood specific density is linked to wood porosity, which is the ratio of the volume of gas (including intercellular air spaces) to the volume of cellular tissue (Armstrong, 1979). Then, lower values indicate high porosity or more intercellular air spaces, reflected in higher GHG emissions. However, this relationship is not always fulfilled. For example, *L. racemosa* and *A. germinans* have lower wood densities than *R. mangle* but they presented lower CH_4 emissions and higher CO_2 emissions, even if *R. mangle* stems are further away from the ground. This reinforced the fact that connected structures can supply a continuous path for gas flow from the roots to the stems.

Furthermore, micro-environmental conditions such as porewater salinity, flooding level, air temperature can affect GHG emissions (Feng *et al.,* 2022; Pangala *et al.,* 2015; Terazawa *et al.,* 2015). These parameters can vary from dry to rainy seasons, which ultimately enhance the methanogenic activity in the soil while limiting respiration. In our study, Seasonality influenced significantly the magnitude of gas emissions, suggesting that soil moisture, temperature, and oxygen availability modulate gas exchange. Rainy season increased the CH_4 emissions of all stem species by 42.55%, 1455.75%, 179.58% and 21.84% for *A. germinans*, *L. racemosa*, scrub *R. mangle* and hammock *R. mangle*, respectively, while CO_2 fluxes were reduced by 28.56% and 16.79% for *A. germinans* and hammock *R. mangle*, respectively. Both *L. racemosa* and scrub *R. mangle* exhibited an increase in CO_2 fluxes from dry to rainy seasons by 38.32% and 24.72% respectively.

Finally, some negative fluxes of CH_4 and CO_2 were present in our data, especially in stems of *L. racemosa* and *A. germinans,* which jointly with the data obtained in other mangrove species suggest that mangrove stems can act as both sources and sinks as has been documented in different mangrove species (Liao *et al.,* 2024; Gao *et al.,* 2021; He *et al.,* 2019). The latter could be explained by differences in the physic-chemical conditions of sediments and water as well as the physiological responses of mangrove species to changes in flooding and salinity, reinforcing the need of consider these variables in our current models.

4.4.2. The roots of GHG emissions

Methane and dioxide emissions from stilt roots were highly variable depending on the order of the stilt and the ecotype. Overall, we found higher emissions from stilt roots compared to stems. Since stilt roots have been poorly considered in CH_4 and CO_2 budgets, direct comparisons are challenging. To simplify, we compared mean ± standard error with mean mangrove stem fluxes or with other kind of aerial roots when possible. CH_4 emission of scrub *R. mangle* was higher in stilt 3 (18.24 ± 3.17 mg m^{-2} d^{-1}) than stilt 1 (11.69 ± 2.58 mg m^{-2} d^{-1}). The same pattern was found for hammock *R. mangle*, with CH_4 emissions of 7.28 ± 0.95 and 0.68 ± 0.12 mg m^{-2} d^{-1}, for stilt 3 and stilt 1, respectively. In general, these emissions were higher than mean stem CH_4 fluxes from mangrove species worldwide, including those from this study (1.85 ± 3.80 mg m^{-2} d^{-1}). However, stilt 1 of hammock *R. mangle* had CH4 emissions rates comparable to those of stems of mangrove species, while stilt 3 of scrub *R. mangle* had higher CH_4 emissions rates than stems of *Aegiceras corniculatum* (16.23 mg m^{-2} d^{-1}; Gao *et al.,* 2021) and dead *A. marina* (17.14 ± 3.22 mg m^{-2} d^{-1}; Jeffrey *et al.,* 2019).

CO_2 emissions were also higher in stilt 3 than stilt 1. Both scrub (599.35 ± 100.86 mg m^{-2} h^{-1}) and hammock (533.60 ± 76.15 mg m^{-2} h^{-1}) stilt 3 emitted more CO_2 than stems of the three species studied, while stilt 1 of scrub (136.63 ± 19.14 mg m^{-2} h^{-1}) and hammock (137.59 ± 15.03 mg m^{-2} h^{-1}) had similar rates than stems of *R. mangle*. The only study reporting CO_2 fluxes from stilts roots of *R. mangle* found magnitudes of 307.37 ± 71.30 mg m^{-2} h^{-1} (Troxler *et al.,* 2015) in a riverine mangrove, which is actually quite similar of the emissions from stilt 1 during the rainy season (hammock, 371.71 ± 55.55; scrub, 371.23 ± 81.63 mg m^{-2} h^{-1}). Stilt 3 emits up to 19.20 times more CH_4 and 3.46 times more CO_2 than stems, indicating that aerial roots are the primary pathways for CH_4 and CO_2 emissions in both scrub and hammock ecotypes. This is likely due to the enhanced gas transport capacity provided by

higher bark proportion, abundant lenticels, and larger intercellular space areas in these roots. Stilt roots of *R. mangle* contributed to the massive emission of both CH_4 and CO_2, just as pneumatophores do for *Avicennia marina* (Zhang *et al.,* 2022; Purvaja *et al.,* 2004) and *A. germinans* (Salas-Rabaza *et al.,* 2024; Troxler *et al.,* 2015; Kristensen *et al.,* 2022; 2008). However, there is still a debate of the transport mechanisms of gases inside the trees. It is hypothesized that it could be rapidly mobilized whether via molecular diffusion through the outer bark (cortex) or by transpiration-driven processes (Jeffrey *et al.,* 2024; Covey and Megonigal*,* 2019). In this sense, it is important to consider the different functions (*i.e.,* physiology) of specialized tissue such as the aerial roots, as well as the trade-off involved.

If flood-adapted species mobilize soil-produced gases through their stems, it is almost evident that they enter by the roots, as has been demonstrated in several studies (Jeffrey *et al.,* 2023, 2021; Villa *et al.,* 2020) and reviewed recently (Määttä and Malhotra, 2024). Although these roots are hidden in many tree species, mangroves exhibit an aerial root system that allowed us to contrast. We demonstrated that stilt roots of *R. mangle* are also a significant source of GHG because these roots are specialized in the transport of gases.

Moreover, the mainly reasons why third-order stilt roots exhibited higher GHG emissions than stems can be summarized as follows: 1) stilt roots are nearer to the methane source in the sediment, which allow axial movement and rapid radial emissions (Jeffrey *et al.,* 2021; Barba *et al.,* 2019a); 2) these roots have a higher bark proportion (73.12 ± 7.90%) than stems (30.09 ± 15.86%) with an extensive aerenchyma forming large intercellular space areas, which is the best pathway for long distance transport of gases (Takahashi *et al.,* 2013; Evans *et al.,* 2005; Colmer, 2003); and 3) the large density and functioning of lenticels in the bark which differs between tissues exposed (stilt roots) *vs* not exposed (stems) to regular flooding, allowing the radial egress of gases (Covey and Megonigal, 2019; Pangala *et al.,* 2013).

4.4.3. Anatomy of the emissions

Plants can mediate the transport of greenhouse gases such as CH_4 and CO_2 produced in the anoxic sediment in flooded ecosystems. The mechanisms and plant traits affecting the gas movement throughout the plant have been widely documented and reviewed mostly for aquatic and herbaceous plants (Määttä and Malhotra, 2024; Villa *et al.,* 2020; Colmer, 2003; Sorrell and Brix, 2013; Strand, 2002; Amstrong, 1979). Recently the processes affecting the

transport, production and consumption of CH_4, and CO_2 by trees have also been included (Salomón *et al.,* 2024; Ge *et al.,* 2024; Anttila *et al.,* 2023; Vroom et al., 2022; Covey and Megonigal, 2019; Barba *et al.,* 2019a; Teskey *et al.,* 2017; Teskey *et al.,* 2008). Nevertheless, most of the studies measuring GHG fluxes from tree stems have also measured macro-anatomical traits such as lenticels density and wood specific density as proxies of the tissue porosity and the relative proportion of intercellular spaces. However, the role of microanatomical features in transporting GHG has been less studied (Ward and Megonigal, 2024; Jeffrey *et al.,* 2024; Takahashi *et al.,* 2022). Even if aerenchyma is assumed to be present in wetland species, it has not been measured yet.

In our study, we were able to separate and measure the proportion of pith, xylem and bark – including cortical parenchyma and outer bark (periderm and epidermis) – from transversal sections of the stem and stilt root of *R. mangle* in two contrasting mangrove ecotypes. The relative proportion of the tissues showed a decrease in xylem and an increase in bark from stems to stilt 3 (*i.e.,* near-soil tissues). This was consistent with the behavior observed in GHG fluxes, suggesting that the main transport of gases in *R. mangle* is via the aerenchymatous cortex, also present in stems, for both scrub and hammock ecotypes.

The exponential increase of CH_4 emissions with bark proportion in scrub *R. mangle* confirmed that bark aerenchyma enhances methane transport and emissions, amplifying these effects during the rainy season. The relationship with CO_2 is less clear but may reflect ecotypes- and season-specific differences in respiration and gas transport dynamics. Lenticel density positively correlates with CH_4 and CO_2 emissions in mangrove tree organs, with scrub *R. mangle* exhibiting steeper slopes, indicating that structural adaptations to gas exchange vary between ecotypes. This is consistent with other studies showing that lenticels facilitate the escape of GHG to the atmosphere (Covey and Megonigal, 2019; Rowland *et al.,* 2018; Pangala *et al.,* 2015). The difference response between ecotypes may be due to environmental pressures such as the hydroperiod, salinity and nutrient availability.

A key finding in this study is the role of cortical aerenchyma in facilitating gas transport from stilt roots near the ground to stems. Larger aerenchyma intercellular spaces in stilt 3, suggest that these tissues are preferred to mobilized gases over the xylem, optimizing the gas exchange in *R. mangle*, particularly for scrub ecotype (Evans *et al.,* 2005; Colmer, 2003; Armstrong, 1979). Additionally, we found an extensive aerenchyma in the pith, which was connected to the cortical aerenchyma by rays in the xylem, then through dilated ray cells in

the axial parenchyma, which suggest that both aerenchyma tissues can exchange gases and improve long distance transport until upper portion of the stem or even the canopy, at least in scrub mangroves.

Furthermore, the structure of the schizogenic aerenchyma in the stem and stilt roots suggests a potential anatomical adaptation to gas flow as described by Yáñez-Espinosa and Ángeles (2022). Polygonal intercellular spaces forming honeycomb-like structures by rounded, Y- and I-shaped cells might reduce their resistance to air flow, while aerenchyma cells with large pits, druses and brachysclereids might reinforce the cortex biomechanics to resist high internal air pressures, maintaining rapid axial transport efficiently. Also, the periderm consisted of multiple compact layers of phellem, surrounding internal aerenchyma with abundant H-trichosclereids and druses, suggesting a structural adaptation for external protection and internal gas exchange. However, other root traits related to gas ingress and transport, such as radial oxygen loss (ROL), root porosity, suberization, must be considered in future research.

4.4.4. Barking up the right tree

It remains to be determined how biotic and abiotic factors influence the magnitudes of CH_4 and CO_2 emissions. However, this study highlights the crucial role of tree anatomy in regulating GHG fluxes and encourages the incorporation of anatomical features whenever possible. To the best of our knowledge, this is the first asses related to tree-CH_4 emissions in mangroves of the Americas, also the first reporting stilt CH_4 emissions. Our findings indicate that scrub *R. mangle* is the species with the highest CH_4 emission rates to the atmosphere, both from stems and stilt roots. Basin mangrove forest contributes to increased CO_2 fluxes through the stems of *A. germinans* and *L. racemosa*. The rainy season appears to limit CO_2 fluxes but enhance CH_4 emissions mediated by stilt roots and stems in mangroves. Notably, CH_4 and CO_2 fluxes are higher in near-ground tissues, such as third-order stilt roots, which have a greater proportion of bark aerenchyma. The marked differences in gas fluxes between ecotypes and the bark structure of the stem/stilt underscore the importance of considering ecological and anatomical variability when assessing the contributions of trees to global carbon budgets. Further investigation into the anatomical and physiological traits driving these differences could help refine models of GHG fluxes in tropical wetlands.

CAPÍTULO V.

DISCUSIÓN, CONCLUSIONES Y PERSPECTIVAS

Los datos de este capítulo forman parte de una revisión de literatura sobre las emisiones de metano y dióxido de carbono de tallos y raíces aéreas de mangles alrededor del mundo, *Overlooked losses of carbon in mangroves: CH_4 and CO_2 emissions beyond the soil*.

5.1. DISCUSIÓN GENERAL

Los protocolos actuales para la medición y cuantificación de gases de efecto invernadero en humedales, como los manglares, requiere de una continua revisión en aras de reducir las incertidumbres derivadas de aspectos aparentemente simples como el modelo de ajuste elegido. A través de una revisión de literatura de los últimos 10 años (Tabla S3 del Anexo I), se encontró que sólo el 9% de los estudios hace uso de un ajuste asintótico en las series de tiempo del aumento de la concentración de GHG acumulada en la cámara, para el cálculo de los flujos de GEI en tallos. Aunque ninguno de los ajustes es malo *per se*, la falta de precisión en las mediciones puede llevar a la subestimación. Se recomienda tomar en consideración los efectos combinados de las fugas y el gradiente de concentración al momento de calcular los flujos, sobre todo en mediciones discretas o cuando no se puede asegurar un perfecto sellado de la cámara con el árbol. Sin embargo, aún sin la medición de ambos fenómenos, es posible solucionar la pérdida de precisión utilizando las recomendaciones detalladas en el Capítulo II. De no considerar las fugas y/o usar métodos de ajuste propuestos, se podría incurrir en una subestimación de 40 ± 20 % y de 22 ± 22 % para el metano y el dióxido de carbono, respectivamente.

Sin duda alguna, los esfuerzos en mejorar nuestra línea base de emisiones naturales en ecosistemas debe continuar, poniendo particular cuidado al tipo de cámara y protocolo de medición. Si bien, no existe un método estandarizado universal, es importante considerar los efectos que pueden producir las fugas y la concentración de gases, estudiados en el Capítulo II, sobre las futuras cuantificaciones del balance global de carbono en los ecosistemas forestales. Asimismo, sería importante un consenso sobre un diagrama de flujo para la toma de decisiones y el reporte de las emisiones de GEI en árboles. Esto es particularmente relevante, debido a que aún es una frontera del conocimiento que requiere

el intercambio de conocimiento para mejorar nuestro entendimiento del ciclo del carbono en humedales.

Recientemente, los árboles fueron sido reconocidos como un componente más en el balance de carbono global. Sin embargo, la mayoría de los estudios de emisiones de gases de efecto invernadero en humedales tropicales se han realizado a nivel de suelo y, como resultado, los flujos de estos gases mediados por árboles no forman parte de las estimaciones locales y regionales actuales de GEI. Hasta donde sabemos, sólo hay nueve estudios que han cuantificado las emisiones de CH_4 o CO_2 mediados por árboles de manglar en China (Liao *et al.,* 2024; Zhang *et al.,* 2022; Gao *et al.,* 2021; He *et al.,* 2019; Zhang *et al.,* 2018), Taiwán (Yong *et al.,* 2024), Japón (Epron *et al.,* 2023), Australia (Jeffrey *et al.,* 2019) y Vietnam (Dušek *et al.,* 2021), que comprende nueve especies de mangle (Fig. 5.1).

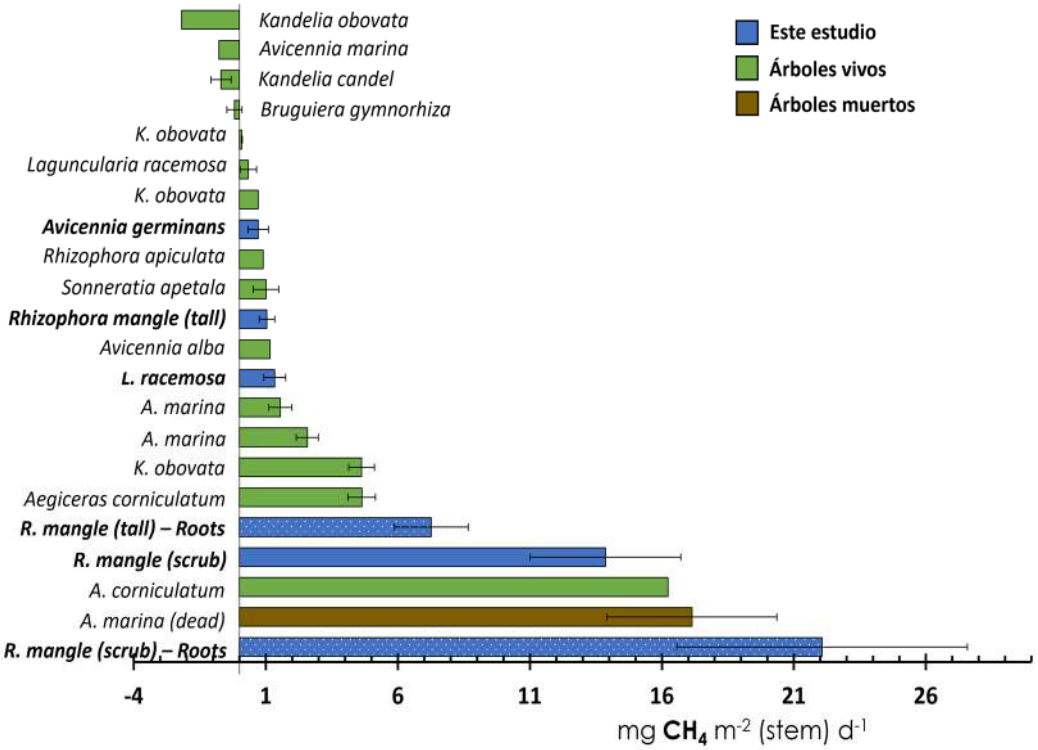

Fig. 5.1. Emisiones de metano en especies de mangle alrededor del mundo.

La presente tesis evidencia que los tallos y raíces aéreas (neumatóforos y zancos) de *R. mangle*, *A. germinans* y *L. racemosa* son una fuente de GEI. Estos hallazgos muestran que los zancos de manglar chaparro son los principales emisores (por área de tejido) de CH_4 reportadas hasta la fecha, incluso mayor que los árboles muertos de *A. marina* (Fig. 5.1).

En el caso de los flujos de CO_2 de los neumatóforos, estos variaron según el ecotipo, la interfaz y la temporada, obteniendo los mayores flujos de CO_2 en el manglar de franja, interfaz sedimento-aire y la temporada de sequía. Estas magnitudes son del orden de tres veces mayores que su contraparte el manglar chaparro en la interfaz agua-aire durante la temporada de lluvias. Además, fue posible inferir la contribución individual de los neumatóforos, así como la línea base de flujo de CO_2 sin neumatóforos con la información de las pendientes y los interceptos de los modelos, respectivamente. Finalmente, encontramos que la respiración (autotrófica) de los neumatóforos representa hasta 69.90% de los flujos de CO_2. Esta información servirá para entender la fisiología de las especies de mangle, mientras se mejoran los balances de carbono del ecosistema. Por tanto, alentamos a que se realicen más investigaciones en torno a estos aspectos, pues, la literatura aún es escasa, y no considera la variabilidad dada por el ecotipo o la interfaz de medición (Fig. 5.2).

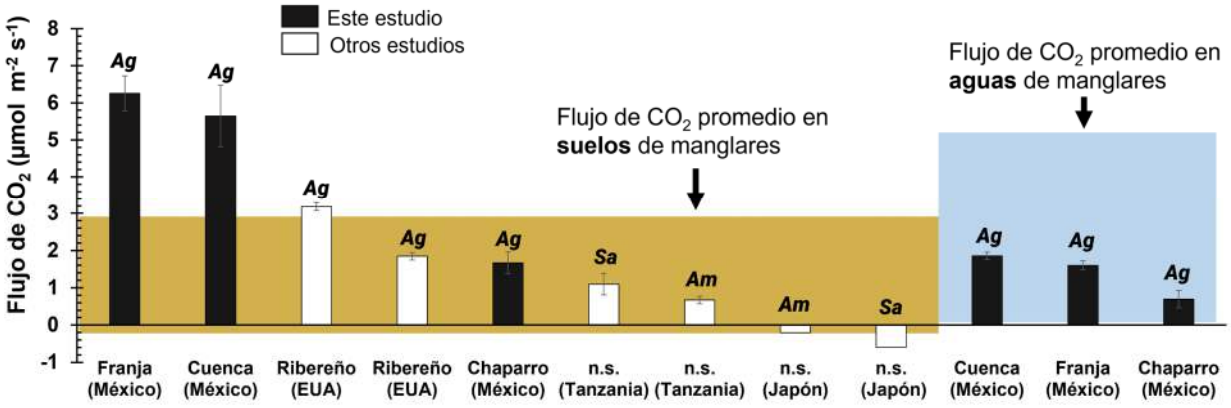

Fig. 5.2. Flujos de CO_2 en neumatóforos de mangles y ecotipos alrededor del mundo. *Ag* = *Avicennia germinans, Am* = *A. marina, Sa* = *Sonneratia alba,* y n.s. = no especificado. Las franjas café y azul representan los rangos de valores de los flujos de CO_2 promedio sin neumatóforos en suelos y agua sin neumatóforos, respectivamente.

También encontramos una mayor contribución de $CO_{2\text{-eq}}$ de *A. germinans* (Fig. 5.3), considerando tanto CH_4 como CO_2 de tallos y zancos (Cap. IV) y CO_2 de neumatóforos (Cap. III). Sin embargo, es importante señalar que la contribución de los zancos en *R. mangle* no debe descuidarse porque estas raíces de tercer orden son numerosas por árbol (hasta más de 30 unidades). Además, el mangle chaparro de *R. mangle* es el bosque de manglar más extenso de la península de Yucatán, donde se encuentra el 60% de toda el

área de manglar en México (Herrera-Silveira *et al.,* 2020), por lo que su papel en las emisiones de GEI debe ser evaluada a escalas más grandes.

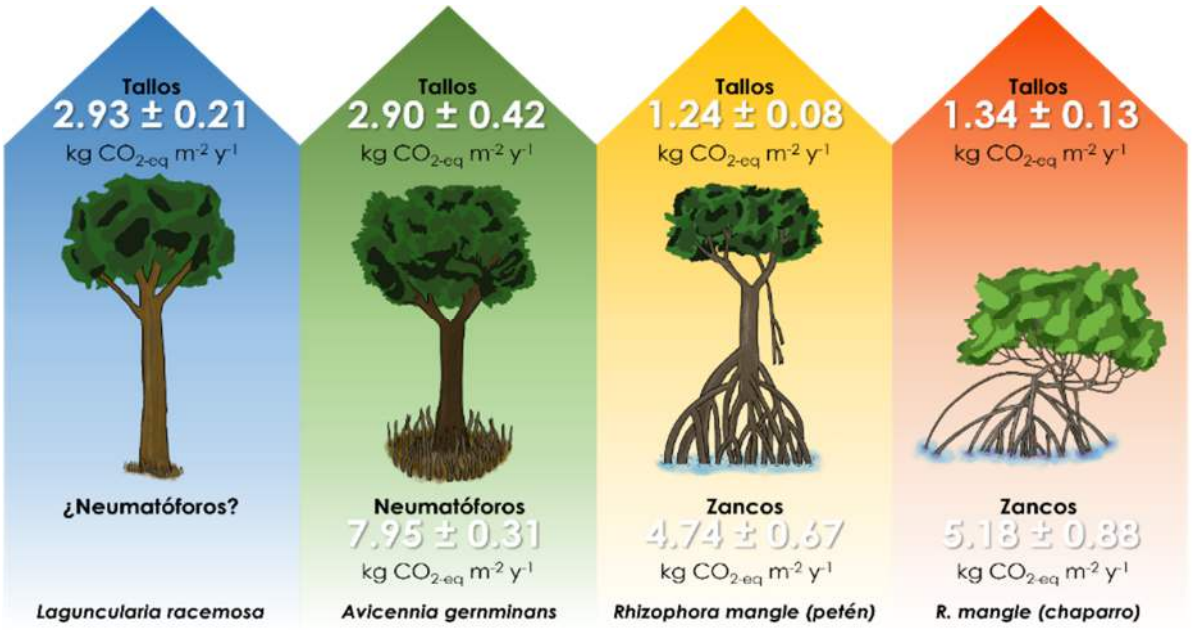

Fig. 5.3. Contribución de las especies de manglares a las emisiones de $CO_{2\text{-eq}}$ hacia la atmósfera, considerando sus tallos y raíces aéreas.

Por lo tanto, alentamos a que las estimaciones de carbono locales a globales incluyan a los árboles. Asimismo, que éstas sean precisas para mejorar los balances y modelos de carbono actuales. También es valioso subrayar que los manglares pueden actuar como fuentes o sumideros de CH_4 (Fig. 5.1) dependiendo de las condiciones fisicoquímicas y microambientales, por lo que deben entenderse desde sus bases fisiológicas y anatómicas. Nuestros resultados sugieren que la discriminación de las emisiones de GEI mediadas por tallos y raíces de árboles (así como por los métodos de medición) resultan en una subestimación significativa de las emisiones totales de GEI del ecosistema. En estudios anteriores se han encontrado emisiones de 0.02 ± 0.06 kg $CO_{2\text{-eq}}$ m^{-2} $año^{-1}$ de suelos en manglares de Celestún (González-Valencia et al., *en preparación*). Lo cual supone que las tasas de emisiones de tallos y zancos de *R. mangle* son del orden de 51 y 198 veces mayores, respectivamente. Finalmente, esperamos que los hallazgos presentados aquí sean relevantes para otros estudios en manglares de México y de las Américas.

5.2. CONCLUSIONES

La función de sumidero de carbono azul de los bosques de manglar, podrían ser parcialmente compensadas por las emisiones de CH_4 y CO_2 a través de tejidos que no se reportan en los balances y modelos de carbono, tales como tallos y raíces aéreas. Por lo tanto, pasar por alto estas pérdidas de carbono puede subestimar las emisiones de CH_4 y CO_2 en los manglares. En resumen, los principales aportes de esta tesis se enlistan a continuación:

- Las estimaciones de los flujos de CH_4 y CO_2 en tallos de árboles mediante cámaras cerradas presentan errores significativos debido a las fugas y la acumulación de gases. Estos efectos pueden subestimar las emisiones hasta en un 40% para CH_4 y un 22% para CO_2. La rugosidad de la corteza juega un papel importante en la variación de estos errores.

- Los neumatóforos de *Avicennia germinans* contribuyen de manera significativa a los flujos de CO_2, especialmente en los manglares de franja, donde se observan mayores tasas de emisión. Los flujos de CO_2 dependen de la densidad de neumatóforos, la salinidad, la interfaz de medición (suelo-aire o agua-aire), la temporada y el ecotipo de manglar, lo que indica que estos componentes deben ser incluidos en los modelos de carbono actuales.

- Los flujos de CH_4 y CO_2 variaron significativamente entre especies de mangle y estaciones del año. *Rhizophora mangle* chaparro mostró las mayores emisiones de CH_4, seguido de *R. mangle* del petén, mientras que *Laguncularia racemosa* y *A. germinans* contribuyeron más al flujo de CO_2. La temporada de lluvias incrementó las emisiones de CH_4 y disminuyó las de CO_2. Estas variaciones temporales y específicas son críticas para mejorar la precisión de los presupuestos de carbono en manglares.

- La anatomía de la corteza de zancos y tallos de *R. mangle* juega un papel clave en los flujos de CH_4 y CO_2. Los tejidos con mayor aerénquima, proporción de corteza y densidad de lenticelas presentaron los flujos más altos de GEI, lo que sugiere que estas estructuras tienen un impacto directo en la capacidad de intercambio gaseoso y, por lo tanto, en las estimaciones de GEI a escalas de bosque.

- Los resultados, en su conjunto, indican que las emisiones de CH_4 y CO_2 a través de tallos y raíces aéreas están subestimadas en los modelos actuales. Es fundamental incluir estos componentes arbóreos en los balances de carbono para obtener estimaciones más precisas de las contribuciones de los ecosistemas al ciclo global del carbono.

5.3. PERSPECTIVAS

- Consenso en las metodologías de medición y el reporte de resultados. Los errores asociados a los métodos de medición deben ser abordados mediante la validación de las técnicas actuales para la medición de GEI en árboles y la estandarización del reporte de resultados.

- Neumatóforos en los modelos de carbono. Se necesita una mayor investigación sobre el papel de los neumatóforos en la dinámica del CO_2, particularmente en su variabilidad estacional a escalas diurnas según el hidroperíodo.

- Interacción entre factores anatómicos y ambientales. El vínculo entre la anatomía del árbol y los factores ambientales debe ser investigado a mayor profundidad. La exploración de cómo la estructura anatómica y el microambiente influyen en la emisión de GEI puede abrir nuevas formas de entender la dinámica de carbono.

- Modelos de transporte de gases en manglares. Los mangles chaparros resultan ser un modelo perfecto para el estudio del transporte de gases a nivel de toda la planta, por lo que este es un paso siguiente a esta tesis.

- Estudio de otras especies, ecotipos y ecosistemas. Expandir este enfoque a otras especies de árboles de humedales y ecosistemas costeros permitirá generalizar los hallazgos y refinar las estrategias globales de mitigación del cambio climático en diferentes regiones y contextos ecológicos.

- Trayectorias de la restauración de manglares. Evaluar la dinámica de los flujos de GEI en tejidos vegetales durante diferentes etapas de restauración permitirá entender mejor el papel de secuestro de carbono de estos bosques y mejorar los planes estratégicos para la mitigación del cambio climático.

BIBLIOGRAFÍA

Adame, M. F., Cormier, N., Taillardat, P., Iram, N., Rovai, A., Sloey, T.M., Yando, E.S., Blanco-Libreros, J.F., Arnaud, M., Jennerjahn,T., Lovelock, C.E., Friess, D., Reithmaier, G.M.S., Buelow, C.A., Muhammad-Nor, S.M., Twilley, R.R., Ribeiro, R.A. (2024a). Deconstructing the Mangrove Carbon Cycle: Gains, Transformation, and Losses. Ecosphere 15(3): e4806. https://doi.org/10.1002/ecs2.4806.

Adame, M.F., R. Reef, R., Santini, N.S., Najera, E., Turschwell, M.P., Hayes, M.A., Masque, P., Lovelock, C.E. (2021). Mangroves in arid regions: Ecology, threats, and opportunities. Estuarine, Coastal and Shelf Science 248. https://doi.org/10.1016/j.ecss.2020.106796

Adame, M.F., Teutli, C., Santini, N.S., Caamal, J.P., Zaldívar-Jiménez, A., Hernández, R. & Herrera-Silveira, J.A. (2014). Root biomass and production of mangroves surrounding a karstic oligotrophic coastal lagoon. Wetlands 34:479488. https://doi.org/10.1007/s13157-014-0514-5

Aguirre, F.J., Squeo, F.A., López, D., Ramiro, D., Buma, B., Carvajal, D., Jaña, R., Casassa, G., Rozzi, R. (2021). Gradientes climáticos y su alta influencia en los ecosistemas terrestres de la Reserva de la Biosfera Cabo de Hornos, Chile. Anales Instituto de la Patagonia. https://doi.org/10.22352/AIP202149012

Aiga, I., Nakano, Y., Ohki, S., Kitaya, Y., Kabuki, K. (1995). Photosynthetic CO_2 fixation in pneumatophores of gray mangrove, *Avicennia marina*. Environ. Control in Biol. 33 (2):97-https://doi.org/101. 10.2525/ecb1963.33.97

Akhand, A. Chanda, A., Das, S., Hazra, S., Kuwae, T. (2019). CO_2 fluxes in mangrove ecosystems. 185 – 221 pp. In: Kuwae, T. y Hori, M. (eds.) Blue carbon in shallow coastal ecosystems, carbon dynamics, policy, and implementation. Springer Nature Singapore Pte. Ltd. https://doi.org/10.1007/978-981-13-1295-3_7

Al-Khayat, J.A., Alatalo, J.M. (2019). Relationship Between Tree Size, Sediment Mud Content, Oxygen Levels, and Pneumatophore Abundance in the Mangrove Tree Species *Avicennia Marina* (Forssk.) Vierh. J. Mar. Sci. Eng. 9, 100. https://doi.org/10.3390/jmse9010100

Allen, D.E., Dalal, R.C., Rennenberg, H., Meyer, R.L., Reeves, S., y S. Schmidt. (2007). Spatial and temporal variation of nitrous oxide and methane flux between subtropical mangrove sediments and the atmosphere. Soil Biol. Biochem. 39, 622–631.

Alongi, D. (2012). Carbon sequestration in mangrove forests. Carbon Manag. 3:313–322

Alongi, D.M. (2014). Carbon cycling and storage in mangrove forests. Ann Rev Mar Sci. 6: 195-219. https://doi.org/10.1146/annurev-marine-010213-135020.

Alongi, D.M., Wattayakorn, G., Pfitzner, J., Tirendi, F., Zagorskis, I., Brunskill, G.J., y B.F. Clough. (2001). Organic carbon accumulation and metabolic pathways in sediments of mangrove forests in southern Thailand. Mar. Geol. 179, 85–103

Alongi, D., y Mukhopadhyay, S. (2015). Contribution of mangroves to coastal carbon cycling in low latitude seas. Agric For Meteorol 213:266–272.

Alvarado-Barrientos, M.S., López-Adame, H., Lazcano-Hernández, H. E., Arellano-Verdejo, J., Hernández-Arana, H. A. (2021). Ecosystem-atmosphere exchange of CO_2, water, and energy in a basin mangrove of the northeastern coast of the Yucatan Peninsula. Journal of Geophysical Research: Biogeosciences, 126, e2020JG005811. https://doi.org/10.1029/2020JG005811

Anderson, B., Barlett, K., Frolking, S., Hayhoe, K., Jenkins, J. y Salas, W. (2010). Methane and Nitrous Oxide Emissions from Natural Sources. Office of Atmospheric Programs, US EPA, EPA 430-R-10-001. Washington, D.C.

Angeles, G., López–Portillo, J.and Ortega-Escalona, F. Functional anatomy of the secondary xylem of roots of the mangrove Laguncularia racemosa (L.) Gaertn. (Combretaceae). Trees 16, 338–345 (2002). https://doi.org/10.1007/s00468-002-0171-9

Anttila, J., Tikkasalo, O.-P., Hölttä, T., Lintunen, A., Vainio, E., Leppä, K. (2024) Model of methane transport in tree stems: Case study of sap flow and radial diffusion. Plant, Cell & Environment, 47: 140–155. https://doi.org/10.1111/pce.14718

Arellano-Martín, F., Dupuy, J. M., Us-Santamaría, R., Andrade, J.L. (2022). Soil CO_2 efflux fluctuates in three different annual seasons in a semideciduous tropical forest in Yucatan, Mexico. Terra Latinoamericana, 40, e968. https://doi.org/10.28940/terra.v40i0.968

Armstrong W. (1979) Aeration in higher plants. Advances in Botanical Research 7, 225–332.

Armstrong W. y J. Armstrong. (2005). Stem photosynthesis not pressurized ventilation is responsible for light-enhanced oxygen supply to submerged roots of alder (Alnus glutinosa). Annals of Botany 96: 591–612.

Bain, W.G., Hutrya, L., Patterson, D.C., Bright, A.V., Daube, B.C., Munger, J.W., Wofsy, S.C. (2005). Wind-induced error in the measurement of soil respiration using closed dynamic chambers. Agricultural and Forest Meteorology 131 (3–4), 225–232. https://doi.org/10.1016/j.agrformet.2005.06.004

Barba, J., Bradford, M.A., Brewer, P.E., Bruhn, D., Covey, K., van Haren, J., Megonigal, J.P., Mikkelsen, T.N., Pangala, S.R., Pihlatie, M., Poulter, B., Rivas-Ubach, A., Schadt, C. W., Terazawa, K., Warner, D. L., Zhang, Z., Vargas, R. (2019a). Methane emissions from tree stems: a new frontier in the global carbon cycle. New Phytologist 222, 18–28. https://doi.org/10.1111/nph.15582

Barba, J., Poyatos, R. y Vargas, R. 2019b. Automated measurements of greenhouse gases fluxes from tree stems and soils: magnitudes, patterns and drivers. Scient. Rep. 9: 4005.

Bastviken, D., Treat, C.C., Pangala, S.R., Gauci, V., Enrich-Prast, A., Karlson, M., Gålfalk, M., Brandini-Romano, M., and Oliveira-Sawakuchi, H. (2022). The importance of plants for methane emission at the ecosystem scale. Aquatic Botany 184 (103596). https://doi.org/10.1016/j.aquabot.2022.103596.

Beckett, H. A. A., Webb, D., Turner, M., Sheppard, A., Ball, M. C., (2023). Bark water uptake through lenticels increases stem hydration and contributes to stem swelling. Plant, Cell & Environment, 1–19. https://doi.org/10.1111/pce.14733

Bloemen, J., McGuire, M.A., Aubrey, D.P., Teskey, R.O., Steppe, K. (2013). Transport of root-respired CO2 via the transpiration stream affects aboveground carbon assimilation and CO2 efflux in trees. New Phytologist 197: 555-565. https://doi.org/10.1111/j.1469-8137.2012.04366.x

Bloemen, J., Agneessens, L., Meulebroek, L., Aubrey, D.P., McGuire, M.A., Teskey, R.O. y K. Steppe. (2014). Stem girdling affects the quantity of CO2 transported in xylem as well as CO2 efflux from soil. New Phytologist 201: 897-907.

Bouillon, S., Borges, A., Castañeda-Moya, E., Diele, K., Dittmar, T., Duke, N.C, Kristensen, E, Lee, S, Marchand, C., Middleburg, J., Rivera-Monroy, V., Smith, T. III, Twilley, R. (2008). Mangrove production and carbon sinks: A revision of global budget estimates. Global Biogeochem Cycles 22, GB2013. https://doi.org/10.1029/2007GB003052

Bowman, W.P., Barbour, M.M., Turnbull, M.H., Tissue, D.T., Whitehead, D. y K.L. Griffin. (2005). Sap flow rates and sapwood density are critical factors in within- and between-tree variation in CO2 efflux from stems of mature Dacrydium cupressinum trees. New Phytologist 167: 815–828.

Bréchet, L.M., Daniel, W., Stahl, C., Burban, B., Goret, J-Y, Salomón, R.L. Janssens, I.A. (2021). Simultaneous tree stem and soil greenhouse gas (CO_2, CH_4, N_2O) flux measurements: a novel design for continuous monitoring towards improving flux estimates and temporal resolution. New Phytologist 230: 2487–2500. https://doi.org/10.1111/nph.17352

Call, M., D.T. Maher, D.T., Santos, I.R., Ruiz-Halpern, R., Mangion, P., Sanders, C.J., Erler, D.V., Oakes, J.M., Rosentreter, J., Murray, R., Eyre, B.D. (2015). Spatial and temporal variability of carbon dioxide and methane fluxes over semi-diurnal and spring–neap–spring timescales in a mangrove creek. Geochim. Cosmochim. Acta 150:211–225. https://doi.org/10.1016/j.gca.2014.11.023

Campioli, M., Malhi. Y., Vicca, S., Luyssaert, S., Papale, D., Peñuelas, J., Reichstein, M., Migliavacca, M., Arain, M.A., Janssens, I.A. (2016). Evaluating the convergence between eddy-covariance and biometric methods for assessing carbon budgets of forests. Nature Communications 7: 13717. https://doi.org/10.1038/ncomms13717

Cattiaux, J., Ribes, A., & Cariou, E. (2024). How extreme were daily global temperatures in 2023 and early 2024? Geophysical Research Letters, 51, e2024GL110531. https://doi.org/10.1029/2024GL110531

Cernusak, L.A. y J.D. Marshall. (2000). Photosynthetic refixation in branches of Western white pine. Functional Ecology 14: 300–311.

Chambers, L., Guevara, R., Boyer, J.N., Troxler, T., Davis, S.E. (2016). Effects of Salinity and Inundation on Microbial Community Structure and Function in a Mangrove Peat Soil. Wetlands 36:361-371. https://doi.org/10.1007/s13157-016-0745-8

Chauhan, R., Ramanathan, AL. y T.K. Adhya. (2008). Assessment of methane and nitrous oxide flux from mangroves along Eastern coast of India. Geofluids 8: 321-332.

Chapin III, F.S., McFarland, J., McGuire, D., Euskirchen, E. S., Ruess, R. W. y K. Kielland. (2009). The changing global carbon cycle: linking plant-soil carbon dynamics to global consequences. Journal of Ecology (97): 840-850.

Chen, G., Tam, N., Ye, Y. (2012). Spatial and seasonal variations of atmospheric N_2O and CO_2 fluxes from a subtropical mangrove swamp and their relationships with soil characteristics. Soil Biol Biochem 48:175–181. https://doi.org/10.1016/j.soilbio.2012.01.029

Chen, G.C., Tam, N.F.Y., Ye, Y. (2010). Summer fluxes of atmospheric greenhouse gases N_2O, CH_4 and CO_2 from mangrove soil in South China. Sci Total Environ 408 (13):2761–2767. https://doi.org/10.1016/j.scitotenv.2010.03.007

Chen, L. (2016). Pneumatophores. In: Kennish, M.J. (eds) Encyclopedia of Estuaries. Encyclopedia of Earth Sciences Series. Springer, Dordrecht. https://doi.org/10.1007/978-94-017-8801-4_282

Chen, G., Chen, B., Yu, D., Tam, N.F.Y, Ye, Y. y S. Chen. (2016). Soil greenhouse gas emissions reduce the contribution of mangrove plants to the atmospheric cooling effect. Environ Res Lett 11(12):124019.

Chen, G.C., Ulumuddin, Y.I.; Chen, S.Y.; Chen, B., Ye, Y., Ou, D.Y., Ma, Z.Y., Huang, H., y J. K. Wang. (2014). Rich soil carbon and nitrogen but low atmospheric greenhouse gas fluxes from North Sulawesi mangrove swamps in Indonesia. Sci. Total Environ. 2014, 487, 91–96.

Cisneros-de la Cruz, D.J., Martínez-Castillo, J., Herrera-Silveira, J.A., Yáñez-Espinosa, L., Ortiz-García, M., Us-Santamaria, R., Andrade, J.L. (2018). Short-distance barriers affect genetic variability of Rhizophora mangle L. in the Yucatan Peninsula. Ecol Evol. 8: 11083–11099. https://doi.org/10.1002/ece3.4575

Colmer, T.D. (2003), Long-distance transport of gases in plants: a perspective on internal aeration and radial oxygen loss from roots. Plant, Cell & Environment, 26: 17-36. https://doi.org/10.1046/j.1365-3040.2003.00846.x

CONAGUA – Comisión Nacional del Agua. (2023). Red de Estaciones Climatológicas Automáticas. Servicio Meteorológico Nacional. https://smn.conagua.gob.mx/es/ (accessed on 24th July 2023).

Cotovicz, L.C., Abril, G., Sanders, C.J., Tait D.R., Maher, D.T., Sippo, J.Z., Holloway, C., Yau, Y.Y., Santos, I.R. (2024). Methane oxidation minimizes emissions and offsets to carbon burial in mangroves. Nat. Clim. Chang. 14: 275–281. https://doi.org/10.1038/s41558-024-01927-1

Covey, K.R., Megonigal, J.P. (2019). Methane production and emissions in trees and forests. New Phytologist 222, 35–51. https://doi.org/10.1111/nph.15624

Dahdouh-Guebas F., Kairo J.G., De Bondt R., Koedam, N. (2007). Pneumatophore height and density in relation to microtopography in the grey mangrove *Avicennia marina*. Belg. J. Bot. 140 (2): 213-221. http://www.jstor.org/stable/20794640

Dalal, R. y Allen, D. 2008. Turner review No. 18. Greenhouse gas fluxes from natural ecosystems. Aust. J. Bot. 56, 369.

De Simone, O., Haase, K., Muller, E., Junk, W.J., Hartmann, K., Schreiber, L. y W. Schmidt. (2003). Apoplasmic barriers and oxygen transport properties of hypodermal cell walls in roots from four Amazonian tree species. Plant Physiology 132: 206–217.

DMC – Dirección Meteorológica de Chile. (2023). Datos históricos de Estaciones Meteorológicas Automatizadas. Dirección General de Aeronáutica Civil. https://climatologia.meteochile.gob.cl/ (accessed on 24th July 2023).

Donato D.C., Kauffman J.B., Murdiyarso D., Kurnianto S., Stidham M., Kanninen, M. (2011). Mangroves among the most carbon-rich forests in the tropics. Nature Geoscience 4: 293. https://doi.org/10.1038/ngeo1123

Drew, M.C., He, C.J. y P.W. Morgan. (2000). Programmed cell death and aerenchyma formation in roots. Trends in Plant Science 5: 123-127.

Dušek, J., Nguyen, V.X., Le, T.X., Pavelka, M. (2021). Methane and carbon dioxide emissions from different ecosystems at the end of dry period in South Vietnam. Tropical Ecology 62: 1–16. https://doi.org/10.1007/s42965-020-00118-1

Epron, D., Mochidome, T., Tanabe, T., Dannoura, M., Sakabe, A. (2022). Variability in stem methane emissions and wood methane production of different tree species in a cold temperate mountain forest. Ecosystems. https://doi.org/10.1007/s10021-022-00795-0

Epron, D., Mochidome, T., Bassar, A. T. M. Z., and Suwa, R. (2023). Variability in methane emissions from stems and buttress roots of Bruguiera gymnorrhiza trees in a subtropical mangrove forest. Ecological Research, 1–11. https://doi.org/10.1111/1440-1703.12415

Evans, D.E. (2004). Aerenchyma formation. New Phytologist, 161: 35-49. https://doi.org/10.1046/j.1469-8137.2003.00907.x

Evans L.S., Okawa, Y. and Searcy, D. (2005). Anatomy and morphology of red mangrove (*Rhizophora mangle*) plants in relation to internal airflow. The J. of the Torrey Botanical Society, 132 (4) :537-550. https://doi.org/10.3159/1095-5674

Feller O.C., McKee, K.L., Whigham, D.F., O'Neill, J.P. (2003). Nitrogen vs. phosphorus limitation across an ecotonal gradient in a mangrove forest. Biogeochemistry 62:145-175. https://doi.org/10.1023/A:1021166010892

Feng, H., Guo, J., Ma, X., Han, M., Kneeshaw, D., Sun, H., Malghani, S., Chen, H. and Wang, W. (2022). Methane emissions may be driven by hydrogenotrophic methanogens inhabiting the stem tissues of poplar. New Phytol, 233: 182-193. https://doi.org/10.1111/nph.17778

Flanagan, L.B., Nikkel, D.J., Scherloski, L.M., Tkach, R.E., Smits, K.M., Selinger, L.B., Rood, S.B. (2021). Multiple processes contribute to methane emission in a riparian cottonwood forest ecosystem. New Phytologist 229: 1970-1982. https://doi.org/10.1111/nph.16977

Fraser-McDonald, A., Boardman, C., Gladding, T., Burnley, S., Gauci, V. (2022). Methane emissions from forested closed landfill sites: variations between tree species and landfill management practices. Science of The Total Environment 838 (2). https://doi.org/10.1016/j.scitotenv.2022.156019

Feller, I.C. y M. Sitnik (Eds.). (1996). Mangrove ecology: a manual for a field course Washington, D.C. 135 p.

Friedlingstein, P., Jones, M.W., O'Sullivan, M., Andrew, R.M., Bakker, D.C.E., Hauck, J., Le Quéré, C., Peters, G.P., Peters, W., Pongratz, J., Sitch, S., Canadell, J.G., Ciais, P., Jackson, R.B., Alin,

S.R., Anthoni, P., Bates, N.R., Becker, M., Bellouin, ... Zeng, J. (2022). Global Carbon Budget 2021. Earth Syst. Sci. Data, 14, 1917–2005. https://doi.org/10.5194/essd-14-1917-2022

Friess, D. A., Adame, M. F., Adams, J. B., Lovelock, C. E. (2022). Mangrove forests under climate change in a 2 °C world. WIREs Climate Change, 13(4), e792. https://doi.org/10.1002/wcc.792

Gao, C.H., Zhang, S., Ding, Q.S., Wei, M.Y., Li, H., Li, J., Wen, C., Gao, G.F., Liu, Y., Zhou, J.J., Zhang, J.Y., You, Y.P., Zheng, H.L. (2021). Source or sink? A study on the methane flux from mangroves stems in Zhangjiang estuary, southeast coast of China. Science of The Total Environment 788. https://doi.org/10.1016/j.scitotenv.2021.147782

Gansert, D. y M. Burgdorf. (20059. Effects of xylem sap flow on carbon dioxide efflux from stems of birch (Betula pendula Roth). Flora 200: 444–455.

Gartner, B.L., Moore, J.R. y B.A. Gardiner. (2004). Gas in stems: abundance and potential consequences for tree biomechanics. Tree Physiology 24: 1239-1250.

Ge, M., Korrensalo, A., Laiho, R., Kohl, L., Lohila, A., Pihlatie, M., Li, X., Laine, A.M. Anttila, J., Putkinen, A., Wang, W., Koskinen, M. (2024). Plant-mediated CH_4 exchange in wetlands: A review of mechanisms and measurement methods with implications for modelling. Science of The Total Environment 914 (169662). https://doi.org/10.1016/j.scitotenv.2023.169662

Giri, C., Ochieng, E., Tieszen, L., Zhu, Z., Singh, A., Loveland, T., Masek, J. y N. Duke. (2011). Status and distribution of mangrove forests of the world using earth observation satellite data. Global Ecology and Biogeography (20): 154-159.

Hanson, P.J., Edwards, N.T., Garten, C.T., Andrews, J.A. (2000). Separating root and soil microbial contributions to soil respiration: a review of methods and observations. Biogeochemistry 48, 115–146. https://doi.org/10.1023/A:1006244819642

He, Y., Guan, W., Xue, D., Liu, L., Peng, C., Liao, B.,Hu, J., Zhu, Q., Yang, Y., Wang, X., Zhou, G., Wu, Z., Chen, H. (2019). Comparison of methane emissions among invasive and native mangrove species in Dongzhaigang, Hainan Island. Science of The Total Environment 697. https://doi.org/10.1016/j.scitotenv.2019.133945

Heinemeyer, A. y McNamara, N.P. (2011). Comparing the closed static versus the closed dynamic chamber flux methodology: Implications for soil respiration studies. Plant Soil 346:145–151.

Herrera-Silveira, J.A., Pech-Cardenas, M.A, Morales-Ojeda, S.M., et al. (2020). Blue carbon of Mexico, carbon stocks and fluxes: a systematic review. PeerJ. 2020; 8:e8790. https://doi.org/10.7717/peerj.8790

Howard, J., Hoyt, S., Isensee, K., Telszewski, M., Pidgeon, E., eds . 2014. Coastal blue carbon : methods for assessing carbon stocks and emissions factors in mangroves, tidal salt marshes, and seagrasses. : 180p. Arlington, VA, USA: Conservation International, Intergovernmental Oceanographic Commission ofUNESCO, International Union for Conservation of Nature.

Hutchinson, G., Livingston, G. (2001). Vents and seals in non-steady-state chambers used for measuring gas exchange between soil and the atmosphere. Eur. J. Soil Sci., 52, 675-682. https://doi.org/10.1046/j.1365-2389.2001.00415.x

Hutchinson, G.L., Mosier, A.R. (1981). Improved soil cover method for field measurement of nitrous oxide fluxes. Soil Sci. Soc. Am. J. 45:311–316. https://doi.org/10.2136/sssaj1981.03615995004500020017x

Inglett, K., Chanton, J., y P. Inglett. (2013). Methanogenesis and methane oxidation in wetlands soils. In: DeLaune, R.D., Reddy, K.R., Richardson, C.J. y J.P. Megonigal (Eds). Methods in biogeochemistry of wetlands. Soil Science Society of America. USA. 1020p.

IPCC (2021) Summary for policymakers Climate Change 2021: The Physical Science Basis. Contribution of Working Group I to the Sixth Assessment Report of the Intergovernmental Panel on Climate Change ed V Masson-Delmotte et al.,

Jackson, R.B., Saunois, M., Martinez, A., Canadell, J.G., Yu, X., Li, M., Poulter, B., Raymond, P.A., Regnier, P., Ciais, P., Davis S.J., Patra, P.K. (2024). Human activities now fuel two-thirds of global methane emissions. Environmental Research Letters 19 (10) 101002. https://doi.org/10.1088/1748-9326/ad6463

Jacotot, A., Marchand, C., Allenbach, M. (2018). Tidal variability of CO_2 and CH_4 emissions from the water column within a *Rhizophora* mangrove forest (New Caledonia). Sci. Total Environ. 631–632: 334-340. https://doi.org/10.1016/j.scitotenv.2018.03.006

Jeffrey, L.C., Maher, D.T., Tait, D.R., Johnston, S.G. (2020). A Small Nimble In Situ Fine-Scale Flux Method for Measuring Tree Stem Greenhouse Gas Emissions and Processes (S.N.I.F.F). Ecosystems 23: 1676–1689. https://doi.org/10.1007/s10021-020-00496-6

Jeffrey, L.C., Reithmaier, G., Sippo, J.Z., Johnston, S.G., Tait, D.R., Harada, Y., Maher, D.T. (2019). Are methane emissions from mangrove stems a cryptic carbon loss pathway? Insights from a catastrophic forest mortality. New Phytologist 224: 146-154. https://doi.org/10.1111/nph.15995

Jeffrey, L.C., Maher, D.T., Tait, D.R., Reading, M.J., Chiri, E., Greening, C. and Johnston, S.G. (2021a). Isotopic evidence for axial tree stem methane oxidation within subtropical lowland forests. New Phytol, 230: 2200-2212. https://doi.org/10.1111/nph.17343

Jeffrey, L., Maher, D.T., Chiri, E., Leung, P.M., Nauer, P.A., Arndt, S.K., Tait, D..R., Greening, C. y S.G. Johnston. 2021b. Bark-dwelling methanotrophic bacteria decrease methane emissions from trees. Nature Communications. 12:2127.

Jeffrey, L. C., Moras, C. A., Tait, D. R., Johnston, S. G., Call, M., Sippo, J. Z. (2023). Large methane emissions from tree stems complicate the wetland methane budget. Journal of Geophysical Research: Biogeosciences, 128, e2023JG007679. https://doi.org/10.1029/2023JG007679

Jeffrey, L.C., Johnston, S.G., Tait, D.R., Dittmann, J., Maher, D.T. (2024). Rapid bark mediated tree stem methane transport occurs independently of the transpiration stream in *Melaleuca quinquenervia.* New Phytol, 242: 49-60. https://doi.org/10.1111/nph.19404

Jiang, J., Hu, J., Xu, X., Li, Y., Sheng, J. (2023). Effect of near-surface winds on the measurement of forest soil CO2 fluxes using closed air chambers. Frontiers in Ecology and Evolution 11:1163704. https://doi.org/10.3389/fevo.2023.1163704

Juszczak, R. (2013). Biases in Methane Chamber Measurements in Peatlands. Int. Agrophys. 27(2), 159–168. https://doi.org/10.2478/V10247-012-0081-Z

Katayama, A., Kume T, Komatsu H, Ohashi M, Nakagawa M, Yamashita M, et al. (2009). Effect of forest structure on the spatial variation in soil respiration in a Bornean tropical rainforest. Agr Forest Meteorol. ;149:1666–73. https://doi.org/10.1016/j.agrformet.2009.05.007

Kauffman, J. B., and D. C. Donato. 2012. Protocols for the measurement, monitoring, & reporting of structure, biomass and carbon stocks in mangrove forests. Working Paper 86. Center for International Forest Research. CIFOR, Bogor, Indonesia.

Kirui, B, Huxham, M, Kairo, J.G., Mencuccini, M. y M.W. Skov. (2009). Seasonal dynamics of soil carbon dioxide flux in a restored young mangrove plantation at Gazi Bay. In: Hoorweg J, Muthiga N (eds) Advances in coastal ecology. African Studies Centre Publisher, Leiden, pp 122–130.

Kitaya Y, Yabuki K, Kiyota M, Tani A, Hirano T., Aiga I. (2002). Gas Exchange and oxygen concentration in pneumatophores and prop roots of four mangrove species. Trees 16:155–158. https://doi.org/10.1007/s00468-002-0167-5

Kohl, L., Koskinen, M., Polvinen, T., Tenhovirta, S., Rissanen, K., Patama, M., Zanetti, A., Pihlatie, M. (2021). An automated system for trace gas flux measurements from plant foliage and other plant compartments. Atmospheric Measurement Techniques 14: 4445–4460. https://doi.org/10.5194/amt-14-4445-2021

Kozlowski, T. (1997). Responses of woody plants to flooding and salinity. Tree physiology monograph 1. https://doi.org/10.1093/treephys/17.7.490

Krauss, K. W., Lovelock, C. E., McKee, K. L., López-Hoffman, L., Ewe, S., Sousa, W.P. (2008). Environmental drivers in mangrove establishment and early development: a review. Aquatic Botany 89: 105–127. https://doi.org/10.1016/j.aquabot.2007.12.014

Krauss, K.W., Whitbeck, J.L. (2012). Soil greenhouse gas fluxes during wetland forest retreat along the lower Savannah River, Gerogia (USA). Wetlands; 32:73–81. https://doi.org/10.1007/s13157-011-0246-8

Kristensen, E., Bouillon, S., Dittmar, T., Marchand, C. (2008). Organic carbon dynamics in mangrove ecosystems: a review. Aquat. Bot. 89, 201–219. https://doi.org/10.1016/j.aquabot.2007.12.005

Kristensen, E., Flindt, M., Ulomi, S., Borges, A., Abril, G., Bouillon, S. (2008). Emission of CO_2 and CH_4 to the atmosphere by sediments and open waters in two Tanzanian mangrove forests. Mar Ecol Prog Ser 370:53–67. https://doi.org/10.3354/meps07642

Kristensen, E., Valdemarsen, T., de Moraes, P. C., Güth, A. Z., Sumida, P. Y. G., Quintana, C.O. (2022). Pneumatophores and crab burrows increase CO_2 and CH_4 emission from sediments in two Brazilian fringe mangrove forests. Marine Ecology Progress Series, 698, 29-39. https://doi.org/10.3354/meps14153

Krithika, K., Purjava, R., Ramesh., R. (2008). Fluxes of methane and nitrous oxide from an Indian mangrove. Current Science 94(2):218-224. http://www.jstor.org/stable/24101861

Kutzbach, L., Schneider, J., Sachs, T., Giebels, M., Nykänen, H., Shurpali, N.J., Martikainen, P.J., Alm, J., Wilmking, M. (2007). CO_2 Flux Determination by Closed-Chamber Methods Can Be Seriously Biased by Inappropriate Application of Linear Regression. Biogeosciences 4(6) : 1005–1025. https://doi.org/10.5194/BG-4-1005-2007

Lambers, H., Oliveira, R. S. (2019). Plant physiological ecology. Third edition. Springer Nature. Cham, Switzerland. 736 p.

Leal, M., Spalding, M.D. (2022). The State of the World's Mangroves 2022. Global Mangrove Alliance.92 pp.

Lendzian, K.J. (2006). Survival strategies of plants during secondary growth: barrier properties of phellems and lenticels towards water, oxygen, and carbon dioxide. Journal of Experimental Botany 57: 2535–2546.

Leon, E., Vargas, R., Bullock, S., Lopez, E., Panosso, A. R., La Scala Jr, N. (2014). Hot spots, hot moments, and spatio-temporal controls on soil CO_2 efflux in a water-limited ecosystem. Soil Biology and Biochemistry, 77, 12-21. http://dx.doi.org/10.1016/j.soilbio.2014.05.029

Leopold, A., Marchand, C., Deborde, J., Chaduteau, C. y M. Allenbach. (2013). Influence of mangrove zonation on CO2 fluxes at the sediment–air interface (New Caledonia). Geoderma 202:62–70.

Li, HL., Zhang, XM., Deng, FD., Han X.G., Xiao, C.W. and Wang, P. (2020). Microbial methane production is affected by secondary metabolites in the heartwood of living trees in upland forests. Trees 34, 243–254. https://doi.org/10.1007/s00468-019-01914-6

Liao, X., Wang, Y., Malghani, S., Zhu, X., Cai, W., Qin, Z., Wang, F. (2024). Methane and nitrous oxide emissions and related microbial communities from mangrove stems on Qi'ao Island, Pearl River Estuary in China. Science of The Total Environment 915 (170062). https://doi.org/10.1016/j.scitotenv.2024.170062

Lin, C.W., Kao, Y.C., Chou, M.C., Wu, H.H., Ho, C.W., Lin, H.J. (2020). Methane emissions from subtropical and tropical mangrove ecosystems in Taiwan. Forests, 11, 470. https://doi.org/10.3390/f11040470

Lin, C.W., Kao, Y.C., Lin, W.J., Ho, C.W., Lin, H.J. (2021). Effect of pneumatophore density on methane emissions in mangroves. Forests 12, 314. https://doi.org/10.3390/f12030314

Litton, C.M., Giardina, C.P., Albano, J.K., Long, M.S., Asner, G.P. (2011). The magnitude and variability of soil-surface CO_2 efflux increase with mean annual temperature in Hawaiian tropical montane wet forests. Soil Biol Biochem 2011;43:2315–23. https://doi.org/10.1016/j.soilbio.2011.08.004

Lopes de Gerenyu, V.O., Yu. A. Kurbatova, Y.A., Kurganova, I.N., Tiunov, A.V., Anichkin, A.Y., Myakshina, T.N., Kuznetsov, A.N. (2011). Daily and seasonal dynamics of CO_2 fluxes from soils under different stands of monsoon tropical forest. Eurasian Soil Science, 44(9), 984-990. https://doi.org/10.1134/S1064229311090067

Lovelock, C.E. (2008). Soil respiration and belowground carbon allocation in mangrove forests. Ecosystems 11:342–354. https://doi.org/10.1007/s10021-008-9125-4

Lovelock, C.E. y C.M. Duarte. (2019). Dimensions of Blue Carbon and emerging perspectives. Biology Letters 15: 20180781.

Lovelock, C., Ruess, R. y Feller, I. (2011). CO2 efflux from cleared mangrove peat. PLoS One 6(6):e21279.

Lovelock, C.E., Feller, I.C., McKee, K.L., Engelbrechts, M.L., Ball, M.C. (2004). The effect of nutrient enrichment on growth, photosynthesis and hydraulic conductance of scrub mangroves in Panama. Functional Ecology 18:25-33. https://doi.org/10.1046/j.0269-8463.2004.00805.x

Lugo, A.E., Snedaker, S.C. (1974). The ecology of mangroves. Annual Review of Ecology and Systematics 5: 39-64. https://doi.org/10.1146/annurev.es.05.110174.000351

Luo, Y., Zhou, X. (2006). Soil respiration and the environment. Elsevier, Burlington, MA., EUA. https://doi.org/10.1016/B978-0-12-088782-8.X5000-1

Määttä, T., and Malhotra, A. (2024). The hidden roots of wetland methane emissions. Global Change Biology, 30, e17127. https://doi.org/10.1111/gcb.17127

Machacova, K., Warlo, H., Svobodová, K., Agyei, T., Uchytilová, T., Horáček, P., Lang, F. (2023). Methane emission from stems of European beech (Fagus sylvatica) offsets as much as half of methane oxidation in soil. New Phytologist 238: 584-597. https://doi.org/10.1111/nph.18726

Maher, D.T., Cowley, K., Santos, I.R., Macklin, P., Eyre, B.D. (2015). Methane and carbon dioxide dynamics in a subtropical estuary over a diel cycle: insights from automated in situ radioactive and stable isotope measurements. Mar. Chem. 168:69–79. https://doi.org/10.1016/j.marchem.2014.10.017

Maier, M., Mayer, S., Laemmel, T. (2019). Rain and wind affect chamber measurements. Agricultural and Forest Meteorology 279. https://doi.org/10.1016/j.agrformet.2019.107754

Maier, M., Machacova, K., Lang, F., Svobodova, K. y O. Urban. (2018). Combining soil and tree-stem flux measurements and soil gas profiles to understand CH4 pathways in Fagus sylvatica forests. Journal of Plant Nutrition and Soil Science 181: 31–35.

Martinez, M., and Ardón, M. (2021). Drivers of greenhouse gas emissions from standing dead trees in ghost forests. Biogeochemistry 154: 471–488. https://doi.org/10.1007/s10533-021-00797-5

McKee, K.L. (1995). Seedling recruitment patterns in a Belizean mangrove forest: effects of establishment ability and physico-chemical factors. Oecologia 101:448--460.

McLeod, E., Chmura, G.L., Bouillon, S., Salm, R., Björk, M., Duarte, C.M., Lovelock, C.E., Schlesinger, W.H., y B.R. Silliman. (2011). A blueprint for blue carbon: toward an improved understanding of the role of vegetated coastal habitats in sequestering CO2. Front Ecol Environ 9:552–560.

Medina, E. (1999). Mangrove physiology: the challenge of salt, heat, and light stress under recurrent flooding, p: 109-126. In: A. Yáñez-Arancibia y A. L. Lara-Domínguez (eds). Ecosistemas de Manglar en América Tropical. Instituto de Ecología A.C. México, UICN/ORMA, Costa Rica, NOAA/NMFS Silver Spring MD USA. 380 pp.

Medina, E., Cuevas, E., Lugo, A.E. (2010). Nutrient relations of scrub *Rhizophora mangle* L. mangroves on peat in eastern Puerto Rico. Plant Ecology 207:13-24. https://doi.org/10.1007/s11258-009-9650-z

Megonigal, J.P., Hines, M.E. y P.T. Visscher. (2004). Anaerobic metabolism: Linkages to trace gases and aerobic processes. In: Schlesinger WH ed. Biogeochemistry. Oxford, UK: Elsevier-Pergamon, 317-424.

Mochidome, T., Epron, D. (2024). Drivers of intra-individual spatial variability in methane emissions from tree trunks in upland forest. Trees 38, 625–636. https://doi.org/10.1007/s00468-024-02501-0

Moisan, M.A., Lajoie, G., Constant, P., Martineau, C., Maire, V. (2024). How tree traits modulate tree methane fluxes: A review. Science of the Total Environment 940 (173730). https://doi.org/10.1016/j.scitotenv.2024.173730

Myhre, G., Shindell, D., Bréon, F., Collins, W., Fuglestvedt, J., Huang, J. et al., 2013. Anthropogenic and Natural Radiative Forcing. In: Climate Change 2013: The Physical Science Basis. Contribution of Working Group I to the Fifth Assessment Report of the Intergovernmental Panel on Climate Change [Stocker, T.F., D. Qin, G.-K. Plattner, M. Tignor, S.K. Allen, J. Boschung, A. Nauels, Y. Xia, V. Bex and P.M. Midgley (eds.)]. Cambridge University Press, Cambridge, United Kingdom and New York, NY, USA.

Neubauer, S. y J. P. Megonigal. (2015). Moving beyond global warming potentials to quantify the climatic role of ecosystems. Ecosystems 18: 1000-1013.

Nie, S., Ouyang, X., Wang, W., Zhu, Z., Guo, F., Yang, Z., Lee, S.Y. (2023). Sediment CO_2 flux from a mangrove in southern China: is it controlled by spatiotemporal, biotic or physical factors? Forests 14, 782. https://doi.org/10.3390/f14040782

NOAA National Centers for Environmental Information, Monthly Global Climate Report for April 2024, published online May 2024, retrieved on October 15, 2024 from https://www.ncei.noaa.gov/access/monitoring/monthly-report/global/202404.

Nóbrega, G.N., Ferreira, T.O., Neto, M.S., Queiroz, H.M., Artur, A.G., Mendonça, E.D.S., Silva, E.D.O., Otero, X.L. (2016). Edaphic factors controlling summer (rainy season) greenhouse gas emissions (CO_2 and CH_4) from semiarid mangrove soils (NE-Brazil). Sci. Total Environ. 542, 685–693. https://doi.org/10.1016/j.scitotenv.2015.10.108

Orellana, R., Espadas, C., Conde, C., Gay, C. (2010). Atlas: Escenarios de cambio climático en la Península de Yucatán. Centro de Investigación Científica de Yucatán A.C. México. 111 pp.

OriginLab Corporation. (2016). Origin(Pro), Version Number 2016. Northampton, MA, USA. https://www.originlab.com/

Pangala, S.R., Enrich-Prast, A., Basso, L.S., Peixoto, R.B., Bastviken, D., Hornibrook, E.R. C., Gatti, L.V., Marotta, H., Calazans, L.S.B., Sakuragui, C.M., Bastos, W.R., Malm, O., Gloor, E., Miller, J.B., Gauci, V. (2017). Large emissions from floodplain trees close the Amazon methane budget. Nature 552: 230–234. https://doi.org/10.1038/nature24639

Pangala, S.R., Hornibrook, E.R.C., Gowing, D.J., Gauci, V. (2015). The contribution of trees to ecosystem methane emissions in a temperate forested wetland. Global Change Biology 21: 2642-2654. https://doi.org/10.1111/gcb.12891

Pangala, S.R., Moore, S., Hornibrook, E.R.C., Gauci, V. (2013). Trees are major conduits for methane egress from tropical forested wetlands. New Phytologist 197: 524-531. https://doi.org/10.1111/nph.12031

Pangala, S.R., Gowing, D.J., Hornibrook, E.R.C. and Gauci, V. (2014), Controls on methane emissions from Alnus glutinosa saplings. New Phytol, 201: 887-896. https://doi.org/10.1111/nph.12561

Pedersen, A.R., Petersen, S.O., Schelde, K. (2010). A comprehensive approach to soil atmosphere trace-gas flux estimation with static chambers. Eur. J. Soil Sci. 61 (6), 888–902. https://doi.org/10.1111/j.1365-2389.2010.01291.x

Pendleton, L., Donato, D., Murray, B., Crooks, S., Jenkins, W., y Sifleet, S. et al., (2012). Estimating global 'blue carbon' emissions from conversion and degradation of vegetated coastal ecosystems. PLoS One 7:e43542. https://doi.org/10.1371/journal.pone.0043542

Penha-Lopes G, Kristensen E, Flindt M, Mangion P, Bouillon S., Paula J. (2010). The role of biogenic structures on the biogeochemical functioning of mangrove constructed wetlands sediments--a mesocosm approach. Mar Pollut Bull. Apr;60(4):560-72. https://doi.org/10.1016/j.marpolbul.2009.11.008

Penha-Lopes, G., Flindt, M.R., Ommen, B., Kristensen, E., Garret, P., Paula, J. (2012). Organic carbon dynamics in a constructed mangrove wastewater wetland populated with benthic fauna: a modelling approach. Ecological Modelling 232. https://doi.org/10.1016/j.ecolmodel.2012.02.005

Pfanz, H. y G. Aschan. (2001). The existence of bark and stem photosynthesis in woody plants and its significance for the overall carbon gain. An eco-physiological and ecological approach. Progress in Botany 62: 477–510.

Pfanz, H., Aschan, G., Langenfeld-Heyser, R., Wittmann, C. y M. Loose. (2002). Ecology and ecophysiology of tree stems: corticular and wood photosynthesis. Naturwissenschaften 89: 147–162.

Pihlatie, M.K., Christiansen, J.R., Aaltonen, H., Korhonen, J.F.J., Nordbo, A., Rasilo, T., Benanti, G., Giebels, M., Helmy, M., Sheehy, J., Jones, S., Juszczak, R., Klefoth, R., Lobo-do-Vale, R., Rosa, A.P., Schreiber, P., Serça, D., Vicca, S., Wolf, B., Pumpanen, J. (2013). Comparison of static chambers to measure CH4 emissions from soils. Agricultural and Forest Meteorology 171-172: 124-136. https://doi.org/10.1016/j.agrformet.2012.11.008

Pihlatie, M.K., Christiansen, J.R., Aaltonen, H., Korhonen, J.F.K., Nordbo, A., Rasilo, T., Benanti, G., Giebels, M., Helmy, M., Sheehy, J., Jones, S., Juszczak, R., Klefoth, R., Lobo-do-Vale, R., Rosa, A.P., Schreiber, P., Serça, D., Vicca, S., Wolf, B., Pumpanen, J. (2013). Comparison of static chambers to measure CH_4 emissions from soils. Agric. For. Meteorol. 171-172, 124–136. https://doi.org/10.1016/j.agrformet.2012.11.008

Pitz, S., Megonigal, J.P. (2017). Temperate forest methane sink diminished by tree emissions. New Phytologist 214 (4): 1432-1439. https://doi.org/10.1111/nph.14559

Pitz, S.L., Megonigal, J.P., Chang, C.H., Szlavecz, K. (2018). Methane fluxes from tree stems and soils along a habitat gradient. Biogeochemistry 137, 307–320. https://doi.org/10.1007/s10533-017-0400-3

Posit Team. (2023). RStudio: Integrated Development Environment for R. Posit Software, PBC, Boston, MA. URL. http://www.posit.co/

Poungparn, S., Komiyama, A., Tanaka, A., Sangtiean, T., Maknual, C., Kato, S., Tanapermpool, P., Patanaponpaiboon, P. (2009). Carbon dioxide emission through soil respiration in a secondary mangrove forest of eastern Thailand. J Trop Ecol 25(4):393–400. http://www.jstor.org/stable/25562632

Prigent, C., F. Papa, F. Aires, W. B. Rossow, and E. Matthews. (2007), Global inundation dynamics inferred from multiple satellite observations, 1993–2000, J. Geophys. Res., 112, D12107. https://doi.org/10.1029/2006JD007847

Pruyn, M.L., Gartner, B.L. y M.E. Harmon. (2005). Storage versus substrate limitation to bole respiratory potential in two coniferous tree species of contrasting sapwood width. Journal of Experimental Botany 56: 2637–2649.

Pruyn, M.L., Harmon, M.E. y B.L. Gartner. (2003). Stem respiratory potential in six softwood and four hardwood tree species in the Central Cascades of Oregon. Oecologia 137: 10–21.

Purjava, R. Ramesh, R., P. Frenzel. (2004). Plant-mediated methane emission from an Indian mangrove. Global Change Biology. 10: 1825-1834. https://doi.org/10.1111/j.1365-2486.2004.00834.x

Purvaja, R., y R. Ramesh. (2001). Natural and anthropogenic methane emission from coastal wetlands of South India.Environ. Manag., 27, 547–555.

Purnobasuki, H., Purnama, P.R., Kobayashi, K. (2017). Morphology of four root types and anatomy of root-root junction in relation gas pathway of Avicennia marina (Forsk.) Vierh roots. Vegetos 30 (2). https://doi.org/10.5958/2229-4473.2017.00143.4

Purnobasuki, H., Suzuki, M. (2005). Aerenchyma tissue development and gas-pathway structure in root of Avicennia marina (Forsk.) Vierh. Journal of Plant Research, 118(4), 285-294. https://doi.org/10.1007/s10265-005-0221-7

Rice, A.L., Butenhoff, C.L., Shearer, M.J., Teama, D., Rosenstiel, T.N. y M.A. Khalil. (2010). Emissions of anaerobically produced methane by trees. Geophysical Research Letters.. 37.

Rodríguez-Zúñiga, M.T., Troche-Souza C., Vázquez-Lule, A. D., Márquez-Mendoza, J. D., Vázquez-Balderas, B., Valderrama-Landeros, L. et al., (2013). Manglares de México/ Extensión, distribución y monitoreo. CONABIO. México D.F. 128 pp

Romero, D., León-Cruz, J. F. (2024). Spatiotemporal changes in hurricane-force wind risk assessment in the Yucatan Peninsula, Mexico. Natural Hazards, 1-24. https://link.springer.com/article/10.1007/s11069-023-06397-w

Rosentreter, J.A, Maher, D.T., Erler, D.V., Murray, R.H., y B.D. Eyre. (2018). Methane emissions partially offset “blue carbon” burial in mangroves. Science Advances 4: eaao4985

Rosner, S., and Morris, H. (2022). Breathing life into trees: the physiological and biomechanical functions of lenticels. IAWA Journal, 43(3): 234-262. https://doi.org/10.1163/22941932-bja10090

Rowland, L., da Costa, A.C.L., Oliveira, A.A.R., Oliveira, R.S., Bittencourt, P.L., Costa, P.B., Giles, A.L., Sosa, A.I., Coughlin, I., Godlee, J.L., Vasconcelos, S.S., Junior, J.A.S., Ferreira, L.V., Mencuccini, M. and Meir, P. (2018). Drought stress and tree size determine stem CO2 efflux in a tropical forest. New Phytol, 218: 1393-1405. https://doi.org/10.1111/nph.15024

Salas-Rabaza, J.A., Andrade, J.L., Us-Santamaría, R., Morales-Rico, P., Mayora, G., Aguirre, F.J., Fecci-Machuca, V., Gade-Palma, E.M., Thalasso, F. (2023). Impacts of leaks and gas accumulation on closed chamber methods for measuring methane and carbon dioxide fluxes from tree stems. Sci. Total Environ. 904. https://doi.org/10.1016/j.scitotenv.2023.166358

Salas-Rabaza, J.A., Yáñez-Espinosa, L., Cejudo, E., Cerón-Aguilera, G., Us-Santamaría, R. and Andrade, J.L. (2024). Pneumatophore CO2 effluxes decrease with increased salinity in mangrove forests of Yucatan, Mexico. Sci Rep 14, 18449. https://doi.org/10.1038/s41598-024-68822-9

Salomón, R.L., Helm, J., Gessler, A., Grams, T.E.E., Hilman, B., Muhr, J., Steppe, K., Wittmann, C., Hartmann, H. (2024) The quandary of sources and sinks of CO2 efflux in tree stems—new insights and future directions, Tree Physiology, Volume 44, Issue 1, January 2024, tpad157, https://doi.org/10.1093/treephys/tpad157

Salomón, R.L., Rodríguez-Calcerrada, J., Staudt, M. (2017). Carbon losses from respiration and emission of volatile organic compounds – the overlooked side of tree carbon budgets, in: Gil-Pelegrín, E., Peguero-Pina, J.J., Sancho-Knapik, D. (Eds.) Oaks physiological ecology. Exploring the functional diversity of genus Quercus L. Cham, Switzerland: Springer International, pp. 327–359. https://doi.org/10.1007/978-3-319-69099-5_10

Sanders, C.J., Maher, D.T., Tait, D.R., Williams, D., Holloway, C., Sippo, J.Z. y I.R. Santos. (2016). Are global mangrove carbon stocks driven by rainfall? Journal of Geophysical Research: Biogeosciences 121: 2600–2609.

Saunois, M., Martinez, A., Poulter, B., Zhang, Z., Raymond, P., Regnier, P., Canadell, J. G., Jackson, R. B., Patra, P. K., Bousquet, P., Ciais, P., Dlugokencky, E. J., Lan, X., Allen, G. H., Bastviken, D., *et al.,* .: Global Methane Budget 2000–2020, Earth Syst. Sci. Data Discuss. [preprint], https://doi.org/10.5194/essd-2024-115, in review, 2024.

Schlesinger, W. H. y Andrews, J. A. (2000). Soil respiration and the global carbon cycle. Biogeochemistry 48, 7–20.

Schneider, C., Rasband, W., Eliceiri, K. (2012). NIH Image to ImageJ: 25 years of image analysis. Nature Methods 9: 671–675. https://doi.org/10.1038/nmeth.2089

Schindler, T., Mander, Ü., Machacova, K., Espenberg, M., Krasnov, D., Escuer-Gatius, J., Veber, G., Pärn, J., Soosaar, K. (2020). Short-term flooding increases CH4 and N2O emissions from trees in a riparian forest soil-stem continuum. Scientific Reports 10: 3204. https://doi.org/10.1038/s41598-020-60058-7

Sheng, N., Wu, F., Liao, B., Xin, K. (2021). Methane and carbon dioxide emissions from cultivated and native mangrove species in Dongzhai Harbor, Hainan. Ecological Engineering 168. https://doi.org/10.1016/j.ecoleng.2021.106285

Siegenthaler, A., Welch, B., Pangala, S.R., Peacock, M., Gauci, V. (2016). Technical Note: Semi-rigid chambers for methane gas flux measurements on tree stems. Biogeosciences, 13: 1197–1207. https://doi.org/10.5194/bg-13-1197-2016.

Siikamäki, J., Sanchirico, J. y Jardine, S. (2012). Global economic potential for reducing carbon dioxide emissions from mangrove loss. Proc Natl Acad Sci. 109:14369–14374.

Sjögersten, S., Siegenthaler, A., López, O.R., Aplin, P., Turner, B. and V. Gauci. (2020). Methane emissions from tree stems in neotropical peatlands. New Phytologist 225: 769-781. https://doi.org/10.1111/nph.16178

Smith, K., Ball, T., Conen, F., Dobbie, K., Massheder, J. y Rey, A. (2018). Exchange of greenhouse gases between soil and atmosphere: interactions of soil physical factors and biological processes. Eur. J. Soil Sci. 69:10-20.

Smith, T. M. y R. L. Smith. (2007). Ecología. Sexta edición. Pearson Education S. A., Madrid, España.

Sorrell, B.K. and Brix, H. (2013). Gas Transport and Exchange through Wetland Plant Aerenchyma. In Methods in Biogeochemistry of Wetlands (eds R.D. DeLaune, K.R. Reddy, C.J. Richardson and J.P. Megonigal). https://doi.org/10.2136/sssabookser10.c11

Spalding, M., Kainuma, M. y Collins, L. (2010). World Atlas of Mangroves. London, UK and Washington, DC, USA: Earthscan.

Stocker, T., Qin, D., Plattner, G., Tignor, M., Allen, S., Boschung, J., Nauels, A., Bex, V. y Midgley, P. (2013). Climate change 2013: the physical science basis. Contribution of Working Group I to the Fifth Assessment Report of the Intergovernmental Panel on Climate Change. Cambridge, UK: Cambridge University Press.

Strand, V.V. (2002). The influence of ventilation systems on water depth penetration of emergent macrophytes. Freshwater Biology, 47: 1097-1105. https://doi.org/10.1046/j.1365-2427.2002.00834.x

Takahashi, K., Sakabe, A., Azuma, W.A., Itoh, M., Imai, T., Matsumura, Y., Tateishi, M. and Kosugi, Y. (2022). Insights into the mechanism of diurnal variations in methane emission from the stem surfaces of Alnus japonica. New Phytol, 235: 1757-1766. https://doi.org/10.1111/nph.18283

Takahashi, H., Yamauchi, T., Colmer, T.D., and Nakazono, M. (2014). Aerenchyma Formation in Plants. In: van Dongen, J., Licausi, F. (eds) Low-Oxygen Stress in Plants. Plant Cell Monographs, vol 21. Springer, Vienna. https://doi.org/10.1007/978-3-7091-1254-0_13

Tenhovirta, S.A.M., Kohl, L., Koskinen, M., Polvinen, T., Salmon, Y., Paljakka, T. and Pihlatie, M. (2024). Aerobic methane production in Scots pine shoots is independent of drought or photosynthesis. New Phytol, 242: 2440-2452. https://doi.org/10.1111/nph.19724

Terazawa, K., Yamada, K., Ohno, Y., Sakata, T., Ishizuka, S., (2015). Spatial and temporal variability in methane emissions from tree stems of Fraxinus mandshurica in a cool-temperate floodplain forest. Biogeochemistry 123: 349–362. https://doi.org/10.1007/s10533-015-0070-y

Teskey, R.O., McGuire, A., Bloemen, J., Aubrey, D.P., Steppe, K. (2017). Respiration and CO_2 Fluxes in Trees, in: Tcherkez, G., Ghashghaie, J. (Eds.), Plant Respiration: Metabolic Fluxes and Carbon Balance, Advances in Photosynthesis and Respiration 43, Cham, Switzerland: Springer, 181–207. https://doi.org/10.1007/978-3-319-68703-2_9

Teskey, R.O y M.A. McGuire. (2007). Measurement of stem respiration of sycamore (Platanus occidentalis L.) trees involves internal and external fluxes of CO2 and possible transport of CO2 from roots. Plant, Cell & Environment 30: 570–579.

Teskey, R.O., Saveyn, A., Steppe, K., McGuire, M.A. (2008)., Origin, fate and significance of CO2 in tree stems. New Phytologist, 177: 17-32. https://doi.org/10.1111/j.1469-8137.2007.02286.x

Teskey, R.O. y M.A. McGuire. (2005). CO2 transported in xylem sap affects CO2 efflux from Liquidambar styraciflua and Platanus occidentalis stems and contributes to observed wound respiration phenomena. Trees – Structure and Function 19: 357–362.

Thalasso, F.; Riquelme, B.; Gómez, A.; Mackenzie, R.; Aguirre, F.J.; Hoyos-Santillan, J.; Rozzi, R.; Sepulveda-Jauregui, A. (2023). Technical note: Skirt chamber – an open dynamic method for the rapid and minimally intrusive measurement of greenhouse gas emissions from peatlands. Biogeosciences, 20, 3737–3749. ISSN 1726-4170. https://doi.org/10.5194/bg-20-3737-2023

Toma, T., Nkamura, K., Patanaponpaiboon, P., Ogino, K. (1991). Effect of Flooding Water Level and Plant Density on Growth of Pneumatophore of *Avicennia marina*. Tropics 1: 75–82. https://doi.org/10.3759/tropics.1.75

Tomlinson P.B. (2016). The botany of mangroves. Second Edition. Cambridge University Press. Cambridge. 418 p.

Troxler, T.G., Barr, J.G., Fuentes, J.D., Engel, V., Anderson, G., Sanchez, C., Lagomasino, D, Price, R., Davis, S.E. (2015). Component-specific dynamics of riverine mangrove CO_2 efflux in the Florida coastal Everglades. Agric For Meteorol 213:273–282. https://doi.org/10.1016/j.agrformet.2014.12.012

Trumbore, S. (2000). Age of soil organic matter and soil respiration: radiocarbon constraints on belowground C dynamics. Ecological Applications, 10 (2), 399-411.

Trumbore, S.E., Angert, A., Kunert, N., Muhr, J. y J. Q. Chambers. (2013). What's the flux? Unraveling how CO2 fluxes from trees reflect underlying physiological processes. New Phytologist 197: 353-355.

van Haren, J., Brewer, P.E., Kurtzberg, L., Wehr, R.N., Springer, V.L., Tello-Espinoza, R., Solignac-Ruiz, J., Cadillo-Quiroz, H. (2021). A versatile gas flux chamber reveals high tree stem CH_4

emissions in Amazonian peatland. Agricultural and Forest Meteorology 307: 108504. https://doi.org/10.1016/j.agrformet.2021.108504.

Vargas, R. y Barba J. (2019). Greenhouse gas fluxes from tree stems. Trends in Plant Science 24-4: 296-299.

Velázquez-Salazar, S., Rodríguez-Zúñiga M.T., Alcántara-Maya J.A., Villeda-Chávez E., Valderrama-Landeros L., Troche-Souza C., Vázquez-Balderas B., Pérez-Espinosa I., Cruz-López M. I., Ressl R., De la Borbolla D. V. G., Paz O., Aguilar-Sierra V., Hruby F., Muñoz-Coutiño J. H. (2021). Manglares de México. Actualización y análisis de los datos 2020. Comisión Nacional para el Conocimiento y Uso de la Biodiversidad. México CDMX. Pp. 168.

Vinh, T.V., Allenbachc, M., Joanne, A. y C. Marchand. (2019). Seasonal variability of CO2 fluxes at different interfaces and vertical CO2 concentration profiles within a Rhizophora mangrove forest (Can Gio, VietNam). Atmospheric Environment 201: 301-309.

Villa, J.A., Ju, Y., Stephen, T., Rey-Sanchez, C., Wrighton, K.C. and Bohrer, G. (2020), Plant-mediated methane transport in emergent and floating-leaved species of a temperate freshwater mineral-soil wetland. Limnol Oceanogr, 65: 1635-1650. https://doi.org/10.1002/lno.11467

Vroom, R.J.E., van den Berg, M., Pangala, S.R., van der Scheer, O.E., Sorrell, B.K. (2022). Physiological processes affecting methane transport by wetland vegetation – A review. Aquatic Botany 182. https://doi.org/10.1016/j.aquabot.2022.103547

Wang, Z.P., Gu, Q., Deng, F.D., Huang, J.H., Megonigal, J.P., Yu, Q., Lü, X.T., Li, L.H., Chang, S., Zhang, Y.H., Feng, J.C. and Han, X.G. (2016). Methane emissions from the trunks of living trees on upland soils. New Phytol, 211: 429-439. https://doi.org/10.1111/nph.13909

Wang, Z.P., Han, S.J., Li, H.L., Deng, F.D., Zheng, Y.H., Liu, H.F., and Han, X.G. (2017). Methane production explained largely by water content in the heartwood of living trees in upland forests. Journal Geophysical Research: Biogeosciences, 122, 2479–2489. https://doi.org/10.1002/2017JG003991

Wang, ZP., Li, HL., Wu, HH., Han, S.J., Huang, J.H., Zhang, X.M., and Han X.G. 2021. Methane Concentration in the Heartwood of Living Trees and Estimated Methane Emission on Stems in Upland Forests. Ecosystems 24, 1485–1499. https://doi.org/10.1007/s10021-020-00596-3

Ward, N.D., and Megonigal, J.P. (2024). Researchers barking up (the right) tree find new mechanisms controlling methane transport by woody vegetation. New Phytol, 242: 5-7. https://doi.org/10.1111/nph.19565

Welles, J.M., Demetriades-Shah, T.H., McDermitt, D.K. (2001). Considerations for measuring ground CO_2 effluxes with chambers. Chemical Geology 177(1–2): 3–13. https://doi.org/10.1016/s0009-2541(00)00388-0.

Wilkinson, J., Bors, C., Burgis, F., Lorke, A., Bodmer, P. (2018). Measuring CO_2 and CH_4 with a portable gas analyzer: Closed-loop operation, optimization and assessment. PLoS ONE 13(4): e0193973. https://doi.org/10.1371/journal.pone.0193973

Wu, J., Zhang, H., Cheng, X., Liu, G. (2024). Tree stem methane emissions: Global patterns and controlling factors. Agricultural and Forest Meteorology 350 (109976). https://doi.org/10.1016/j.agrformet.2024.109976

Xiao, S., Wang, C., Wilkinson, R.J., Liu, D., Zhang, C., Xu, W., Yang, Z., Wang, Y., Lei, D. (2016). Theoretical model for diffusive greenhouse gas fluxes estimation across water-air interfaces measured with the static floating chamber method. Atmospheric Environment 137: 45-52. https://doi.org/10.1016/j.atmosenv.2016.04.036

Yabuki, K. (2004). Gas Exchange between the Pneumatophores and Roots of Mangroves by Photosynthesis of Pneumatophore. In: Photosynthetic Rate and Dynamic Environment. Springer, Dordrecht. https://doi.org/10.1007/978-94-017-2640-5_5

Yamauchi, T., Shimamura, S., Nakazono, M., and Mochizuki, T. (2013). Aerenchyma formation in crop species: A review.Field Crops Research 152: 8-16. https://doi.org/10.1016/j.fcr.2012.12.008.

Yánez-Espinosa, L., Ángeles, G. (2022). Does mangrove stem bark have an internal pathway for gas flow? Trees 36, 361–377. https://doi.org/10.1007/s00468-02102210-y

Yáñez-Espinosa L, and Flores J. (2011). A review of sea-level rise effect on mangrove forest species: anatomical and morphological modifications. In: Casalegno S (ed) Global warming impacts—case studies on the economy, human health, and on urban and natural environments. InTech, Texas, pp 253–276. https://doi.org/10.5772/24662

Yáñez-Espinosa L., Terrazas T., Angeles G. (2008). The effect of prolonged flooding on the bark off mangrove trees. Trees 22:77–86. https://doi.org/10.1007/s00468-007-0171-x

Yang, J., He, Y., Aubrey, D.P., Zhuang, Q., Teskey, R.O. (2016). Global patterns and predictors of stem CO_2 efflux in forest ecosystems. Global Change Biology 22: 1433–1444. https://doi.org/10.1111/gcb.13188

Yang, H., Wang, S., Son, R., Lee, H., Benson, V., Zhang, W., Zhang, Y., Zhang, Y., Kattge, J., Boenisch, G., Schepaschenko, D., Karaszewski, Z., Stereńczak, K., Moreno-Martínez, Á., Nabais, C., Birnbaum, P., Vieilledent, G., Weber, U., Carvalhais, N. (2024). Global patterns of tree wood density. Global Change Biology, 30, e17224. https://doi.org/10.1111/gcb.17224

Youssef, T., and Saenger, P. (1996). Anatomical adaptive strategies to flooding and rhizosphere oxidation in mangrove seedlings. Aust J Bot 44: 297–313. https://doi.org/10.1071/BT9960297

Yong, Z.J., Lin, W., Lin, C.W., and Lin, H.J.L. (2024). Tidal influence on carbon dioxide and methane fluxes from tree stems and soils in mangrove forests, EGUsphere [preprint], https://doi.org/10.5194/egusphere-2024-533, 2024.

Yu, K., Hiscox, A. y R. DeLaune. (2013). Greenhouse gas emission by static chamber and eddy flux methods. In: DeLaune, R.D., Reddy, K.R., Richardson, C.J. y J.P. Megonigal (Eds). Methods in biogeochemistry of wetlands. Soil Science Society of America. USA. 1020p.

Zaldívar-Jiménez, M.A., Herrera-Silveira, J. A., Teutli-Hernández, C., Comín, J. A., Andrade, J. L., Coronado-Molina, C., Pérez-Ceballos, R. (2010). Conceptual Framework for Mangrove Restoration in the Yucatán Peninsula. Ecological Restoration 28:3. https://doi.org/10.3368/er.28.3.333

Zhang, C., Zhang, Y., Luo, M., Tan, J., Chen, X., Tan, F., Huang, J. (2022). Massive methane emission from tree stems and pneumatophores in a subtropical mangrove wetland. Plant Soil 473, 489–505. https://doi.org/10.1007/s11104-022-05300-z

Zhang, Y.X., Huang, J.F., Luo, M., Wu, Z., Li, H., Chen, K.L., Tan, J. (2019). Rate of methane transport and respiration from the stem of mangrove Kandelia obovata at different part of intertidal zone in Zhangjiang river estuary. Research of Environmental Sciences 32 (5): 839-847. https://doi.org/10.13198/j.issn.1001-6929.2018.09.14

ANEXOS

ANEXO I. MATERIAL SUPLEMENTARIO DEL CAPÍTULO II

La siguiente información corresponde a la sección de *Supplementary Materials* del artículo correspondiente publicado en la revista científica *Science of The Total Environment* y debe ser citado y referido según las normas de dicha revista.

Para más información visitar el siguiente enlace:

Salas-Rabaza, J.A., Andrade, J.L., Us-Santamaría, R., Morales-Rico, P., Mayora, G., Aguirre, F.J., Fecci-Machuca, V., Gade-Palma, E.M., Thalasso, F., 2023. Impacts of leaks and gas accumulation on closed chamber methods for measuring methane and carbon dioxide fluxes from tree stems. Science of The Total Environment 904 (166358). https://doi.org/10.1016/j.scitotenv.2023.166358

Supplementary Materials

Impacts of leaks and gas accumulation on closed chamber methods for measuring methane and carbon dioxide fluxes from tree stems

Julio A. Salas-Rabaza[1,2], José Luis Andrade[1], Roberth Us-Santamaría[1], Pablo Morales-Rico[3], Gisela Mayora[4], Francisco Javier Aguirre[2], Vicente Fecci-Machuca[2], Eugenia M. Gade-Palma[2], Frederic Thalasso[2,3*]

[1] Unidad de Recursos Naturales, Centro de Investigación Científica de Yucatán, A.C. (CICY), Calle 43 No. 130, Chuburná de Hidalgo, 97205 Mérida, México

[2] Cape Horn International Center, Universidad de Magallanes, Av. Bulnes 01855, Punta Arenas 6210427, Chile.

[3] Departamento de Biotecnología y Bioingeniería, Centro de Investigación y de Estudios Avanzados del Instituto Politécnico Nacional (Cinvestav), Av. IPN 2508, Mexico City 07360, Mexico.

[4] Instituto Nacional de Limnología (Inali) Ciudad Universitaria, Colectora Ruta Nac. 168, Paraje El Pozo, (3000), Santa Fé, Argentina.

Section S1. Extended information about mass balance, leak detection, and pneumatic behavior of the chambers

S1.1. Mass balance of closed chambers

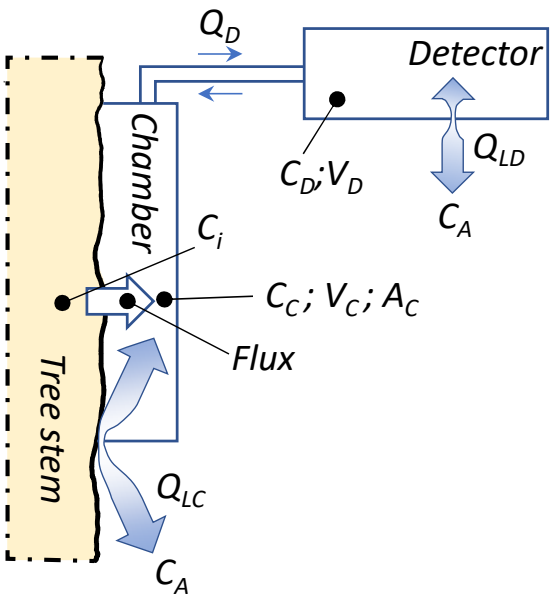

Figure S1. Conceptual scheme of mass balance in closed chambers (extended)

Notations:

V_C	Chamber volume (m^3)
V_D	Detector and pneumatic circuit volume (m^3)
V_T	Total volume (V_C + V_D; m^3)
A_C	Chamber area in contact with the tree (m^2)
C_C	CH_4/CO_2 concentration within the chamber (g m^{-3})
C_D	CH_4/CO_2 concentration within the detector (g m^{-3})
C_A	Atmospheric CH_4/CO_2 concentration (g m^{-3})
Q_D	Gas flowrate to/from the detector (m^3 h^{-1})
Q_{LC}	Leak flowrate of the chamber (m^3 h^{-1})
Q_{LD}	Leak flowrate of the detector and pneumatic circuit (m^3 h^{-1})
F	CH_4/CO_2 flux from the tree (g m^{-2} h^{-1})

Prior to flux measurement, the chamber is tidily fixed on the tree and connected to the greenhouse gas analyzer in a closed loop, according to Figure S1. Under this configuration, the mass balance of the closed chamber is;

$$\frac{dC_C}{dt} = F \cdot \frac{A_C}{V_T} - \frac{Q_D}{V_T} \cdot C_C + \frac{Q_D}{V_T} \cdot C_D - \frac{Q_{LD}}{V_T} \cdot C_D + \frac{Q_{LD}}{V_T} \cdot C_A - \frac{Q_{LC}}{V_T} \cdot C_C + \frac{Q_{LC}}{V_T} \cdot C_A \quad \text{(S1)}$$

where:

$\frac{dC_C}{dt}$ Is the observed variation of the CH_4/CO_2 concentration within the chamber

$F \cdot \frac{A_C}{V_T}$ Is the Flux component.

$\frac{Q_D}{V_T} \cdot C_C$ Is the chamber output (chamber to detector).

$\frac{Q_D}{V_T} \cdot C_D$ Is the chamber input (detector to chamber).

$\frac{Q_{LD}}{V_T} \cdot C_D$ Is the detector/pneumatic circuit leak to the atmosphere.

$\frac{Q_{LD}}{V_T} \cdot C_A$ Is the detector/pneumatic circuit leak from the atmosphere.

$\frac{Q_{LC}}{V_T} \cdot C_C$ Is the chamber leak to the atmosphere.

$\frac{Q_{LC}}{V_T} \cdot C_A$ Is the chamber leak from the atmosphere.

Reorganizing Eq. S1, we obtain:

$$\frac{dC_C}{dt} = F \cdot \frac{A_C}{V_T} + \frac{Q_D}{V_T} \cdot (C_D - C_C) + \frac{Q_{LD}}{V_T} \cdot (C_A - C_D) + \frac{Q_{LC}}{V_T} \cdot (C_A - C_C) \quad \text{(S2)}$$

After a significant measurement time, equilibrium is reached and $C_D = C_C$, thus:

$$\frac{dC_C}{dt} = F \cdot \frac{A_C}{V_T} + \frac{Q_{LD}}{V_T} \cdot (C_A - C_C) + \frac{Q_{LC}}{V_T} \cdot (C_A - C_C) \quad \text{(S3)}$$

When required, Q_{LD} and Q_{LC} can be combined into a total leak flowrate (Q_L), which includes potential leaks of the detector, permeability of the chamber and the pneumatic circuit, and leaks caused by imperfect sealing between the chamber and the tree bark.

$$\frac{dC_C}{dt} = F \cdot \frac{A_C}{V_T} + \frac{Q_L}{V_T} \cdot (C_A - C_C) \quad \text{(S4)}$$

In Eq. S4, leaks can be described by a kinetic constant, called leak constant (k_L), which represents the frequency to which the content of the chamber is replaced by external air:

$$\frac{Q_L}{V_T} = k_L \quad \text{(S5)}$$

in such manner that Eq, S4 becomes;

$$\frac{dC_C}{dt} = F \cdot \frac{A_C}{V_T} + k_L \cdot (C_A - C_C) \quad \text{(S6)}$$

In Equation S6, F is the flux measured when the chamber is positioned on the tree stem, which is exposed to C_C, potentially different from atmospheric concentration C_A. Thus, the actual flux (F^*), naturally occurring when the bark is exposed to C_A might be different from F. Since mass transfer is a lineal function of the concentration gradient, we can estimate that the measured flux is a function of the ration between the concentration gradient with and without a chamber:

$$F = F^* \cdot \frac{(C_i - C_C)}{(C_i - C_A)} \quad \text{(S7)}$$

Where (C_i-C_C) and (C_i-C_A) are the concentration gradient actually observed during the chamber measurement and the gradient that would be otherwise observed in absence of a chamber, respectively. Equation 2 is similar to those commonly used in the study of aquatic ecosystems (Matthews et al., 2003) and wetlands (Juszczak, 2013; Kutzbach et al., 2007). Therefore, Equation S6 becomes:

$$\frac{dC_C}{dt} = F^* \cdot \frac{(C_i - C_C)}{(C_i - C_A)} \cdot \frac{A_C}{V_T} + k_L \cdot (C_A - C_C) \quad \text{(3)}$$

S1.2. Leak detection and measurements

The determination of k_L is based on the injection of a pulse of CH_4 into the pneumatic circuit, through a septum, while CH_4 concentration measurement is maintained. In the main article, we indicate that, in a well-mixed device, the mass balance of the closed chamber after a pulse injection, is well described by Equation 6, where $C_{C,0}$ and $C_{C,f}$ are the CH_4 chamber concentration at time zero (shortly after pulse injection) and after a long time (when the chamber reaches a new equilibrium).

$$C_{C,t} = C_{C,0} + (C_{C,0} - C_{C,f}) \cdot (1 - exp(-k_L \cdot t)) \quad \text{(6)}$$

However, Equation 6 does not contemplate the complex pneumatic behavior of the closed chamber, because, just after pulse injection, the gas concentration within the chamber is relatively high, while the gas contained in the detector and tubing, is still close to atmospheric concentration.

This concentration gradient recirculates within the loop, while being progressively diluted by mixing, causing a damped oscillatory phenomenon, that we described with a semi-empirical equation (Eqs. S8).

$$C_{C,t} = C_{C,0} \cdot exp(-k_L \cdot t) + sin(\alpha) \cdot A \cdot exp\left(-\frac{t}{\theta_A}\right) \quad \text{(S8)}$$

$$\alpha = 1.5\pi + \left(\frac{t}{\omega}\right) \cdot 2\pi = \left(1.5 + \frac{2t}{\omega}\right) \cdot \pi \quad \text{(S8)}$$

Where α is expressed in radians; A is the initial amplitude of the oscillatory signal, which is function of the mass of CH_4 injected and V_T; θ_A is the damping time constant, which represents the mixing time of the measurement device; and ω is the period of the observed oscillatory phenomena, which represents the recirculation time along the loop and is equal to the ration V_T/Q_D, where Q_D is the gas flowrate to/from the detector. It is noteworthy to mention that Equation S8 can be applied even when no oscillatory behavior is observed, the second term of Equation S8 being in that case equal to zero.

By calibration of Equation S8, using k_L, A, and θ_A, as adjustment parameters, leaks can be quantified. However, k_L determination requires the assumption that, during pulse injection the flux from/to the tree stem has a negligible impact. The latter was discussed in the Results and Discussion Section.

S1.3. Pneumatic behavior and method validity

Abiotic tests were performed to establish the pneumatic behavior of our flux measurement setup and to confirm the validity of Equations 6 and S8. A closed loop tubing without chamber, i.e. from/to the detector, of 6, 12 and 24 m of total length was used, and CH_4 pulses were injected into the circuit. An example of the observed behavior is presented on Figure S2A. In all cases, a damped sinusoidal behavior was observed, combined with a slow asymptotic decrease of the CH_4 concentration (Fig. S2A), which indicates that the pneumatic circuit and the detector presented significant leaks. No difference in k_L was observed among the different lengths of tubing used, suggesting that the leaks observed were caused by the UGGA only. Leaks in a similar UGGA have been previously reported (Wilkinson et al., 2018), and are therefore confirmed here. The leak flowrate (Q_L) of the analyzer was estimated to 0.27 ± 0.05 L h^{-1} (median ± one standard deviation).

When the method was applied on trees, varying the chamber, and using 4−24 m of tubing (2−12 m between the chamber and the detector), the damped oscillatory effect was also often but not always observed, after CH_4 pulse injection. The oscillatory behavior was varying in both amplitude and frequency, according to the size of the chamber and the length of the pneumatic circuit, i.e. long tubing and small chamber volume increased both the amplitude and the frequency of the oscillation. To illustrate the latter, Figure S2 shows examples of three distinctive observed behaviors (B-D), as well as the model fitting (Eq. S8). Immediately after each pulse injection, the damped sinusoidal Equation failed to describe C_C, probably due to complex mixing phenomena within the chamber, just after pulse injection. However, after that initial period, the model adjusted well to the experimental data with a mean R^2 of 0.981 ± 0.035, whatever the oscillatory magnitude.

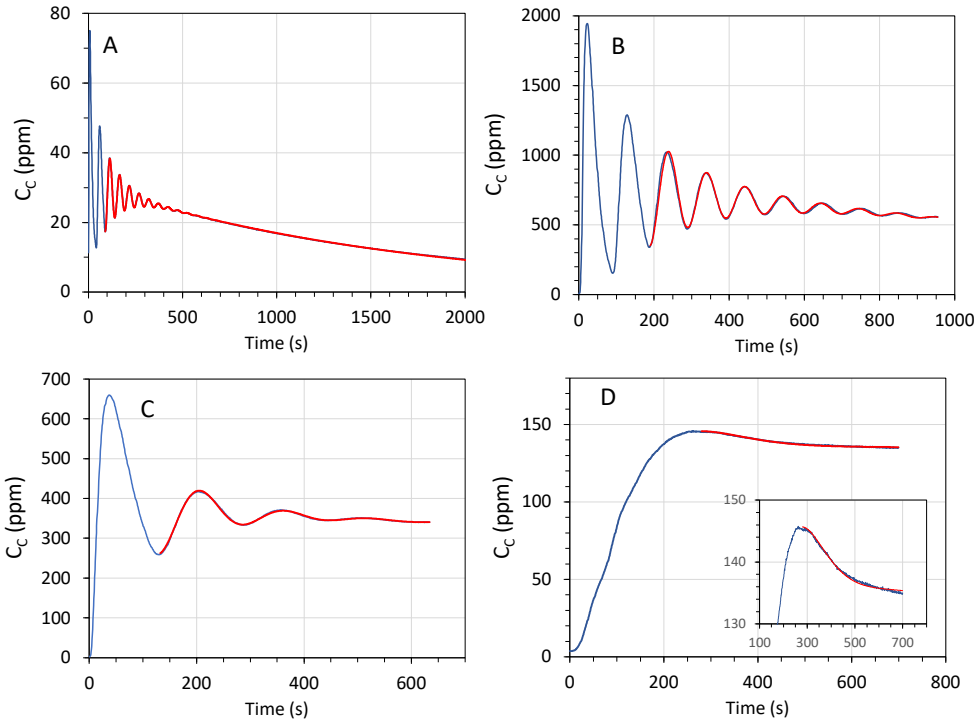

Figure S2. Examples of the oscillatory behavior of C_C observed after a pulse injection in the pneumatic circuit without chamber (abiotic test, A), in a small chamber fixed on a tree with long tubing (B), medium size chamber fixed on a tree with long tubing (C), and large chamber fixed on a tree with short tubing (D), where a close-up window shows the transient behavior observed.

S1.4. Simplified mass balance equation

When deploying a chamber on a tree, C_C will increase, as capturing the gas emitted by the tree stem. In the absence of any leak and any impact of concentration buildup, C_C would increase

linearly and endlessly. In real case scenario, C_C will increase asymptotically until reaching a steady-state concentration $C_{C,2}$, where leaks equal flux, which in turn is limited to a certain extent by the concentration buildup. Under these conditions, the mass balance of the chamber can be described by:

$$\frac{dC_C}{dt} = (C_{C,2} - C_C) \cdot k_t \quad \text{(S9)}$$

This mass balance can be integrated over time, with a variable change, as follows:

$$\frac{d(C_{C,2}-C_C)}{(C_{C,2}-C_C)} = -dt \cdot k_t \quad \text{(S10)}$$

$$\int_{C_{C,1}}^{C_{C,t}} \frac{d(C_{C,2}-C_{C,t})}{(C_{C,2}-C_{C,1})} = k_t \cdot \int_{t=0}^{t} -dt \quad \text{(S11)}$$

$$ln\left(\frac{(C_{C,2}-C_{C,t})}{(C_{C,2}-C_{C.1})}\right) = -k_t \cdot t \quad \text{(S12)}$$

$$\frac{(C_{C,2}-C_{C,t})}{(C_{C,2}-C_{C.1})} = exp(-k_t \cdot t) \quad \text{(S13)}$$

$$C_{C,t} = C_{C,2} - (C_{C,2} - C_{C,1}) \cdot \exp(-k_t \cdot t) \quad \text{(14)}$$

Supplementary Figures and Tables

Figure S3. Photographs of the bark of the six tree species tested.

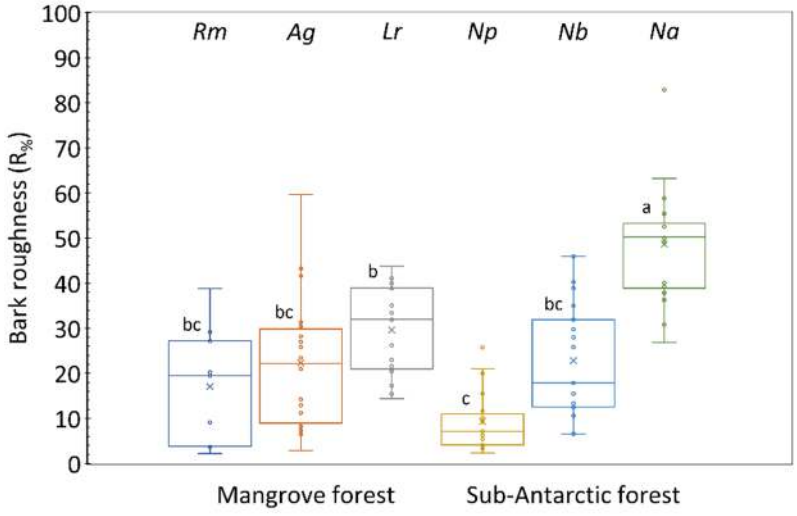

Figure S4. Bark roughness ($R_{\%}$) of the six tree species.

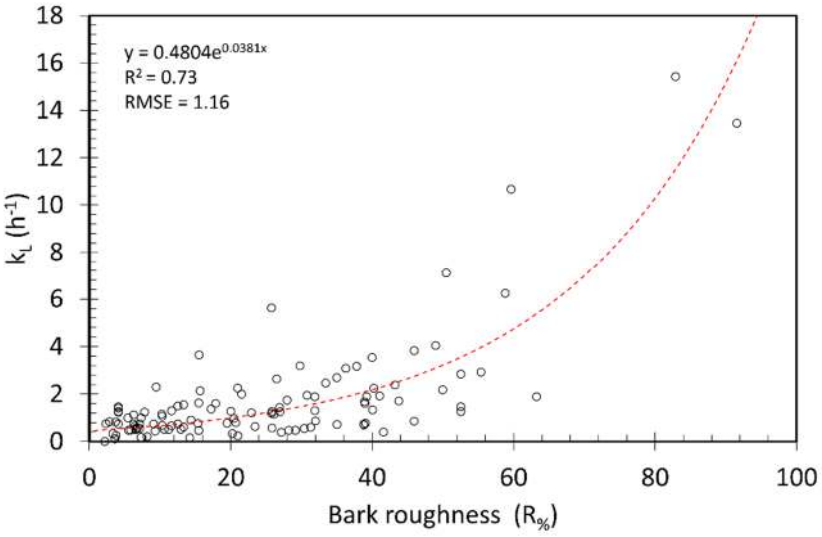

Figure S5. k_L as a function of the tree bark roughness ($R_{\%}$).

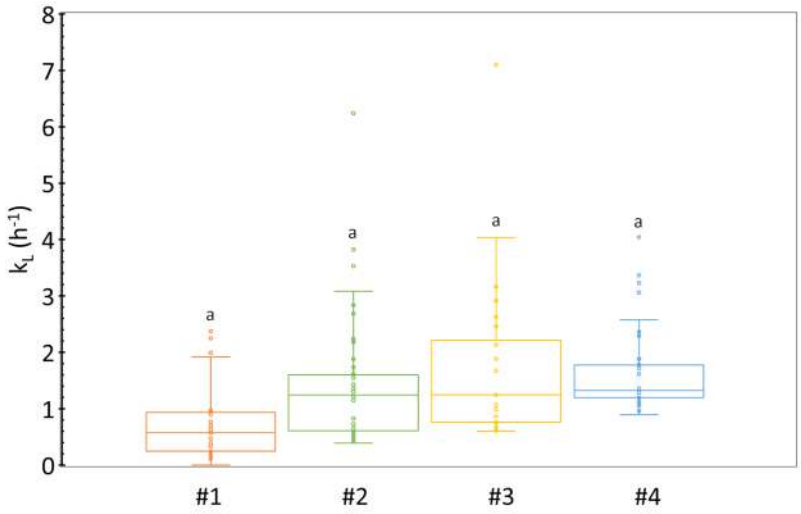

Figure S6. k_L vs chamber number.

Table S1. Bark roughness ($R_{\%}$) by species at each tree height. Equal letters indicate no difference of $R_{\%}$ between tree heights within each species.

Species	Tree height	n	$R_{\%}$ (mean ± SD)	
Rm	0.25	9	17.08 ± 13.12	a
Ag	0.25	9	23.21 ± 16.39	a
	1.40	9	21.45 ± 15.12	a
Lr	0.25	9	32.77 ± 9.45	a
	1.40	9	26.47 ± 9.58	a
Np	0.25	13	8.99 ± 6.97	a
	1.40	13	8.46 ± 2.28	a
Nb	0.25	12	24.42 ± 11.05	a
	1.40	12	24.54 ± 9.81	a
Na	0.25	12	47.17 ± 19.96	a
	1.40	12	46.39 ± 7.58	a

Table S2. Summary of the chamber used, measurements height (m), number of measurements (n), and tree stem diameters (mean **±** standard deviation and ranges; cm), by tree species. Note: in *Rm*, measurement height was always 0.25 m above the last stilt root.

Forest type	Species	Chamber	Height	n	Mean diam. ± SD	Diam. Range
Mangrove	Rm	#1	0.25	7	18.6 ± 3.6	14.6 - 24.3
		#2	0.25	2	15.8 ± 8.5	9.9 - 21.8
		#4	0.25	9	4.6 ± 0.9	3.4 - 6.3
	Ag	#1	0.25	4	29.1 ± 13.7	18.1 - 49.1
			1.4	4	29.7 ± 14.9	17.9 - 51.6
		#2	0.25	4	11.8 ± 4.1	9.1 - 17.8
			1.4	4	10.9 ± 3.2	8.6 - 15.4
		#3	0.25	1	9.2	
			1.4	1	10	
	Lr	#1	0.25	3	17.9 ± 1.3	17 - 19.4
			1.4	3	16.6 ± 1	15.9 - 17.8
		#2	0.25	3	17 ± 3.1	13.7 - 19.9
			1.4	3	15 ± 2.6	12.3 - 17.6
		#3	0.25	3	6.1 ± 0.3	5.7 - 6.4
			1.4	3	5.5 ± 0.5	5.1 - 6
Sub-Antarctic	Np	#1	0.25	2	33.8 ± 2.7	32 - 35.7
		#2	0.25	11	26.8 ± 8.3	14.2 - 45.8
			1.4	3	35.9 ± 6.3	29.1 - 44
		#3	1.4	10	24.5 ± 7.4	13.7 - 42.4
	Nb	#2	0.25	12	25.9 ± 7.1	15.8 - 38.4
			1.4	2	34 ± 3.3	31.6 - 37.8
		#3	1.4	10	24.8 ± 8.1	15 - 41.5
	Na	#1	0.25	2	32.1 ± 3.2	29.9 - 34.4
		#2	0.25	9	30.6 ± 8.4	18.9 - 42.8
			1.4	6	36.6 ± 13.5	20.2 - 56.2
		#3	0.25	1	19.8	
			1.4	6	27.8 ± 8.6	17.5 - 43.1

Table S3 (1/2). Literature review of the last ten years regarding stem CH_4 fluxes in trees and the adjustment used. We considered only literature reporting CH_4 fluxes. A = asymptotic-like adjustment**; L = linear models; L-NL = the best among combined linear or non-linear models (unspecified); NS = Not Specified; D = discrete sampling using static closed chamber; C= continuous measurements using dynamic closed chamber; or B = both of them. Measurements times are given in terms of the total time and the interval between sampling (enclosed in parentheses).

REFERENCE	ADJUSTMENT	MEASUREMENT	TIME (min)
Daniel et al., 2023	L-NL	D	30 (10)
Gorgolewski et al., 2023	L-NL	C	3-8
Machacova et al., 2023	A	D	
Petaja et al., 2023	L	C	
Ranniku et al., 2023	L	D	180 (60)
Berg, 2022	L	C	7-10
Epron et al., 2022	L	C	4
Fraser-McDonald et al., 2022a	L	C	10
Fraser-McDonald et al., 2022b	L	C	10
Gómez, 2022	L	C	5
Gorgolewski et al., 2022	A	C	
Han et al., 2022	L	D	
Lazdins et al., 2022	L	D	30 (2-6)
Ma, 2022	L	C	
Martínez et al., 2022	L-NL	B	10; 30-40 (5)
Soosaar et al., 2022	L	D	180 (60)
Takahashi et al., 2022	L	C	6-10
Vainio et al., 2022	A	D	
Barba et al., 2021	L-NL	C	5
Bréchet et al., 2021	L-NL	C	
Dušek et al., 2021	L	C	4-5
Feng et al., 2021	L	D	
Flanagan et al., 2021	L	C	3
Gao et al., 2021	L	C	+3
Gauci et al., 2021	L	D	20 (1-5)
Iddris et al., 2021	L	D	60 (20)
Jeffrey et al., 2021	L	C	
Kohl et al., 2021	L	C	3
Mander et al., 2021	L-NL	D	
Martínez and Ardón, 2021	L-NL	C	10
Moldaschl et al., 2021	L	D	
Plain and Epron, 2021	L	C	
Sakabe et al., 2021	L	C	6
Schindler et al., 2021	L	D	180 (60)

**Asymptotic-like adjustments are those similar to Equation 14 (asymptotic) or those using similar models such as the steady-state diffusion model "HM" (Hutchinson and Mosier, 1981), and its extension "HMP" (Pedersen et al., 2001), non-steady-state diffusive flux estimator "NDFE" (Livingston et al., 2005; 2006), or “HMR” (Pedersen et al., 2010).

Table S3 (continued, 2/2).

REFERENCE	ADJUSTMENT	MEASUREMENT	TIME (min)
Takahashi et al., 2021	NS	B	15-30
van Haren et al., 2021	L	C	4-6
Jeffrey et al., 2020a	L	C	2
Jeffrey et al., 2020b	L	C	
Megonigal et al., 2020	L	C	
Schindler et al., 2020	A	D	180 (60)
Sjogersten et al., 2020	L	C	5
Barba et al., 2019	L-NL	C	5.83
Ghasemi, 2019	A	C	10
He et al., 2019	NS	D	240 (30)
Jeffrey et al., 2019	L	C	2-3
Kohl et al., 2019	L	C	20
Koks, 2019	L	D	60 (20)
Machacova et al., 2019	L	D	
Plain et al., 2019	L	C	8
Pyykkö, 2019	A	C	10-20
Welch et al., 2019	L	D	15 (5)
Zhang et al., 2019	L	C	
Carmichael et al., 2018	L	D	80 (~11)
Maier et al., 2018	L	D	360 (30)
Pitz et al., 2018	L	B	5-30
Pangala et al., 2017	L	C	
Pitz and Megonigal et al., 2017	L	C	5-10
Wang et al., 2017	L	D	45 (15)
Warner et al., 2017	L	C	3
Kutschera et al., 2016	L	D	30 (5)
Machacova et al., 2016	L	D	
Siegenthaler et al., 2016	L-NL	B	
Wang et al., 2016	L	D	45 (15)
Pangala et al., 2015	L	D	80 (5-20)
Terezawa et al., 2015	L	D	20 (10)
Pangala et al., 2014	L	C	5
Machacova et al., 2013	L	D	80-200 (20-30)
Pangala et al., 2013	L	D	80 (5-20)
Takahashi et al., 2012	L	C	

ANEXO II. INFORMACIÓN SUPLEMENTARIA DEL CAPÍTULO III

La siguiente información corresponde a la sección de *Supplementary Information* del artículo *en revisión* en la revista científica *Scientific Reports* y debe ser citado y referido según las normas de la revista final de publicación.

Supplementary Information

Pneumatophores increase CO_2 effluxes from sediment and water along a salinity gradient in mangrove forests of Yucatan, Mexico

Julio A. Salas-Rabaza[1], Laura Yáñez-Espinosa[2], Eduardo Cejudo[3], Gabriela Cerón-Aguilera[1], Roberth Us-Santamaría[1], José Luis Andrade[1,*]

[1] Unidad de Recursos Naturales, Centro de Investigación Científica de Yucatán A.C., Calle 43 No. 130, Chuburná de Hidalgo, 97205 Mérida, Mexico.

[2] Instituto de Investigación de Zonas Desérticas, Universidad Autónoma de San Luis Potosí, De Altair 200, Col del Llano, 78377 San Luis Potosí, S.L.P., Mexico.

[3] Unidad de Ciencias del Agua, Centro de Investigación Científica de Yucatán A.C., Calle 8, No. 39, Mz 29, SM 64, 77524. Cancún, Quintana Roo, Mexico.

Table S1. Models of CO_2 effluxes explained by pneumatophore's density for all data and for each combination of seasons, mangrove forest and exchange interfaces. Slopes are given in 10^{-3} in order to facilitate comparisons.

Model	R^2_{-adj}	Intercept	Slope × 10^{-3}	RMSE	AIC	F-statistic	N
General	0.37	1.55	4.44	2.69	829.27	98.77	171
Dry	0.28	2.31	4.30	3.12	563.19	43.93	109
Rainy	0.82	0.84	3.49	0.70	137.38	278.69	62
Basin	0.50	1.79	2.29	0.94	162.88	57.70	58
Fringe	0.51	2.94	6.24	2.96	296.50	59.86	58
Scrub	0.86	-0.01	4.40	0.82	140.64	339.87	55
Sediment	0.32	3.17	4.54	3.09	403.38	36.64	78
Water	0.78	0.80	3.20	0.74	213.16	335.17	93
Dry - Basin	0.39	2.10	2.08	1.11	115.38	23.71	36
Rainy - Basin	0.50	1.71	1.65	0.37	25.09	22.16	22
Dry - Fringe	0.64	6.04	4.51	1.71	150.87	66.34	37
Rainy - Fringe	0.87	0.92	2.98	0.35	21.46	139.49	21
Dry - Scrub	0.84	-0.06	4.50	0.81	92.88	179.04	36
Rainy - Scrub	0.88	0.03	4.31	0.84	53.51	137.75	19
Basin - Sediment	0.74	3.45	3.04	0.42	14.82	20.94	8
Basin - Water	0.83	1.43	2.34	0.45	67.77	245.76	50
Fringe - Sediment	0.64	6.04	4.51	1.71	150.87	66.34	37
Fringe - Water	0.87	0.92	2.98	0.35	21.46	139.49	21
Scrub - Sediment	0.83	0.49	3.98	0.77	82.57	160.65	33
Scrub - Water	0.91	-0.56	4.78	0.74	55.16	222.02	22
Dry - Basin - Sediment	0.74	3.45	3.04	0.42	14.82	20.94	8
Dry - Basin - Water	0.86	1.23	2.55	0.46	42.50	173.30	28
Rainy - Basin - Water	0.50	1.71	1.65	0.37	25.09	22.16	22
Dry - Fringe - Sediment	0.64	6.04	4.51	1.71	150.87	66.34	37
Rainy - Fringe - Water	0.87	0.92	2.98	0.35	21.46	139.49	21
Dry - Scrub - Sediment	0.83	0.34	4.14	0.80	68.02	120.13	26
Rainy - Scrub - Sediment	0.86	1.16	3.36	0.56	17.66	39.07	7
Dry - Scrub - Water	0.89	-0.91	5.48	0.57	23.15	75.63	10
Rainy - Scrub - Water	0.91	-0.41	4.61	0.82	35.39	114.70	12

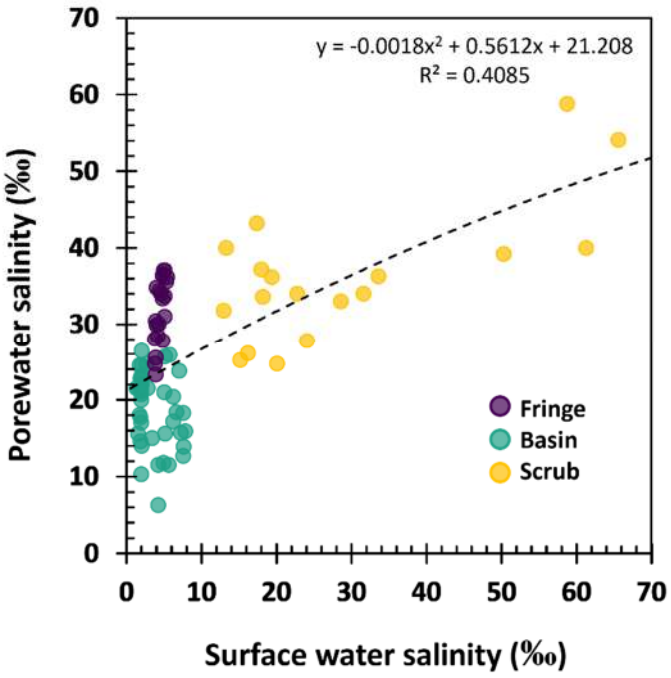

Figure S1. Relationship between surface water salinity and porewater salinity at the water-air interface when sediments were flooded.

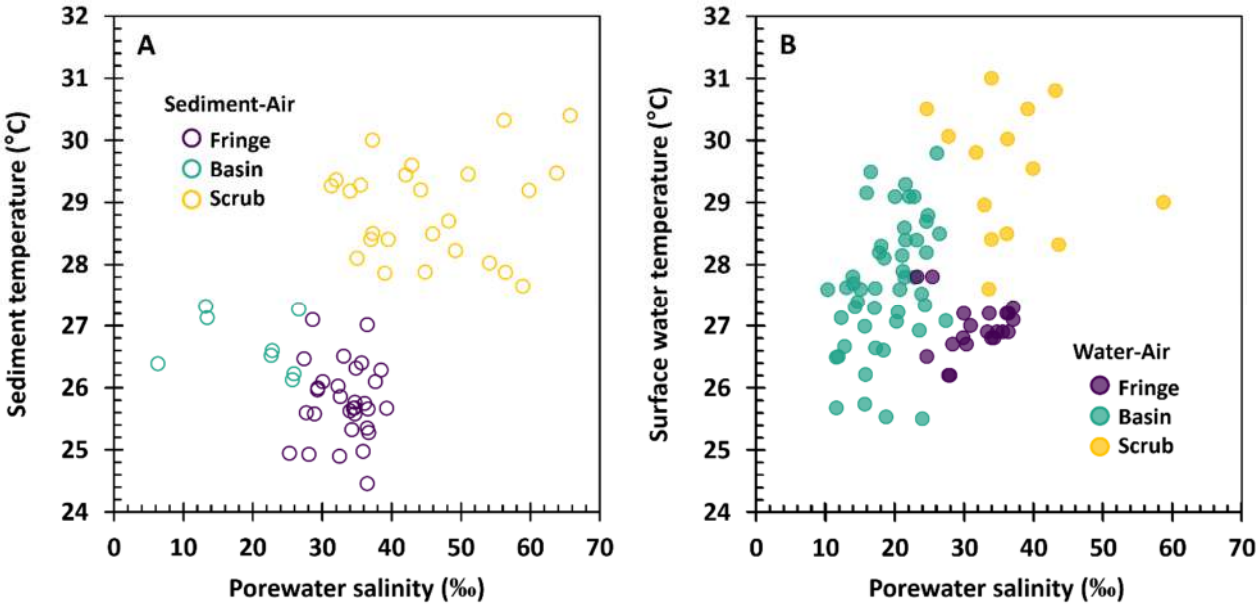

Figure S2. Porewater salinity and temperature relationship at the sediment-air (A, open dots) and water-air (B, filled dots).

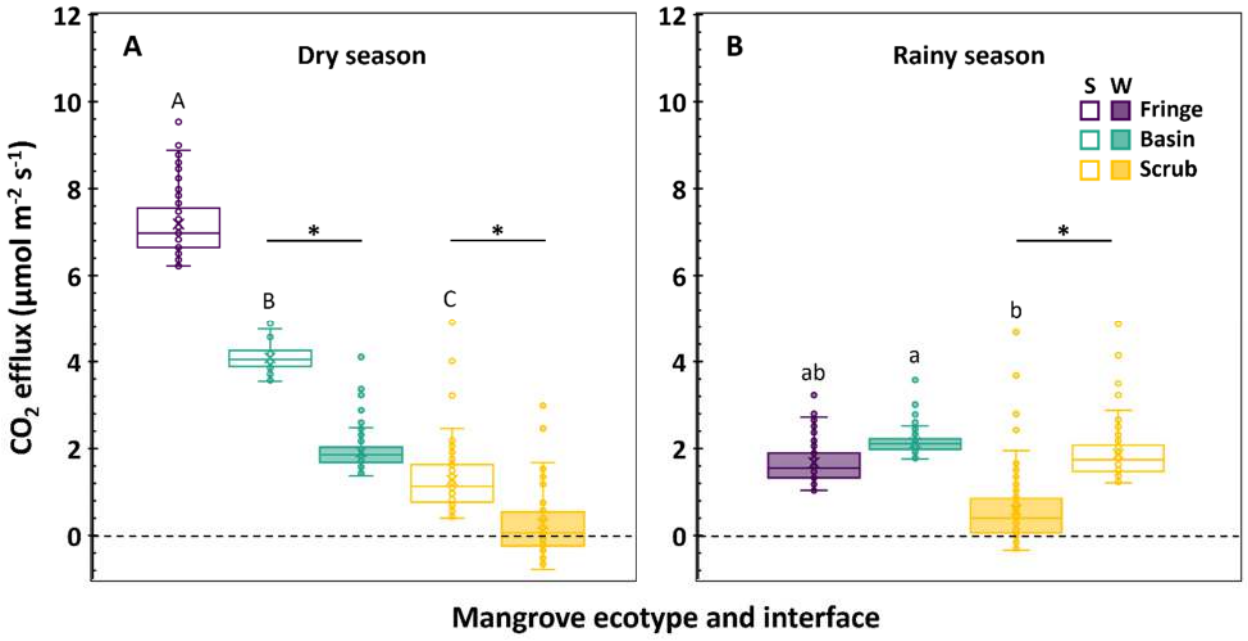

Figure S3. CO_2 effluxes from three different mangrove ecotypes during the dry (A) and rainy (B) seasons, at the sediment-air (S, open boxes) and water-air (W, filled boxes) interface. Data are medians, boxes correspond from first to third quartiles. Letters denote significant differences between mangrove ecotypes within seasons, being upper cases for dry and lower cases for rainy. Asterisks denote differences between interfaces within same mangrove ecotype (A) or between mangrove ecotypes within interfaces (B; $P < 0.01$).

ANEXO III. INFORMACIÓN SUPLEMENTARIA DEL CAPÍTULO IV

Figure S4.1. Structural traits of *R. mangle* trees at the ecological type of hammock (left) and scrub (right) mangrove forests.